

Coulomb Interaction in Atomically Thin Semiconductors and Density-Independent Exciton-Scattering Processes

Henry Mittenzwey,^{1, 2, *} Andreas Knorr,² and Thorsten Deilmann³

¹ Institut für Theoretische Physik und Zentrum für Materialforschung,
Justus-Liebig-Universität Gießen, 35392 Gießen, Germany

² Nichtlineare Optik und Quantenelektronik, Institut für Physik und Astronomie (IFPA),
Technische Universität Berlin, 10623 Berlin, Germany

³ Institut für Festkörpertheorie, Universität Münster, 48149 Münster, Germany
(Dated: February 17, 2026)

In quantum-kinetic approaches to the dynamics of Coulomb-bound many-body correlations such as excitons, trions, biexcitons or higher-order correlations, a detailed knowledge of the many-body Coulomb Hamiltonian serving as a starting point is important. In this manuscript, the second-quantized description of the Coulomb interaction between Bloch electrons in a Heisenberg-equation-of-motion approach in atomically thin semiconductors is derived and reviewed. Emphasis is put on a discussion of Umklapp processes and the dielectric screening including all local-field effects. A link between *ab initio* methods of screening and few-band models in effective-mass approximations for the quantum kinetics is established and all important Coulomb scattering processes contributing to the exciton energy landscape and density-independent exciton scattering are discussed.

CONTENTS

I. Introduction	1
II. Many-Body Coulomb Interaction Hamiltonian	2
A. Evaluating the Form Factors	5
B. Expansion Over the Band Extrema	6
C. Taylor Expansion of the Form Factor in Small Momentum Transfers	6
III. Screening	7
A. Microscopic Screening	10
B. Macroscopic Screening	12
1. Poisson's Equation in Layered Media	13
2. Analytical Model of Screening	16
IV. Excitons and Optical Spectra	17
V. Coulomb Scattering Processes	21
A. Direct Electron-Hole Interaction	21
Small Momentum Transfer	21
Large Momentum Transfer	22
B. Electron-Hole Exchange Interaction	23
Small Momentum Transfer	24
Large Momentum Transfer	26
VI. Conclusion	27
Acknowledgments	28
A. Supercell Hamiltonian	28
B. Fourier Transformation in Periodic Lattices	30
C. Parameters	31

References

31

I. INTRODUCTION

In this manuscript, we review and discuss a Heisenberg-equations-of-motion approach to the second-quantized Coulomb interaction between Bloch electrons in thin semiconductors. Our theory serves as a starting point for the calculation of many-body complexes such as excitons [1–3], trions [4–14], biexcitons [15–20] and higher correlations in intense optical fields in undoped semiconductors [21–26] or in small optical fields in heavily doped semiconductors [27, 28] and their quantum kinetics. Within a projection technique on electron-hole pair operators [2, 29] up to second order dynamics-controlled truncation [30, 31], the exciton dynamics in the undoped limit within an effective-mass approximation are dominated by incoherent exciton scattering via exciton-phonon interaction [32–36] and density-independent incoherent Coulomb scattering such as intervalley exchange [37–40], Dexter interaction [41–43] or disorder-mediated coherent intervalley exchange [44]. Recent advances go beyond an effective-mass approximation by marrying *ab initio* methods with quantum-kinetic approaches [45–55].

While the topic of second-quantized many-body Coulomb interaction is covered by various textbooks [56–61], its derivation starting from the classical Hamiltonian and a detailed discussion of Umklapp processes and the origin of local-field effects and microscopic screening in atomically thin semiconductors is often not provided. Our approach shall serve as a starting point to combine state-of-the-art *ab initio* methods with many-body quantum kinetics.

The manuscript is organized as follows: In Sec. II, we derive the general many-body Coulomb Hamiltonian in

* henry.mittenzwey@uni-giessen.de

second quantization, cf. Eq. (29):

$$\hat{H}_{\text{Coul}} = \frac{1}{2} \sum_{\substack{\lambda_1, \dots, \lambda_4, \mathbf{k}_{\parallel}, \mathbf{k}'_{\parallel}, \mathbf{q}_{\parallel}, \\ \mathbf{G}_{\parallel}, \mathbf{G}'_{\parallel}, s, s', n_1, \dots, n_4, \\ \mathbf{G}''_{\parallel} |_{\mathbf{k}_{\parallel} + \mathbf{q}_{\parallel} + \mathbf{G}''_{\parallel} \in \text{1st BZ}}, \\ \mathbf{G}'''_{\parallel} |_{\mathbf{k}'_{\parallel} - \mathbf{q}_{\parallel} - \mathbf{G}'''_{\parallel} \in \text{1st BZ}}} \int_{-\infty}^t dt' V_{\mathbf{q}_{\parallel}, \mathbf{G}_{\parallel}, \mathbf{G}'_{\parallel}}^{n_1, n_2, n_3, n_4}(t, t') \times \bar{\Upsilon}_{\mathbf{k}_{\parallel} + \mathbf{q}_{\parallel} + \mathbf{G}_{\parallel}}^{\lambda_1, \lambda_4, s} \bar{\Upsilon}_{\mathbf{k}'_{\parallel} - \mathbf{q}_{\parallel} - \mathbf{G}'_{\parallel}, \mathbf{k}'_{\parallel}}^{\lambda_2, \lambda_3, s'} \times \left(\hat{a}_{\lambda_1, \mathbf{k}_{\parallel} + \mathbf{q}_{\parallel} + \mathbf{G}''_{\parallel}}^{\dagger, s, n_1}(t) \hat{a}_{\lambda_2, \mathbf{k}'_{\parallel} - \mathbf{q}_{\parallel} - \mathbf{G}'''_{\parallel}}^{\dagger, s', n_2}(t') \hat{a}_{\lambda_3, \mathbf{k}'_{\parallel}}^{s', n_3}(t') \hat{a}_{\lambda_4, \mathbf{k}_{\parallel}}^{s, n_4}(t) \right. \\ \left. + \delta_{\lambda_2, \lambda_4}^{\mathbf{k}'_{\parallel}, \mathbf{k}_{\parallel} + \mathbf{q}_{\parallel} + \mathbf{G}''_{\parallel}} \delta_{\mathbf{G}''_{\parallel}, \mathbf{G}'''_{\parallel}}^{n_2, n_4} \delta(t - t') \right. \\ \left. \times \hat{a}_{\lambda_1, \mathbf{k}_{\parallel} + \mathbf{q}_{\parallel} + \mathbf{G}_{\parallel}}^{\dagger, s, n_1}(t) \hat{a}_{\lambda_3, \mathbf{k}'_{\parallel}}^{s', n_3}(t) \right), \quad (1)$$

in its most general form including all possible Coulomb-scattering processes ($\hat{a}_1^{\dagger} \hat{a}_2^{\dagger} \hat{a}_3 \hat{a}_4$), local-field effects ($\mathbf{G}_{\parallel}, \mathbf{G}'_{\parallel}$) and Umklapp processes ($\mathbf{G}''_{\parallel}, \mathbf{G}'''_{\parallel}$) with the screened quantum-confined Coulomb potential $V_{\mathbf{q}_{\parallel}, \mathbf{G}_{\parallel}, \mathbf{G}'_{\parallel}}^{n_1, n_2, n_3, n_4}(t, t')$, cf. Eq. (4), (reduced) Bloch form factors $\bar{\Upsilon}_{\mathbf{k}'_{\parallel}, \mathbf{k}_{\parallel}}^{\lambda, \lambda', s}$, cf. Eq. (30), and annihilation (creation) operators $\hat{a}_{\lambda, \mathbf{k}_{\parallel}}^{(\dagger) s, n}$ in band λ , in-plane quasi-momentum \mathbf{k}_{\parallel} , spin s and confinement quantum number n .

In Sec. III, we discuss the concepts of screening, where we, first, provide a microscopic model (Sec. III A) for the quantum-confined Coulomb potential $V_{\mathbf{q}_{\parallel}, \mathbf{G}_{\parallel}, \mathbf{G}'_{\parallel}}^{n_1, n_2, n_3, n_4}(\omega, \omega')$, cf. Eq. (89):

$$V_{\mathbf{q}_{\parallel}, \mathbf{G}_{\parallel}, \mathbf{G}'_{\parallel}}^{n_1, n_2, n_3, n_4}(\omega, \omega') = \sum_{G_z, G'_z} (\varepsilon_{\text{mic}}^{-1})_{\mathbf{q}_{\parallel}, \mathbf{G}_{\parallel}, \mathbf{G}'_{\parallel}, G_z, G'_z}(\omega, \omega') F_{G_z}^{n_1, n_4} F_{-G'_z}^{n_2, n_3} \times V_{0, \mathbf{q}_{\parallel} + \mathbf{G}'_{\parallel}, G'_z}^{\text{trunc}}, \quad (2)$$

with the three-dimensional microscopic dielectric function $\varepsilon_{\text{mic}, \mathbf{q}, \mathbf{G}, \mathbf{G}'}(\omega, -\omega')$ from *ab initio* supercell calculations in random-phase approximation, cf. Eq. (83):

$$\varepsilon_{\text{mic}, \mathbf{q}, \mathbf{G}, \mathbf{G}'}(\omega, -\omega') = 2\pi\delta(\omega - \omega')\delta_{\mathbf{G}, \mathbf{G}'} - 2\pi\delta(\omega - \omega')V_{0, \mathbf{q} + \mathbf{G}} + \sum_{\lambda, \lambda', \mathbf{k}} \frac{\bar{\Upsilon}_{\mathbf{k} - \mathbf{G}, \mathbf{k}}^{\lambda, \lambda', s} \bar{\Upsilon}_{\mathbf{k}, \mathbf{k} - \mathbf{G}'}^{\lambda', \lambda, s} \left(f_{\lambda, \mathbf{k} - \mathbf{q}}^s - f_{\lambda', \mathbf{k}}^s \right)}{\tilde{E}_{\lambda, \mathbf{k} - \mathbf{q}}^s - \tilde{E}_{\lambda', \mathbf{k}}^s + \hbar\omega + i\hbar\gamma}, \quad (3)$$

with renormalized single-particle dispersions $\tilde{E}_{\lambda, \mathbf{k}}^s$ and Fermi distributions $f_{\lambda, \mathbf{k}}^s$, and, second, review an analytical macroscopic approach (Sec. III B), where the quantum-confined Coulomb potential in a layered dielectric environment with substrate and superstrate without local fields ($\mathbf{G}_{\parallel} = \mathbf{G}'_{\parallel} = \mathbf{0}$) in a static, i.e., memory-free limit ($\omega = \omega' = 0$) with $V_{\mathbf{q}_{\parallel}, \mathbf{G}_{\parallel}, \mathbf{G}'_{\parallel}}^{n_1, n_2, n_3, n_4}(\omega, \omega') \rightarrow V_{\mathbf{q}_{\parallel}}$ can be

expressed as, cf. Eq. (112):

$$V_{\mathbf{q}_{\parallel}} = \frac{e^2}{2\mathcal{A}\epsilon_0\epsilon_{\text{M}}|\mathbf{q}_{\parallel}|} \frac{\gamma_- + \delta_+ - \gamma_+e^{|\mathbf{q}_{\parallel}|d} - \delta_-e^{-|\mathbf{q}_{\parallel}|d}}{\delta_-e^{-|\mathbf{q}_{\parallel}|d} - \gamma_+e^{|\mathbf{q}_{\parallel}|d}}. \quad (4)$$

In Sec. IV, we derive the Bethe-Salpeter equation in COHSEX- and Tamm-Danoff approximation, cf. Eq. (124):

$$(E_{c, \mathbf{q}} - E_{v, \mathbf{q}} + \Sigma_{v, c, \mathbf{q}}^{\text{H}} + \Sigma_{c, \mathbf{q}}^{\text{COH}} + \Sigma_{c, \mathbf{q}}^{\text{SEX}}) \Phi_{\mu, v, c, \mathbf{q}} + \sum_{\mathbf{q}', v', c'} \left(K_{\text{eh}}^{\text{dir} v', c', \mathbf{q}'} + K_{\text{eh}}^{\text{exch} v', c', \mathbf{q}'} \right) \Phi_{\mu, v', c', \mathbf{q}'} = E_{\mu} \Phi_{\mu, v, c, \mathbf{q}}, \quad (5)$$

for the excitonic energies E_{μ} and excitonic wave functions $\Phi_{\mu, v, c, \mathbf{q}}$ defined over the entire Brillouin zone, and its few-band effective-mass version, the Wannier equation, cf. Eq. (131):

$$\left(\tilde{E}_{\text{gap}}^{\xi, \xi', s, s'} + \frac{\hbar^2 \mathbf{q}^2}{2m_{r, s, s'}^{\xi, \xi'}} \right) \varphi_{\mu, \mathbf{q}}^{\xi, \xi', s, s'} - \sum_{\mathbf{q}'} K_{\text{eh}}^{\text{dir} \xi, \xi', s, s'} \varphi_{\mu, \mathbf{q} - \mathbf{q}'}^{\xi, \xi', s, s'} = E_{\mu}^{\xi, \xi', s, s'} \varphi_{\mu, \mathbf{q}}^{\xi, \xi', s, s'}, \quad (6)$$

for excitonic energies $E_{\mu}^{\xi, \xi', s, s'}$ and excitonic wave functions $\varphi_{\mu, \mathbf{q}}^{\xi, \xi', s, s'}$ defined in the vicinity of the high-symmetry points ξ (ξ') with respect to holes (electrons), which describe Coulomb-bound electron-hole pairs, the excitons, and discuss their signatures in optical absorption spectra.

In Sec. V A (direct electron-hole interaction $\hat{a}_{\lambda, \mathbf{k}_{\parallel} + \mathbf{q}_{\parallel}}^{\dagger s} \hat{a}_{\lambda', \mathbf{k}'_{\parallel} - \mathbf{q}_{\parallel}}^{\dagger s'} \hat{a}_{\lambda', \mathbf{k}'_{\parallel}}^{s'} \hat{a}_{\lambda, \mathbf{k}_{\parallel}}^s$ with $\lambda \neq \lambda'$) and Sec. V B (electron-hole exchange interaction $\hat{a}_{\lambda', \mathbf{k}_{\parallel} + \mathbf{q}_{\parallel}}^{\dagger s} \hat{a}_{\lambda, \mathbf{k}'_{\parallel} - \mathbf{q}_{\parallel}}^{\dagger s'} \hat{a}_{\lambda', \mathbf{k}'_{\parallel}}^{s'} \hat{a}_{\lambda, \mathbf{k}_{\parallel}}^s$ with $\lambda \neq \lambda'$), we dissect all contributions of many-body Coulomb scattering processes described by Eq. (1) beyond the Wannier equation in an effective-mass two-band model, which are important for exciton quantum kinetics in the density-independent limit.

II. MANY-BODY COULOMB INTERACTION HAMILTONIAN

The classical electron-electron Coulomb interaction Hamiltonian in Coulomb gauge reads [62]:

$$H_{\text{Coul}} = \frac{1}{2} \int d^3r \rho(\mathbf{r}, t) \phi(\mathbf{r}, t), \quad (7)$$

where $\rho(\mathbf{r}, t) = \sum_i q_i \delta(\mathbf{r} - \mathbf{r}_i(t))$ is the electronic charge density with charge $q_i = -e$ and location $\mathbf{r}_i(t)$ of the i -th electron and $\phi(\mathbf{r}, t)$ is the electron-electron Coulomb potential, which solves the generalized Poisson equation:

$$\nabla_{\mathbf{r}} \cdot \int d^3r' dt' \epsilon(\mathbf{r}, \mathbf{r}', t, t') \nabla_{\mathbf{r}'} \phi(\mathbf{r}', t') = -\frac{1}{\epsilon_0} \rho(\mathbf{r}, t). \quad (8)$$

Here, $\epsilon(\mathbf{r}, \mathbf{r}', t, t')$ is the relative spatially and temporally nonlocal background permittivity covering the dielectric environment and the thin semiconductor itself. The solution of Eq. (8) can be written in terms of a Green's function $G(\mathbf{r}, \mathbf{r}', t, t')$:

$$\phi(\mathbf{r}, t) = \int d^3r' dt' G(\mathbf{r}, \mathbf{r}', t, t') \rho(\mathbf{r}', t'). \quad (9)$$

Plugging this into the Hamiltonian, we obtain:

$$H_{\text{Coul}} = \frac{1}{2} \int d^3r d^3r' \int_{-\infty}^t dt' \rho(\mathbf{r}, t) G(\mathbf{r}, \mathbf{r}', t, t') \rho(\mathbf{r}', t'). \quad (10)$$

The quantized electron charge density $\rho(\mathbf{r}, t) \rightarrow \hat{\rho}(\mathbf{r}, t)$ reads [63]:

$$\begin{aligned} \hat{\rho}(\mathbf{r}, t) &= -e \int d^3r' \hat{\Psi}^\dagger(\mathbf{r}', t) \delta(\mathbf{r} - \mathbf{r}') \hat{\Psi}(\mathbf{r}', t) \\ &= -e \hat{\Psi}^\dagger(\mathbf{r}, t) \hat{\Psi}(\mathbf{r}, t), \end{aligned} \quad (11)$$

where $\hat{\Psi}(\mathbf{r}, t)$ is the corresponding fermionic Schrödinger field operator with fermionic equal-time commutation relations for a constrained system [64–67]:

$$\begin{aligned} [\hat{\Psi}(\mathbf{r}, t), \hat{\Psi}^\dagger(\mathbf{r}', t')]_+ &= \hat{\Psi}(\mathbf{r}, t) \hat{\Psi}^\dagger(\mathbf{r}', t') + \hat{\Psi}^\dagger(\mathbf{r}', t') \hat{\Psi}(\mathbf{r}, t) \\ &= \delta(\mathbf{r} - \mathbf{r}') \delta(t - t'). \end{aligned} \quad (12)$$

In the following, we set $\mathbf{r} = (\mathbf{r}_\parallel \ z)^\top$, where \mathbf{r}_\parallel (z) represent the in-plane (out-of-plane) coordinates. The field operator is expanded in single-particle states:

$$\hat{\Psi}(\mathbf{r}_\parallel, z, t) = \sum_{\lambda, \mathbf{k}_\parallel, s, n} \psi_{\lambda, \mathbf{k}_\parallel}^s(\mathbf{r}_\parallel) \chi_s \zeta_n(z) \hat{a}_{\lambda, \mathbf{k}_\parallel}^{s, n}(t), \quad (13)$$

where:

$$\psi_{\lambda, \mathbf{k}_\parallel}^s(\mathbf{r}_\parallel) = \frac{1}{\sqrt{\mathcal{A}}} e^{i\mathbf{k}_\parallel \cdot \mathbf{r}_\parallel} u_{\lambda, \mathbf{k}_\parallel}^s(\mathbf{r}_\parallel) \quad (14)$$

are the Bloch functions with lattice-periodic Bloch factors $u_{\lambda, \mathbf{k}_\parallel}^s(\mathbf{r}_\parallel)$ describing electrons in a two-dimensional periodic lattice in band λ and in-plane momentum \mathbf{k}_\parallel from within the first Brillouin zone (BZ) normalization area \mathcal{A} within Born-von Kármán boundary conditions [68]. By Fourier-expanding $u_{\lambda, \mathbf{k}_\parallel}^s(\mathbf{r}_\parallel) = \sum_{\mathbf{G}_\parallel} e^{i\mathbf{G}_\parallel \cdot \mathbf{r}_\parallel} u_{\lambda, \mathbf{k}_\parallel + \mathbf{G}_\parallel}^s$ within the periodic-gauge condition satisfying $\psi_{\lambda, \mathbf{k}_\parallel + \mathbf{G}_\parallel}^s = \psi_{\lambda, \mathbf{k}_\parallel}^s$ [69–71], we can also obtain the expression:

$$\psi_{\lambda, \mathbf{k}_\parallel}^s(\mathbf{r}_\parallel) = \frac{1}{\sqrt{\mathcal{A}}} \sum_{\mathbf{G}_\parallel} e^{i(\mathbf{k}_\parallel + \mathbf{G}_\parallel) \cdot \mathbf{r}_\parallel} u_{\lambda, \mathbf{k}_\parallel + \mathbf{G}_\parallel}^s. \quad (15)$$

Hence, a Bloch electron – in contrast to a free electron – does not possess a single momentum but is rather described as a wave packet, i.e., a superposition of plane

waves with momenta $\mathbf{k}_\parallel + \mathbf{G}_\parallel$ weighted by the corresponding Bloch factor in reciprocal space $u_{\lambda, \mathbf{k}_\parallel + \mathbf{G}_\parallel}^s$. Moreover, in Eq. (13), χ_s are the eigenfunctions of the spin angular momentum operator in z -direction $\hat{S}_z = \frac{\hbar}{2} \sigma_z$ with Pauli matrix σ_z , which are normalized according to $\bar{\chi}_s \cdot \chi_{s'} = \delta_{s, s'}$, and $\zeta_n(z)$ are the confinement functions in z -direction with confinement quantum number n . $a_{\lambda, \mathbf{k}_\parallel}^{(\dagger)s, n}(t)$ are the annihilation (creation) operators, whose commutation relations follow from Eq. (12):

$$[\hat{a}_i(t), \hat{a}_j^\dagger(t')] = \delta_{i,j} \delta(t - t'). \quad (16)$$

The factorization in Eq. (13) is a quasi-mesoscopic ansatz, which assumes in-plane, out-of-plane and spin contributions to be separable. We note, that this is an approximation to simplify the notation. In App. A, we show an exact approach, which is able to incorporate Bloch functions obtained from *ab initio* calculations using supercells. We also note, that we work in the reduced-zone scheme throughout the manuscript, i.e., the quasi-or crystal momenta \mathbf{k}_\parallel are always restricted to the first Brillouin zone. In second quantization $H_{\text{Coul}} \rightarrow \hat{H}_{\text{Coul}}$ and a subsequent normal ordering of the occurring operator products, Eq. (10) translates to:

$$\begin{aligned} \hat{H}_{\text{Coul}} &= \frac{1}{2} \sum_{\substack{\lambda_1, \dots, \lambda_4, \\ \mathbf{k}_{\parallel, 1}, \dots, \mathbf{k}_{\parallel, 4}, \\ s_1, \dots, s_4, \\ n_1, \dots, n_4}} \int_{-\infty}^t dt' \frac{e^2}{\mathcal{A}^2} \int d^2r_\parallel d^2r'_\parallel dz dz' \\ &\quad \times G(\mathbf{r}_\parallel, \mathbf{r}'_\parallel, z, z', t, t') (\bar{\chi}_{s_1} \cdot \chi_{s_4}) (\bar{\chi}_{s_2} \cdot \chi_{s_3}) \\ &\quad \times e^{-i(\mathbf{k}_{\parallel, 1} - \mathbf{k}_{\parallel, 4}) \cdot \mathbf{r}_\parallel} u_{\lambda_1, \mathbf{k}_{\parallel, 1}}^{s_1}(\mathbf{r}_\parallel) u_{\lambda_4, \mathbf{k}_{\parallel, 4}}^{s_4}(\mathbf{r}'_\parallel) \zeta_{n_1}(z) \zeta_{n_4}(z') \\ &\quad \times e^{-i(\mathbf{k}_{\parallel, 2} - \mathbf{k}_{\parallel, 3}) \cdot \mathbf{r}'_\parallel} u_{\lambda_2, \mathbf{k}_{\parallel, 2}}^{s_2}(\mathbf{r}'_\parallel) u_{\lambda_3, \mathbf{k}_{\parallel, 3}}^{s_3}(\mathbf{r}'_\parallel) \zeta_{n_2}(z') \zeta_{n_3}(z') \\ &\quad \times \left(\hat{a}_{\lambda_1, \mathbf{k}_{\parallel, 1}}^{\dagger s_1, n_1}(t) \hat{a}_{\lambda_2, \mathbf{k}_{\parallel, 2}}^{\dagger s_2, n_2}(t') \hat{a}_{\lambda_3, \mathbf{k}_{\parallel, 3}}^{s_3, n_3}(t') \hat{a}_{\lambda_4, \mathbf{k}_{\parallel, 4}}^{s_4, n_4}(t) \right. \\ &\quad \left. + \delta_{\lambda_2, \lambda_4}^{\mathbf{k}_{\parallel, 2}, \mathbf{k}_{\parallel, 4}} \delta_{s_2, s_4}^{n_2, n_4} \delta(t - t') \hat{a}_{\lambda_1, \mathbf{k}_{\parallel, 1}}^{\dagger s_1, n_1}(t) \hat{a}_{\lambda_3, \mathbf{k}_{\parallel, 3}}^{s_3, n_3}(t') \right). \end{aligned} \quad (17)$$

We expand the Coulomb Green's function $G(\mathbf{r}_\parallel, \mathbf{r}'_\parallel, z, z', t, t')$ in terms of its Fourier components [72–74]:

$$\begin{aligned} G(\mathbf{r}_\parallel, \mathbf{r}'_\parallel, z, z', t, t') &= \frac{1}{\mathcal{A}} \sum_{\mathbf{q}_\parallel, \mathbf{G}_\parallel, \mathbf{G}'_\parallel} e^{i(\mathbf{q}_\parallel + \mathbf{G}_\parallel) \cdot \mathbf{r}_\parallel} \\ &\quad \times G_{\mathbf{q}_\parallel, \mathbf{G}_\parallel, \mathbf{G}'_\parallel}(z, z', t, t') e^{-i(\mathbf{q}_\parallel + \mathbf{G}'_\parallel) \cdot \mathbf{r}'_\parallel}, \end{aligned} \quad (18)$$

where \mathbf{q}_\parallel is a momentum within the first Brillouin zone and \mathbf{G}_\parallel and \mathbf{G}'_\parallel are in-plane reciprocal lattice vectors. Here, the summation runs over all reciprocal lattice vectors \mathbf{G}_\parallel and \mathbf{G}'_\parallel to cover the total reciprocal lattice. The restriction to \mathbf{q}_\parallel results from demanding lattice periodicity:

$G(\mathbf{r}_\parallel + \mathbf{R}_\parallel, \mathbf{r}'_\parallel + \mathbf{R}_\parallel, z, z', t, t') \stackrel{!}{=} G(\mathbf{r}_\parallel, \mathbf{r}'_\parallel, z, z', t, t')$. In Fourier space, it also holds: $G_{\mathbf{q}_\parallel + \mathbf{G}''_\parallel, \mathbf{G}_\parallel, \mathbf{G}'_\parallel}(z, z', t, t') =$

$G_{\mathbf{q}_{\parallel}, \mathbf{G}_{\parallel} + \mathbf{G}_{\parallel}''} (z, z', t, t')$. The Fourier expansion in Eq. (18) accounts for all microscopic local-field effects with $\mathbf{G}_{\parallel} \neq \mathbf{G}'_{\parallel}$ [72, 75], whose explicit calculation requires *ab initio* methods [74–83]. These local-field effects originate from spatial variations of the charge distributions within the unit cell, which are on the scale of the lattice constant of approximately 0.3 nm for the common TMDC monolayers [84] or below, much smaller than the exciton Bohr radius of approximately 1 nm. From a rigorous theoretical viewpoint, they are the result of an elimination of unwanted degrees of freedom [85–87], i.e., deeper valence/core bands or specific quantum-mechanical hierarchy strains, which will be discussed later on.

To illustrate the distinction between macroscopic and microscopic, i.e., local fields, we perform an averaging on the scale of the lattice vectors \mathbf{R}_{\parallel} and \mathbf{R}'_{\parallel} over the unit-cell area \mathcal{A}_{UC} by:

$$\begin{aligned} & G(\mathbf{R}_{\parallel}, \mathbf{R}'_{\parallel}, z, z', t, t') \\ &= \frac{1}{\mathcal{A}_{\text{UC}}} \int d^2 r_{\parallel} \frac{1}{\mathcal{A}_{\text{UC}}} \int d^2 r'_{\parallel} G(\mathbf{r}_{\parallel} + \mathbf{R}_{\parallel}, \mathbf{r}_{\parallel} + \mathbf{R}'_{\parallel}, z, z', t, t') \\ &= \frac{1}{\mathcal{A}} \sum_{\mathbf{q}_{\parallel}, \mathbf{G}_{\parallel}, \mathbf{G}'_{\parallel}} G_{\mathbf{q}_{\parallel}, \mathbf{G}_{\parallel}, \mathbf{G}'_{\parallel}} (z, z', t, t') \\ & \quad \times \frac{1}{\mathcal{A}_{\text{UC}}} \int_{\mathcal{A}_{\text{UC}}} d^2 r_{\parallel} e^{i(\mathbf{q}_{\parallel} + \mathbf{G}_{\parallel}) \cdot (\mathbf{r}_{\parallel} + \mathbf{R}_{\parallel})} \\ & \quad \times \frac{1}{\mathcal{A}_{\text{UC}}} \int_{\mathcal{A}_{\text{UC}}} d^2 r'_{\parallel} e^{-i(\mathbf{q}_{\parallel} + \mathbf{G}'_{\parallel}) \cdot (\mathbf{r}'_{\parallel} + \mathbf{R}'_{\parallel})} \\ &= \frac{1}{\mathcal{A}} \sum_{\mathbf{q}_{\parallel}, \mathbf{G}_{\parallel}, \mathbf{G}'_{\parallel}} G_{\mathbf{q}_{\parallel}, \mathbf{G}_{\parallel}, \mathbf{G}'_{\parallel}} (z, z', t, t') e^{i\mathbf{q}_{\parallel} \cdot (\mathbf{R}_{\parallel} - \mathbf{R}'_{\parallel})} \\ & \quad \times \frac{1}{\mathcal{A}_{\text{UC}}} \int_{\mathcal{A}_{\text{UC}}} d^2 r_{\parallel} e^{i(\mathbf{q}_{\parallel} + \mathbf{G}_{\parallel}) \cdot \mathbf{r}_{\parallel}} \\ & \quad \times \frac{1}{\mathcal{A}_{\text{UC}}} \int_{\mathcal{A}_{\text{UC}}} d^2 r'_{\parallel} e^{-i(\mathbf{q}_{\parallel} + \mathbf{G}'_{\parallel}) \cdot \mathbf{r}'_{\parallel}}, \end{aligned} \quad (19)$$

where we used $e^{i\mathbf{G}_{\parallel} \cdot \mathbf{R}_{\parallel}} = 1$ in the last step. The spatial integrals can be evaluated by assuming $|\mathbf{q}_{\parallel}| \ll |\mathbf{G}_{\parallel}|$:

$$\begin{aligned} & \frac{1}{\mathcal{A}_{\text{UC}}} \int_{\mathcal{A}_{\text{UC}}} d^2 r_{\parallel} e^{i(\mathbf{q}_{\parallel} + \mathbf{G}_{\parallel}) \cdot \mathbf{r}_{\parallel}} \approx \frac{1}{\mathcal{A}_{\text{UC}}} \int_{\mathcal{A}_{\text{UC}}} d^2 r_{\parallel} e^{i\mathbf{G}_{\parallel} \cdot \mathbf{r}_{\parallel}} \\ &= \delta_{\mathbf{G}_{\parallel}, \mathbf{0}}, \end{aligned} \quad (20)$$

as $e^{i\mathbf{G}_{\parallel} \cdot \mathbf{r}_{\parallel}}$ varies rapidly within the unit cell. Altogether, we obtain:

$$\begin{aligned} & G(\mathbf{R}_{\parallel}, \mathbf{R}'_{\parallel}, z, z', t, t') = \frac{1}{\mathcal{A}} \sum_{\mathbf{q}} G_{\mathbf{q}_{\parallel}, \mathbf{0}, \mathbf{0}} (z, z', t, t') e^{i\mathbf{q}_{\parallel} \cdot (\mathbf{R}_{\parallel} - \mathbf{R}'_{\parallel})} \\ & \equiv G(\mathbf{R}_{\parallel} - \mathbf{R}'_{\parallel}, z, z', t, t'). \end{aligned} \quad (21)$$

Hence, the macroscopic Coulomb Green's function $G(\mathbf{R}_{\parallel}, \mathbf{R}'_{\parallel}, z, z', t, t')$, which is the average over

the unit cell of the microscopic Green's function $G(\mathbf{r}_{\parallel}, \mathbf{r}'_{\parallel}, z, z', t, t')$, does not contain any local fields anymore and depends only on spatial distances. From Eq. (21), the macroscopic limit – not to be confused with the limit $\mathbf{q}_{\parallel} \rightarrow 0$ – in Fourier space can be identified as $G_{\mathbf{q}_{\parallel}, \mathbf{0}, \mathbf{0}} (z, z')$.

With the microscopic Coulomb Green's function in Eq. (18), we obtain:

$$\begin{aligned} \hat{H}_{\text{Coul}} &= \frac{1}{2} \sum_{\substack{\lambda_1, \dots, \lambda_4, \\ \mathbf{k}_{\parallel 1}, \dots, \mathbf{k}_{\parallel 4}, \\ \mathbf{q}_{\parallel}, \mathbf{G}_{\parallel}, \mathbf{G}'_{\parallel}, s, s', \\ n_1, \dots, n_4}} \int_{-\infty}^t dt' V_{\mathbf{q}_{\parallel}, \mathbf{G}_{\parallel}, \mathbf{G}'_{\parallel}}^{n_1, n_2, n_3, n_4} (t, t') \\ & \quad \times \Upsilon_{\mathbf{k}_{\parallel 1}, \mathbf{k}_{\parallel 2}, \mathbf{q}_{\parallel} + \mathbf{G}_{\parallel}}^{\lambda_1, \lambda_4, s} \Upsilon_{\mathbf{k}_{\parallel 2}, \mathbf{k}_{\parallel 3}, -\mathbf{q}_{\parallel} - \mathbf{G}'_{\parallel}}^{\lambda_2, \lambda_3, s'} \\ & \quad \times \left(\hat{a}_{\lambda_1, \mathbf{k}_{\parallel 1}}^{\dagger, s, n_1} (t) \hat{a}_{\lambda_2, \mathbf{k}_{\parallel 2}}^{\dagger, s', n_2} (t') \hat{a}_{\lambda_3, \mathbf{k}_{\parallel 3}}^{s', n_3} (t') \hat{a}_{\lambda_4, \mathbf{k}_{\parallel 4}}^{s, n_4} (t) \right. \\ & \quad \left. + \delta_{\lambda_2, \lambda_4}^{\mathbf{k}_{\parallel 2}, \mathbf{k}_{\parallel 4}} \delta_{s, s'}^{n_2, n_4} \delta(t - t') \hat{a}_{\lambda_1, \mathbf{k}_{\parallel 1}}^{\dagger, s, n_1} (t) \hat{a}_{\lambda_3, \mathbf{k}_{\parallel 3}}^{s', n_3} (t') \right), \end{aligned} \quad (22)$$

where we defined the form factors as:

$$\Upsilon_{\mathbf{k}_{\parallel}, \mathbf{k}'_{\parallel}, \mathbf{q}_{\parallel}}^{\lambda, \lambda', s} = \frac{1}{\mathcal{A}} \int d^2 r_{\parallel} e^{-i(\mathbf{k}_{\parallel} - \mathbf{k}'_{\parallel} - \mathbf{q}_{\parallel}) \cdot \mathbf{r}_{\parallel}} u_{\lambda, \mathbf{k}_{\parallel}}^{*s} (\mathbf{r}_{\parallel}) u_{\lambda', \mathbf{k}'_{\parallel}}^s (\mathbf{r}_{\parallel}), \quad (23)$$

and identified the time-nonlocal quantum-confined Coulomb potential with all local-field contributions \mathbf{G}_{\parallel} and \mathbf{G}'_{\parallel} as:

$$\begin{aligned} & V_{\mathbf{q}_{\parallel}, \mathbf{G}_{\parallel}, \mathbf{G}'_{\parallel}}^{n_1, n_2, n_3, n_4} (t, t') \\ &= \frac{e^2}{\mathcal{A}} \int dz dz' \zeta_{n_1}^* (z) \zeta_{n_4} (z) \zeta_{n_2}^* (z') \zeta_{n_3} (z') \\ & \quad \times G_{\mathbf{q}_{\parallel}, \mathbf{G}_{\parallel}, \mathbf{G}'_{\parallel}} (z, z', t, t'). \end{aligned} \quad (24)$$

Note, that the Coulomb Hamiltonian in Eq. (22) equally assumes a screened Coulomb interaction for direct electron-hole processes ($\hat{a}_{\lambda, \mathbf{k}_{\parallel 1}}^{\dagger} \hat{a}_{\lambda', \mathbf{k}_{\parallel 2}}^{\dagger} \hat{a}_{\lambda', \mathbf{k}_{\parallel 3}} \hat{a}_{\lambda, \mathbf{k}_{\parallel 4}}$, $\lambda \neq \lambda'$) and electron-hole exchange processes ($\hat{a}_{\lambda, \mathbf{k}_{\parallel 1}}^{\dagger} \hat{a}_{\lambda', \mathbf{k}_{\parallel 2}}^{\dagger} \hat{a}_{\lambda, \mathbf{k}_{\parallel 3}} \hat{a}_{\lambda', \mathbf{k}_{\parallel 4}}$, $\lambda \neq \lambda'$). In a fully microscopic treatment, the exchange contributions are unscreened, while the direct contributions are screened [74, 78]. However, within a reduced few-band model, it turns out, that screening the exchange interaction via the dielectric function of the material itself is necessary [88], since the interaction with all other bands is neglected. Similarly, if any substrate/superstrate material is present, the exchange contributions also have to take into account the screening by the dielectric environment [89, 90]. Hence, within a few-band model, exchange and direct interaction can be treated on the same footing with respect to the screening. This way, we avoid an overestimation of the exchange-interaction strength at the expense of a minor underestimation, since, if we use the full dielectric function, we double-count the influence of

those bands, which we consider in the few-band model as active. We note, that the exchange effects in, e.g., TMDCs are comparably small.

A. Evaluating the Form Factors

Expanding the spatial integrals in Eq. (23) over the unit cells in a periodic lattice [58]:

$$\begin{aligned} \Upsilon_{\mathbf{k}_{\parallel}, \mathbf{k}'_{\parallel}, \mathbf{q}_{\parallel} + \mathbf{G}_{\parallel}}^{\lambda, \lambda', s} &= \frac{1}{\mathcal{A}} \sum_{\mathbf{R}_{\parallel}} e^{-i(\mathbf{k}_{\parallel} - \mathbf{k}'_{\parallel} - \mathbf{q}_{\parallel}) \cdot \mathbf{R}_{\parallel}} \\ &\times \int_{\mathcal{A}_{\text{UC}}} d^2 r_{\parallel} e^{-i(\mathbf{k}_{\parallel} - \mathbf{k}'_{\parallel} - \mathbf{q}_{\parallel} - \mathbf{G}_{\parallel}) \cdot \mathbf{r}} u_{\lambda, \mathbf{k}_{\parallel}}^{*s}(\mathbf{r}_{\parallel}) u_{\lambda', \mathbf{k}'_{\parallel}}^s(\mathbf{r}_{\parallel}), \end{aligned} \quad (25)$$

evaluating the lattice sum:

$$\sum_{\mathbf{R}_{\parallel}} e^{-i(\mathbf{k}_{\parallel} - \mathbf{k}'_{\parallel} - \mathbf{q}_{\parallel}) \cdot \mathbf{R}_{\parallel}} = \mathcal{N} \sum_{\mathbf{G}''_{\parallel}} \delta_{\mathbf{G}''_{\parallel}, \mathbf{k}_{\parallel} - \mathbf{k}'_{\parallel} - \mathbf{q}_{\parallel}}, \quad (26)$$

where \mathcal{N} is the total number of unit cells with area \mathcal{A}_{UC} , and Fourier expanding the Bloch factors as follows:

$$u_{\lambda, \mathbf{k}_{\parallel}}^s(\mathbf{r}_{\parallel}) = \sum_{\mathbf{G}_{\parallel}} u_{\lambda, \mathbf{k}_{\parallel}, \mathbf{G}_{\parallel}}^s e^{i \mathbf{G}_{\parallel} \cdot \mathbf{r}_{\parallel}}, \quad (27)$$

which satisfy the periodic-gauge condition of the Bloch functions: $\psi_{\lambda, \mathbf{k}_{\parallel} + \mathbf{G}_{\parallel}}^s = \psi_{\lambda, \mathbf{k}_{\parallel}}^s$ [69–71], the form factors can be expressed as:

$$\begin{aligned} \Upsilon_{\mathbf{k}_{\parallel}, \mathbf{k}'_{\parallel}, \mathbf{q}_{\parallel} + \mathbf{G}_{\parallel}}^{\lambda, \lambda', s} &= \sum_{\mathbf{G}''_{\parallel}, \mathbf{G}_{\parallel 1}, \mathbf{G}_{\parallel 2}} u_{\lambda, \mathbf{k}'_{\parallel} + \mathbf{q}_{\parallel} + \mathbf{G}''_{\parallel}, -\mathbf{G}_{\parallel 1}}^{*s} u_{\lambda', \mathbf{k}'_{\parallel}, \mathbf{G}_{\parallel 2}}^s \\ &\times \delta_{\mathbf{G}''_{\parallel}, \mathbf{k}_{\parallel} - \mathbf{k}'_{\parallel} - \mathbf{q}_{\parallel}} \delta_{\mathbf{G}''_{\parallel}, \mathbf{G}_{\parallel 1} + \mathbf{G}_{\parallel 2}}. \end{aligned} \quad (28)$$

This expression is often used in explicit DFT/GW methods [70, 91, 92], as it relies on a full reciprocal-space formulation. Here, the first Kronecker delta ensures, that $\mathbf{k}'_{\parallel} + \mathbf{q}_{\parallel} + \mathbf{G}''_{\parallel} \in 1\text{st BZ}$ after evaluating the \mathbf{k}_{\parallel} -sum in the Hamiltonian, while the second Kronecker delta ensures momentum conservation of the total scattering process. In an extended classification, we call processes with $\mathbf{G}_{\parallel} = \mathbf{G}''_{\parallel} = \mathbf{0}$ *normal* processes, cf. Fig. 1(a), and processes with $\mathbf{G}_{\parallel} \neq \mathbf{0}$ or $\mathbf{G}''_{\parallel} \neq \mathbf{0}$ *Umklapp* processes, cf. Fig. 1(b). This implies, that even a process with $\mathbf{k}'_{\parallel} + \mathbf{q}_{\parallel} \in 1\text{st BZ}$ is classified as an *Umklapp* process, as long as a nonzero reciprocal lattice vector \mathbf{G}_{\parallel} entering the argument of the Coulomb potential $V_{\mathbf{q}_{\parallel}, \mathbf{G}_{\parallel}, \mathbf{G}'_{\parallel}}$ is involved, cf. Fig. 1(b). Our definition of Umklapp processes closely resembles the one in Refs. [57, 92, 93] and is not equal to the usual narrower definition in textbooks [56, 58, 59, 94], which only relates processes with $\mathbf{k}_{\parallel} + \mathbf{q}_{\parallel} \notin 1\text{st BZ}$ to Umklapp processes, i.e., processes with $\mathbf{G}''_{\parallel} \neq \mathbf{0}$. However, even the classification of a process being Umklapp

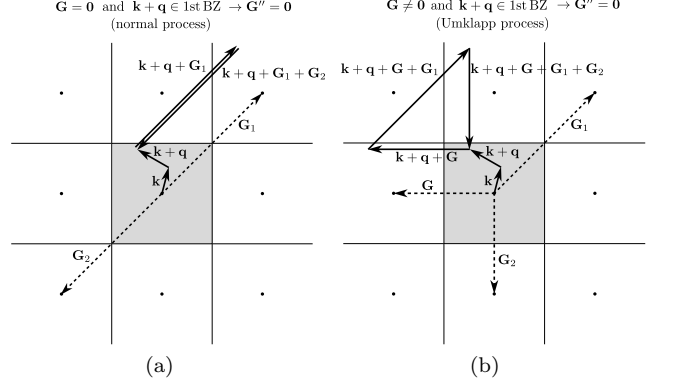


FIG. 1. Normal (a) and Umklapp (b) processes for a vanishing reciprocal lattice vector \mathbf{G}'' in an example square lattice.

in the standard and narrower sense contains some arbitrariness, i.e., the same process $\mathbf{k}_{\parallel} + \mathbf{q}_{\parallel}$ can be classified as Umklapp or not depending on the exact choice of the Brillouin zone. As a consequence, the magnitude of the scattering matrix elements, i.e., the Bloch form factors $\Upsilon_{\mathbf{k}_{\parallel}, \mathbf{k}'_{\parallel}, \mathbf{q}_{\parallel} + \mathbf{G}_{\parallel}}^{\lambda, \lambda', s}$, *do not* depend on the reciprocal lattice vector \mathbf{G}''_{\parallel} originating from the lattice sum in Eq. (26) – in contrast to the reciprocal lattice vector \mathbf{G}_{\parallel} originating from the Fourier transformation in Eq. (18). In the end, it is just a classification. What matters, is, that the description captures all possible processes, and not, how they are labeled.

The resulting Hamiltonian reads:

$$\begin{aligned} \hat{H}_{\text{Coul}} &= \frac{1}{2} \sum_{\substack{\lambda_1, \dots, \lambda_4, \mathbf{k}_{\parallel}, \mathbf{k}'_{\parallel}, \mathbf{q}_{\parallel}, \\ \mathbf{G}_{\parallel}, \mathbf{G}'_{\parallel}, s, s', n_1, \dots, n_4, \\ \mathbf{G}'''_{\parallel} | \mathbf{k}_{\parallel} + \mathbf{q}_{\parallel} + \mathbf{G}'''_{\parallel} \in 1\text{st BZ}, \\ \mathbf{G}'''_{\parallel} | \mathbf{k}'_{\parallel} - \mathbf{q}_{\parallel} - \mathbf{G}'''_{\parallel} \in 1\text{st BZ}}} \int_{-\infty}^t dt' V_{\mathbf{q}_{\parallel}, \mathbf{G}_{\parallel}, \mathbf{G}'_{\parallel}}^{n_1, n_2, n_3, n_4}(t, t') \\ &\times \bar{\Upsilon}_{\mathbf{k}_{\parallel} + \mathbf{q}_{\parallel} + \mathbf{G}_{\parallel}, \mathbf{k}_{\parallel}}^{\lambda_1, \lambda_4, s} \bar{\Upsilon}_{\mathbf{k}'_{\parallel} - \mathbf{q}_{\parallel} - \mathbf{G}'_{\parallel}, \mathbf{k}'_{\parallel}}^{\lambda_2, \lambda_3, s'} \\ &\times \left(\hat{a}_{\lambda_1, \mathbf{k}_{\parallel} + \mathbf{q}_{\parallel} + \mathbf{G}'''_{\parallel}}^{\dagger, s, n_1}(t) \hat{a}_{\lambda_2, \mathbf{k}'_{\parallel} - \mathbf{q}_{\parallel} - \mathbf{G}'''_{\parallel}}^{\dagger, s', n_2}(t') \hat{a}_{\lambda_3, \mathbf{k}'_{\parallel}}^{s', n_3}(t') \hat{a}_{\lambda_4, \mathbf{k}_{\parallel}}^{s, n_4}(t) \right. \\ &\left. + \delta_{\lambda_2, \lambda_4}^{\mathbf{k}'_{\parallel}, \mathbf{k}_{\parallel} + \mathbf{q}_{\parallel} + \mathbf{G}'''_{\parallel}} \delta_{\mathbf{G}'''_{\parallel}, \mathbf{G}'''_{\parallel}}^{n_2, n_4} \delta_{s, s'}(t - t') \right. \\ &\left. \times \hat{a}_{\lambda_1, \mathbf{k}_{\parallel} + \mathbf{q}_{\parallel} + \mathbf{G}'''_{\parallel}}^{\dagger, s, n_1}(t) \hat{a}_{\lambda_3, \mathbf{k}'_{\parallel}}^{s', n_3}(t') \right), \end{aligned} \quad (29)$$

where:

$$\bar{\Upsilon}_{\mathbf{k}_{\parallel}, \mathbf{k}'_{\parallel}}^{\lambda, \lambda', s} = \sum_{\mathbf{G}_{\parallel}} u_{\lambda, \mathbf{k}_{\parallel}, \mathbf{G}_{\parallel}}^{*s} u_{\lambda', \mathbf{k}'_{\parallel}, \mathbf{G}_{\parallel}}^s, \quad (30)$$

is the reduced form factor. In Fig. 2, we schematically depict the scattering processes described by Eq. (29).

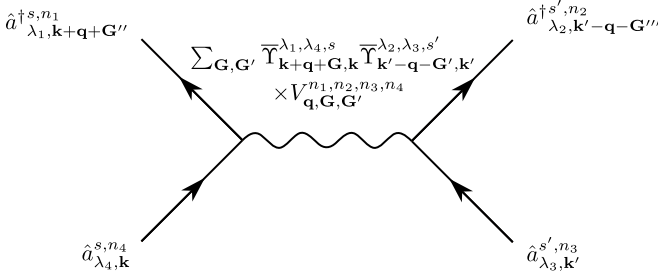


FIG. 2. Scheme of the Coulomb scattering processes described by Eq. (29).

Note, that in the calculation of standard BSE kernels [78, 95], only the reciprocal lattice vectors \mathbf{G}_{\parallel} and \mathbf{G}'_{\parallel} originating from the Fourier transformation in Eq. (18) appear, as \mathbf{G}''_{\parallel} and $\mathbf{G}'''_{\parallel}$ originate from explicitly evaluating the lattice sum in Eq. (26), which is often only done implicitly.

Also, we note, that, contrary to their outer appearance in Eq. (29) and Fig. 2, many-body scattering processes with $\mathbf{G}''_{\parallel} \neq \mathbf{G}'''_{\parallel}$ do not violate actual momentum conservation, since the quasi-momentum of a Bloch electron is not equal to the kinetic momentum of a bare electron.

In the following, we neglect the one-particle contributions arising from normal ordering, as they describe constant energy offsets, which cancel out in the evaluation of Heisenberg's equations of motion.

Moreover, from now on, we treat the reciprocal lattice vectors \mathbf{G}''_{\parallel} and $\mathbf{G}'''_{\parallel}$ describing Umklapp processes in the narrower sense implicitly, which is often done in the literature, and drop their summation. This can be safely done, since the matrix elements do not depend on these specific reciprocal lattice vectors \mathbf{G}''_{\parallel} and $\mathbf{G}'''_{\parallel}$, as discussed earlier.

B. Expansion Over the Band Extrema

We expand the momenta around the band extrema denoted by ξ , i.e., for a TMDC, the high-symmetry points \mathbf{K}^{ξ} :

$$\mathbf{k}_{\parallel} \rightarrow \mathbf{k}_{\parallel} + \mathbf{K}^{\xi}, \quad \mathbf{k}'_{\parallel} \rightarrow \mathbf{k}'_{\parallel} + \mathbf{K}^{\xi'}. \quad (31)$$

where $\xi = \Gamma, K, K', \Lambda, \Lambda'$ with $\mathbf{K}^{\Gamma} = \mathbf{0}$. Momentum transfers \mathbf{q}_{\parallel} within the first Brillouin zone can also be expanded around the band extrema:

$$\mathbf{q}_{\parallel} \rightarrow \mathbf{q}_{\parallel} + \mathbf{K}^{\xi''}. \quad (32)$$

The Bloch factors are then written as:

$$u_{\lambda, \mathbf{k}_{\parallel}}^s \rightarrow u_{\lambda, \mathbf{k}_{\parallel} + \mathbf{K}^{\xi}}^s \equiv u_{\lambda, \mathbf{k}_{\parallel}}^{\xi, s}, \quad (33)$$

where $u_{\lambda, \mathbf{k}_{\parallel}}^{\xi, s}$ is the Bloch factor valid for small momenta \mathbf{k}_{\parallel} around valley ξ . Correspondingly, the valley-

expanded Bloch factors read:

$$\overline{\Upsilon}_{\mathbf{k}_{\parallel}, \mathbf{k}'_{\parallel}}^{\lambda, \lambda', \xi, \xi', s} = \sum_{\mathbf{G}_{\parallel}} u_{\lambda, \mathbf{k}_{\parallel}, \mathbf{G}_{\parallel}}^{*, \xi, s} u_{\lambda', \mathbf{k}'_{\parallel}, \mathbf{G}'_{\parallel}}^{\xi', s}. \quad (34)$$

The resulting Hamiltonian reads:

$$\begin{aligned} \hat{H}_{\text{Coul}} = & \frac{1}{2} \sum_{\substack{\lambda_1, \dots, \lambda_4, \mathbf{k}_{\parallel}, \mathbf{k}'_{\parallel}, \\ \mathbf{q}_{\parallel}, \mathbf{G}_{\parallel}, \mathbf{G}'_{\parallel}, \\ s, s', \xi, \xi', \xi'', n_1, \dots, n_4,}} \int_{-\infty}^t dt' V_{\mathbf{q}_{\parallel} + \mathbf{K}^{\xi''}, \mathbf{G}_{\parallel}, \mathbf{G}'_{\parallel}}^{n_1, n_2, n_3, n_4}(t, t') \\ & \times \overline{\Upsilon}_{\mathbf{k}_{\parallel} + \mathbf{q}_{\parallel} + \mathbf{G}_{\parallel}, \mathbf{k}'_{\parallel}}^{\lambda_1, \lambda_4, \xi + \xi'', \xi, s} \overline{\Upsilon}_{\mathbf{k}'_{\parallel} - \mathbf{q}_{\parallel} - \mathbf{G}'_{\parallel}, \mathbf{k}'_{\parallel}}^{\lambda_2, \lambda_3, \xi' - \xi'', \xi', s'} \\ & \times \hat{a}_{\lambda_1, \mathbf{k}_{\parallel} + \mathbf{q}_{\parallel} + \mathbf{G}''_{\parallel}}^{\dagger, \xi + \xi'', s, n_1}(t) \hat{a}_{\lambda_2, \mathbf{k}'_{\parallel} - \mathbf{q}_{\parallel} - \mathbf{G}'''_{\parallel}}^{\dagger, \xi' - \xi'', s', n_2}(t') \hat{a}_{\lambda_3, \mathbf{k}'_{\parallel}}^{\xi', s', n_3}(t') \hat{a}_{\lambda_4, \mathbf{k}_{\parallel}}^{\xi, s, n_4}(t). \end{aligned} \quad (35)$$

Here, as a shorthand notation, we write: $\xi - \xi' \equiv \mathbf{K}^{\xi} - \mathbf{K}^{\xi'}$.

C. Taylor Expansion of the Form Factor in Small Momentum Transfers

A Taylor expansion of the reduced form factors for small momentum transfer \mathbf{q}_{\parallel} yields:

$$\begin{aligned} & \overline{\Upsilon}_{\mathbf{k}_{\parallel} + \mathbf{q}_{\parallel}, \mathbf{k}_{\parallel}, \mathbf{G}_{\parallel}}^{\lambda, \lambda', \xi, \xi', s} \\ &= \frac{1}{\mathcal{A}_{\text{UC}}} \int_{\mathcal{A}_{\text{UC}}} d^2 r_{\parallel} u_{\lambda, \mathbf{k}_{\parallel} + \mathbf{q}_{\parallel}}^{*, \xi, s}(\mathbf{r}_{\parallel}) e^{i \mathbf{G}_{\parallel} \cdot \mathbf{r}_{\parallel}} u_{\lambda', \mathbf{k}_{\parallel}}^{\xi', s}(\mathbf{r}_{\parallel}) \\ &= \frac{1}{\mathcal{A}_{\text{UC}}} \int_{\mathcal{A}_{\text{UC}}} d^2 r_{\parallel} \left(\left(1 + \mathbf{q}_{\parallel} \cdot \nabla_{\mathbf{k}_{\parallel}} + \frac{1}{2} (\mathbf{q}_{\parallel} \cdot \nabla_{\mathbf{k}_{\parallel}}) \right. \right. \\ & \times \left. \left. (\mathbf{q}_{\parallel} \cdot \nabla_{\mathbf{k}_{\parallel}}) + \mathcal{O}((\mathbf{q}_{\parallel})^3) \right) u_{\lambda, \mathbf{k}_{\parallel}}^{*, \xi, s}(\mathbf{r}_{\parallel}) \right) e^{i \mathbf{G}_{\parallel} \cdot \mathbf{r}_{\parallel}} u_{\lambda', \mathbf{k}_{\parallel}}^{\xi', s}(\mathbf{r}_{\parallel}). \end{aligned} \quad (36)$$

We consider terms up to second order:

$$\begin{aligned} & \overline{\Upsilon}_{\mathbf{k}_{\parallel} + \mathbf{q}_{\parallel}, \mathbf{k}_{\parallel}, \mathbf{G}_{\parallel}}^{\lambda, \lambda', \xi, \xi', s} \\ & \approx \frac{1}{\mathcal{A}_{\text{UC}}} \int_{\mathcal{A}_{\text{UC}}} d^2 r_{\parallel} u_{\lambda, \mathbf{k}_{\parallel}}^{*, \xi, s}(\mathbf{r}_{\parallel}) e^{i \mathbf{G}_{\parallel} \cdot \mathbf{r}_{\parallel}} u_{\lambda', \mathbf{k}_{\parallel}}^{\xi', s}(\mathbf{r}_{\parallel}) \\ & + \frac{1}{\mathcal{A}_{\text{UC}}} \int_{\mathcal{A}_{\text{UC}}} d^2 r_{\parallel} \left((\mathbf{q}_{\parallel} \cdot \nabla_{\mathbf{k}_{\parallel}}) u_{\lambda, \mathbf{k}_{\parallel}}^{*, \xi, s}(\mathbf{r}_{\parallel}) \right) e^{i \mathbf{G}_{\parallel} \cdot \mathbf{r}_{\parallel}} u_{\lambda', \mathbf{k}_{\parallel}}^{\xi', s}(\mathbf{r}_{\parallel}) \\ & - \frac{1}{2} \frac{1}{\mathcal{A}_{\text{UC}}} \int_{\mathcal{A}_{\text{UC}}} d^2 r_{\parallel} \left((\mathbf{q}_{\parallel} \cdot \nabla_{\mathbf{k}_{\parallel}}) u_{\lambda, \mathbf{k}_{\parallel}}^{*, \xi, s}(\mathbf{r}_{\parallel}) \right) e^{i \mathbf{G}_{\parallel} \cdot \mathbf{r}_{\parallel}} \\ & \times (\mathbf{q}_{\parallel} \cdot \nabla_{\mathbf{k}_{\parallel}}) u_{\lambda', \mathbf{k}_{\parallel}}^{\xi', s}(\mathbf{r}_{\parallel}). \end{aligned} \quad (37)$$

In the last term, we shifted the momentum derivative to the second Bloch factor by assuming vanishing boundary terms in \mathbf{k}_{\parallel} and by neglecting any \mathbf{k}_{\parallel} -derivative on the creation/annihilation operators. Inserting a unit matrix

where appropriate, we obtain:

$$\begin{aligned}
& \bar{\Gamma}_{\mathbf{k}_{\parallel} + \mathbf{q}_{\parallel}, \mathbf{k}_{\parallel}, \mathbf{G}_{\parallel}}^{\lambda, \lambda', \xi, \xi', s} \\
& \approx \frac{1}{\mathcal{A}_{\text{UC}}} \int_{\mathcal{A}_{\text{UC}}} d^2 r_{\parallel} u_{\lambda, \mathbf{k}_{\parallel}}^{*\xi, s}(\mathbf{r}_{\parallel}) e^{i \mathbf{G}_{\parallel} \cdot \mathbf{r}_{\parallel}} u_{\lambda', \mathbf{k}_{\parallel}}^{\xi', s}(\mathbf{r}_{\parallel}) \\
& + \sum_{\lambda''} \frac{1}{\mathcal{A}_{\text{UC}}} \int_{\mathcal{A}_{\text{UC}}} d^2 r_{\parallel} \left((\mathbf{q}_{\parallel} \cdot \nabla_{\mathbf{k}_{\parallel}}) u_{\lambda, \mathbf{k}_{\parallel}}^{*\xi, s}(\mathbf{r}_{\parallel}) \right) u_{\lambda'', \mathbf{k}_{\parallel}}^{\xi', s}(\mathbf{r}_{\parallel}) \\
& \quad \times \frac{1}{\mathcal{A}_{\text{UC}}} \int_{\mathcal{A}_{\text{UC}}} d^2 r'_{\parallel} u_{\lambda'', \mathbf{k}_{\parallel}}^{*\xi, s}(\mathbf{r}'_{\parallel}) e^{i \mathbf{G}_{\parallel} \cdot \mathbf{r}'_{\parallel}} u_{\lambda', \mathbf{k}_{\parallel}}^{\xi', s}(\mathbf{r}'_{\parallel}) \\
& - \frac{1}{2} \sum_{\lambda'', \lambda'''} \frac{1}{\mathcal{A}_{\text{UC}}} \int_{\mathcal{A}_{\text{UC}}} d^2 r_{\parallel} \left((\mathbf{q}_{\parallel} \cdot \nabla_{\mathbf{k}_{\parallel}}) u_{\lambda, \mathbf{k}_{\parallel}}^{*\xi, s}(\mathbf{r}_{\parallel}) \right) \\
& \quad \times u_{\lambda'', \mathbf{k}_{\parallel}}^{\xi, s}(\mathbf{r}_{\parallel}) \\
& \quad \times \frac{1}{\mathcal{A}_{\text{UC}}} \int_{\mathcal{A}_{\text{UC}}} d^2 r'_{\parallel} u_{\lambda'', \mathbf{k}_{\parallel}}^{*\xi, s}(\mathbf{r}'_{\parallel}) e^{i \mathbf{G}_{\parallel} \cdot \mathbf{r}'_{\parallel}} u_{\lambda''', \mathbf{k}_{\parallel}}^{\xi, s}(\mathbf{r}'_{\parallel}) \\
& \quad \times \frac{1}{\mathcal{A}_{\text{UC}}} \int_{\mathcal{A}_{\text{UC}}} d^2 r''_{\parallel} u_{\lambda''', \mathbf{k}_{\parallel}}^{*\xi, s}(\mathbf{r}''_{\parallel}) (\mathbf{q}_{\parallel} \cdot \nabla_{\mathbf{k}_{\parallel}}) u_{\lambda', \mathbf{k}_{\parallel}}^{\xi', s}(\mathbf{r}''_{\parallel}). \tag{38}
\end{aligned}$$

By identifying:

$$\mathbf{d}_{\mathbf{k}_{\parallel}}^{\lambda, \lambda', \xi, \xi', s} = -ie \frac{1}{\mathcal{A}_{\text{UC}}} \int_{\mathcal{A}_{\text{UC}}} d^2 r_{\parallel} u_{\lambda, \mathbf{k}_{\parallel}}^{*\xi, s}(\mathbf{r}_{\parallel}) \nabla_{\mathbf{k}_{\parallel}} u_{\lambda', \mathbf{k}_{\parallel}}^{\xi', s}(\mathbf{r}_{\parallel}), \tag{39}$$

which constitutes the dipole matrix element for $\lambda' = \bar{\lambda}$ and the Berry connection for $\lambda' = \lambda$ [96–98], we can write:

$$\bar{\Gamma}_{\mathbf{k}_{\parallel} + \mathbf{q}_{\parallel}, \mathbf{k}_{\parallel}, \mathbf{G}_{\parallel}}^{\lambda, \lambda', \xi, \xi', s} \approx \bar{\Gamma}_{\mathbf{k}_{\parallel}, \mathbf{k}_{\parallel}, \mathbf{G}_{\parallel}}^{\lambda, \lambda', \xi, \xi', s} \tag{40}$$

$$- \frac{i}{e} \sum_{\lambda''} \left(\mathbf{q}_{\parallel} \cdot \mathbf{d}_{\mathbf{k}_{\parallel}}^{\lambda, \lambda'', \xi, \xi, s} \right) \bar{\Gamma}_{\mathbf{k}_{\parallel}, \mathbf{k}_{\parallel}, \mathbf{G}_{\parallel}}^{\lambda'', \lambda', \xi, \xi', s} \tag{41}$$

$$- \frac{1}{2e^2} \sum_{\lambda'', \lambda'''} \left(\mathbf{q}_{\parallel} \cdot \mathbf{d}_{\mathbf{k}_{\parallel}}^{\lambda, \lambda'', \xi, \xi, s} \right) \bar{\Gamma}_{\mathbf{k}_{\parallel}, \mathbf{k}_{\parallel}, \mathbf{G}_{\parallel}}^{\lambda'', \lambda''', \xi, \xi, s} \\
\times \left(\mathbf{q}_{\parallel} \cdot \mathbf{d}_{\mathbf{k}_{\parallel}}^{\lambda''', \lambda', \xi, \xi', s} \right). \tag{42}$$

This expression is similar to a $\mathbf{q}_{\parallel} \cdot \mathbf{p}_{\parallel}$ expansion up to second order at the band extrema.

III. SCREENING

In this section, we discuss the validity of applying the *generalized* Poisson equation in Eq. (8) giving rise to the screened quantum-confined Coulomb potential in Eq. (24) entering the many-body Coulomb Hamiltonian in Eq. (22).

Starting from scratch, we have to consider the unscreened Poisson equation for the total potential ϕ_{tot} induced by the total charge density of the system ρ_{tot} derived from Gauss's law $(\nabla_{\mathbf{r}_{\parallel}} \partial_z)^{\top}$.

$\mathbf{E}_{\parallel}(\mathbf{r}_{\parallel}, z, t) = \frac{1}{\epsilon_0} \rho_{\text{tot}}(\mathbf{r}_{\parallel}, z, t)$ for a longitudinal electric field $\mathbf{E}_{\parallel}(\mathbf{r}_{\parallel}, z, t) = -(\nabla_{\mathbf{r}_{\parallel}} \partial_z)^{\top} \phi_{\text{tot}}(\mathbf{r}_{\parallel}, z, t)$:

$$\left(\frac{\nabla_{\mathbf{r}_{\parallel}}}{\partial_z} \right) \cdot \left(\frac{\nabla_{\mathbf{r}_{\parallel}}}{\partial_z} \right) \phi_{\text{tot}}(\mathbf{r}_{\parallel}, z, t) = -\frac{1}{\epsilon_0} \rho_{\text{tot}}(\mathbf{r}_{\parallel}, z, t). \tag{43}$$

Expanding the total potential in terms of the bare Green's function $G_0(\mathbf{r}_{\parallel}, \mathbf{r}'_{\parallel}, z, z', t, t')$:

$$\begin{aligned}
& \phi_{\text{tot}}(\mathbf{r}_{\parallel}, z, t) \\
& = \int d^2 r'_{\parallel} dz' dt' G_0(\mathbf{r}_{\parallel}, \mathbf{r}'_{\parallel}, z, z', t, t') \rho_{\text{tot}}(\mathbf{r}'_{\parallel}, z', t'), \tag{44}
\end{aligned}$$

and performing a Fourier transformation with respect to the in-plane coordinates \mathbf{r}_{\parallel} , yields the following equation for the bare Green's function $G_{0, \mathbf{q}_{\parallel}, \mathbf{G}_{\parallel}, \mathbf{G}'_{\parallel}}$:

$$\begin{aligned}
& \left(-(\mathbf{q}_{\parallel} + \mathbf{G}_{\parallel})^2 + \partial_z^2 \right) G_{0, \mathbf{q}_{\parallel}, \mathbf{G}_{\parallel}, \mathbf{G}'_{\parallel}}(z, z', t, t') \\
& = -\frac{1}{\epsilon_0} \delta(z - z') \delta(t - t') \delta_{\mathbf{G}_{\parallel}, \mathbf{G}'_{\parallel}}. \tag{45}
\end{aligned}$$

The solution reads:

$$\begin{aligned}
G_{0, \mathbf{q}_{\parallel}, \mathbf{G}_{\parallel}, \mathbf{G}'_{\parallel}}(z, z', t, t') & = \delta_{\mathbf{G}_{\parallel}, \mathbf{G}'_{\parallel}} \delta(t - t') \frac{e^{-|\mathbf{q}_{\parallel} + \mathbf{G}_{\parallel}| |z - z'|}}{2\epsilon_0 |\mathbf{q}_{\parallel} + \mathbf{G}_{\parallel}|} \\
& \equiv G_{0, \mathbf{q}_{\parallel} + \mathbf{G}_{\parallel}}(z - z') \delta_{\mathbf{G}_{\parallel}, \mathbf{G}'_{\parallel}} \delta(t - t'), \tag{46}
\end{aligned}$$

is diagonal in \mathbf{G}_{\parallel} and does not include any memory effects. In this case, if we wanted to calculate the optical response of a thin semiconductor, we would have to include a large amount of bands in the many-body Coulomb interaction, which would result in a large amount of correlations via Heisenberg equations of motion. Hence, we would strongly underestimate the screening if we restricted the considered bands to just a few e.g., restricting the phase space to the topmost valence band and the lowest conduction band.

To circumvent the necessity of computing a large amount of correlations, we divide the total charge density $\rho_{\text{tot}}(\mathbf{r}_{\parallel}, z, t)$ in a background contribution $\rho_b(\mathbf{r}_{\parallel}, z, t)$ and an active contribution $\rho(\mathbf{r}_{\parallel}, z, t)$ with:

$$\rho_{\text{tot}}(\mathbf{r}_{\parallel}, z, t) = \rho_b(\mathbf{r}_{\parallel}, z, t) + \rho(\mathbf{r}_{\parallel}, z, t), \tag{47}$$

where the active contribution $\rho(\mathbf{r}_{\parallel}, z, t)$ contains the reduced number of active bands and the background contribution $\rho_b(\mathbf{r}_{\parallel}, z, t)$ contains all other bands including possible sub-/superstrate materials. Then, from $\rho_b(\mathbf{r}_{\parallel}, z, t) = -(\nabla_{\mathbf{r}_{\parallel}} \partial_z)^{\top} \cdot \mathbf{P}_{\parallel}(\mathbf{r}_{\parallel}, z, t)$ and using the linear response of a longitudinal polarization density $\mathbf{P}_{\parallel}(\mathbf{r}_{\parallel}, z, t)$ due to a spatially and temporally nonlocal background described by the electronic susceptibility $\chi(\mathbf{r}_{\parallel}, \mathbf{r}'_{\parallel}, z, z', t, t')$, $\mathbf{P}_{\parallel}(\mathbf{r}_{\parallel}, z, t) =$

$\epsilon_0 \int d^2r'_{\parallel} dz' dt' \chi(\mathbf{r}_{\parallel}, \mathbf{r}'_{\parallel}, z, z', t, t') \mathbf{E}_{\parallel}(\mathbf{r}'_{\parallel}, z', t')$, we obtain the relation:

$$\begin{aligned} \rho_b(\mathbf{r}_{\parallel}, z, t) &= \epsilon_0 \left(\frac{\nabla_{\mathbf{r}_{\parallel}}}{\partial_z} \right) \cdot \int d^2r'_{\parallel} dz' dt' \\ &\times \chi(\mathbf{r}_{\parallel}, \mathbf{r}'_{\parallel}, z, z', t, t') \left(\frac{\nabla_{\mathbf{r}'_{\parallel}}}{\partial_{z'}} \right) \phi_{\text{tot}}(\mathbf{r}'_{\parallel}, z', t'), \end{aligned} \quad (48)$$

which, via defining the nonlocal dielectric function:

$$\begin{aligned} \epsilon(\mathbf{r}_{\parallel}, \mathbf{r}'_{\parallel}, z, z', t, t') &= \delta(\mathbf{r}_{\parallel} - \mathbf{r}'_{\parallel}) \delta(z - z') \delta(t - t') + \chi(\mathbf{r}_{\parallel}, \mathbf{r}'_{\parallel}, z, z', t, t'), \end{aligned} \quad (49)$$

yields the generalized or screened Poisson equation [99, 100], cf. also Eq. (8):

$$\begin{aligned} \left(\frac{\nabla_{\mathbf{r}_{\parallel}}}{\partial_z} \right) \cdot \int d^2r'_{\parallel} dz' dt' \epsilon(\mathbf{r}_{\parallel}, \mathbf{r}'_{\parallel}, z, z', t, t') \\ \times \left(\frac{\nabla_{\mathbf{r}'_{\parallel}}}{\partial_{z'}} \right) \phi_{\text{tot}}(\mathbf{r}'_{\parallel}, z', t') = -\frac{1}{\epsilon_0} \rho(\mathbf{r}_{\parallel}, z, t). \end{aligned} \quad (50)$$

Now, the total potential $\phi_{\text{tot}}(\mathbf{r}_{\parallel}, z, t)$ is induced via the active charge density $\rho(\mathbf{r}_{\parallel}, z, t)$ only, while the influence of the background is encoded in the nonlocal permittivity $\epsilon(\mathbf{r}_{\parallel}, \mathbf{r}'_{\parallel}, z, z', t, t')$. We expand the total potential in terms of a screened Green's function $G(\mathbf{r}_{\parallel}, \mathbf{r}'_{\parallel}, z, z', t, t')$ and the active charge density $\rho(\mathbf{r}_{\parallel}, z, t)$, cf. also Eq. (9):

$$\phi_{\text{tot}}(\mathbf{r}_{\parallel}, z, t) = \int d^2r'_{\parallel} dz' dt' G(\mathbf{r}_{\parallel}, \mathbf{r}'_{\parallel}, z, z', t, t') \rho(\mathbf{r}'_{\parallel}, z', t'), \quad (51)$$

and, after an in-plane Fourier transformation, we obtain:

$$\begin{aligned} \sum_{\mathbf{G}'_{\parallel}} \int_{-\infty}^t dt' \int dz' \left(\frac{i(\mathbf{q}_{\parallel} + \mathbf{G}_{\parallel})}{\partial_z} \right)^{\top} \epsilon_{\mathbf{q}_{\parallel}, \mathbf{G}_{\parallel}, \mathbf{G}'_{\parallel}}(z, z', t, t') \\ \times \left(\frac{i(\mathbf{q}_{\parallel} + \mathbf{G}'_{\parallel})}{\partial_{z'}} \right) G_{\mathbf{q}_{\parallel}, \mathbf{G}'_{\parallel}, \mathbf{G}''_{\parallel}}(z', z'', t', t'') \\ = -\frac{1}{\epsilon_0} \delta_{\mathbf{G}_{\parallel}, \mathbf{G}''_{\parallel}} \delta(z - z'') \delta(t - t''). \end{aligned} \quad (52)$$

We observe, that the screened Green's function $G_{\mathbf{q}_{\parallel}, \mathbf{G}'_{\parallel}, \mathbf{G}''_{\parallel}}(z, z', t, t')$ is not diagonal in \mathbf{G}_{\parallel} and includes memory effects, as long as the dielectric function $\epsilon_{\mathbf{q}_{\parallel}, \mathbf{G}_{\parallel}, \mathbf{G}'_{\parallel}}(z, z', t, t')$ is non-local in space and time. Hence, with the corresponding dielectric function, $G_{\mathbf{q}_{\parallel}, \mathbf{G}'_{\parallel}, \mathbf{G}''_{\parallel}}(z, z', t, t')$ is the correct Green's function to use in our few-band many-body Coulomb Hamiltonian in Eq. (29) or Eq. (35) and the problem of screening is shifted to the evaluation of the microscopic dielectric function $\epsilon_{\mathbf{q}_{\parallel}, \mathbf{G}_{\parallel}, \mathbf{G}'_{\parallel}}(z, z', t, t')$.

In the following, we provide the link to usual literature definitions of the dielectric function in the macroscopic

limit in three and two dimensions. In a three-dimensional periodic lattice in the static limit ($\omega = 0$) and by redefining:

$$\tilde{\epsilon}_{\mathbf{q}, \mathbf{G}, \mathbf{G}'} = \frac{(\mathbf{q} + \mathbf{G}) \cdot (\mathbf{q} + \mathbf{G}')}{|\mathbf{q} + \mathbf{G}| |\mathbf{q} + \mathbf{G}'|} \epsilon_{\mathbf{q}, \mathbf{G}, \mathbf{G}'}, \quad (53)$$

i.e., including the angle-dependent part of the scalar product in the dielectric matrix $\tilde{\epsilon}_{\mathbf{q}, \mathbf{G}, \mathbf{G}'}$, we find for the screened Green's function in the static limit via matrix inversion:

$$G_{\mathbf{q}, \mathbf{G}, \mathbf{G}'} = \frac{(\tilde{\epsilon}^{-1})_{\mathbf{q}, \mathbf{G}, \mathbf{G}'}}{|\mathbf{q} + \mathbf{G}| |\mathbf{q} + \mathbf{G}'|}, \quad (54)$$

which corresponds exactly to the expression from Rohlfing and Louie in Ref. [74]. Note, that $(\tilde{\epsilon}^{-1})_{\mathbf{q}, \mathbf{G}, \mathbf{G}'}$ is the inverse of the full dielectric matrix $\tilde{\epsilon}_{\mathbf{q}, \mathbf{G}, \mathbf{G}'}$.

However, in practical calculations, the dielectric function is defined via relating an external perturbing potential ϕ_{ext} to the total potential ϕ_{tot} in the material. To obtain such a description, we combine Eq. (44), Eq. (47) and Eq. (48):

$$\begin{aligned} \phi_{\text{tot}, \mathbf{q} + \mathbf{G}}(\omega) &= \sum_{\mathbf{G}'} \frac{1}{2\pi} \int d\omega' (\varepsilon_{\text{mic}}^{-1})_{\mathbf{q}, \mathbf{G}, \mathbf{G}'}(\omega, -\omega') \\ &\times \phi_{\text{ext}, \mathbf{q} + \mathbf{G}'}(\omega'), \end{aligned} \quad (55)$$

with:

$$\begin{aligned} \varepsilon_{\text{mic}, \mathbf{q}, \mathbf{G}, \mathbf{G}'}(\omega, -\omega') &= \delta_{\mathbf{G}, \mathbf{G}'} 2\pi \delta(\omega - \omega') \\ &+ \frac{(\mathbf{q} + \mathbf{G}) \cdot (\mathbf{q} + \mathbf{G}')}{(\mathbf{q} + \mathbf{G}) \cdot (\mathbf{q} + \mathbf{G})} \chi_{\mathbf{q}, \mathbf{G}, \mathbf{G}'}(\omega, -\omega'), \end{aligned} \quad (56)$$

or, analog, in real space:

$$\phi_{\text{tot}}(\mathbf{r}, t) = \int d^3r' dt' \varepsilon_{\text{mic}}^{-1}(\mathbf{r}, \mathbf{r}', t, t') \phi_{\text{ext}}(\mathbf{r}', t'). \quad (57)$$

Note, that the dielectric function ϵ from Eq. (49) appearing in the generalized Poisson equation in Eq. (50) is not equal to the dielectric function ε_{mic} from Eq. (56) appearing in Eq. (55) or Eq. (57), as long as all local-field effects with $\mathbf{G} \neq \mathbf{G}'$ are included.

In the following, we provide the expressions for the static ($\omega = 0$) macroscopic dielectric function in three and two dimensions, which are useful in relating macroscopic screening approaches to fully microscopic calculations.

First, we consider the three-dimensional case. We perform a macroscopic averaging over the total potential in Eq. (57):

$$\begin{aligned} \phi_{\text{tot}}(\mathbf{R}) &= \frac{1}{V_{\text{UC}}} \int_{V_{\text{UC}}} d^3r \phi_{\text{tot}}(\mathbf{r} + \mathbf{R}) \\ &= \int d^3r' \varepsilon_{\text{mic}}^{-1}(\mathbf{R}, \mathbf{r}') \phi_{\text{ext}}(\mathbf{r}') \\ &= \sum_{\mathbf{R}'} \int_{V_{\text{UC}}} d^3r' \varepsilon_{\text{mic}}^{-1}(\mathbf{R}, \mathbf{r}' + \mathbf{R}') \phi_{\text{ext}}(\mathbf{r}' + \mathbf{R}'), \end{aligned} \quad (58)$$

where \mathcal{V}_{UC} is the volume of the three-dimensional unit cell. Next, we assume the external perturbation as macroscopic, i.e., ϕ_{ext} is constant over the size of a unit cell:

$$\phi_{\text{ext}}(\mathbf{r}' + \mathbf{R}') \approx \phi_{\text{ext}}(\mathbf{R}') \quad \text{for } \mathbf{r} \in \mathcal{V}_{\text{UC}}, \quad (59)$$

which yields:

$$\phi_{\text{tot}}(\mathbf{R}) \approx \mathcal{V}_{\text{UC}} \sum_{\mathbf{R}'} \varepsilon_{\text{mic}}^{-1}(\mathbf{R}, \mathbf{R}') \phi_{\text{ext}}(\mathbf{R}'). \quad (60)$$

After a Fourier transformation, this expression can be rearranged:

$$\frac{\phi_{\text{tot}, \mathbf{q}}}{\phi_{\text{ext}, \mathbf{q}}} = (\varepsilon_{\text{mic}}^{-1})_{\mathbf{q}, \mathbf{0}, \mathbf{0}} =: \frac{1}{\epsilon_{\mathbf{q}}^{3D}} \quad (\text{three dimensions}), \quad (61)$$

and yields the definition of the macroscopic dielectric function $\epsilon_{\mathbf{q}, q_z}^{3D}$ in three dimensions. Note, that $\epsilon_{\mathbf{q}}^{3D} \neq \varepsilon_{\text{mic}, \mathbf{q}, \mathbf{0}, \mathbf{0}}$ due to local-field effects.

In two-dimensional confined semiconductors, special care must be taken with respect to the out-of-plane direction. In *ab initio* calculations, an array of periodically arranged layers with supercell distance L_z is usually created. The monolayer case is then obtained by choosing L_z in such a way, that the individual layers behave as electrostatically decoupled with the help of a truncated Coulomb potential [101, 102]. Hence, if we spatially averaged over the supercell distance L_z , which can be chosen as arbitrarily large, we would obtain a two-dimensional dielectric function of unity [103, 104], which is meaningless. Thus, it can be argued, that not the dielectric function, but rather the polarizability or susceptibility should be regarded as the fundamental quantity determining the dielectric properties [103]. However, as long as we know, how and where which quantity evaluated via *ab initio* methods enters our description of screening, such reasoning can be avoided. In this work, we take the route of incorporating the results from the Computational Materials Repository established by the workgroup of Thygesen [80]. Within this approach, it is possible to obtain a meaningful two-dimensional dielectric function, if we average over the layer thickness d around the center of the material $z_0 = 0$ and not over the supercell length L_z , where d is assumed as the layer distance in the corresponding bulk material [82, 104]:

$$\begin{aligned} \phi_{\text{tot}}(\mathbf{R}_{\parallel}, 0) &= \frac{1}{\mathcal{A}_{\text{UC}}} \int_{\mathcal{A}_{\text{UC}}} d^2 r_{\parallel} \frac{1}{d} \int_{-\frac{d}{2}}^{\frac{d}{2}} dz \phi_{\text{tot}}(\mathbf{r}_{\parallel} + \mathbf{R}_{\parallel}, z) \\ &= \frac{1}{\mathcal{A}_{\text{UC}}} \int_{\mathcal{A}_{\text{UC}}} d^2 r_{\parallel} \frac{1}{d} \int_{-\frac{d}{2}}^{\frac{d}{2}} dz \sum_{\mathbf{R}'_{\parallel}} \int_{\mathcal{A}_{\text{UC}}} d^2 r'_{\parallel} \int dz' \\ &\times \varepsilon_{\text{mic}}^{-1}(\mathbf{r}_{\parallel} + \mathbf{R}_{\parallel}, \mathbf{r}'_{\parallel} + \mathbf{R}'_{\parallel}, z, z') \phi_{\text{ext}}(\mathbf{r}'_{\parallel} + \mathbf{R}'_{\parallel}, z'). \end{aligned} \quad (62)$$

Similar to the three-dimensional case, we assume the external perturbation as in-plane macroscopic, but completely independent of the out-of-plane direction: $\phi_{\text{ext}}(\mathbf{r}'_{\parallel} + \mathbf{R}'_{\parallel}, z') \equiv \phi_{\text{ext}}(\mathbf{r}'_{\parallel})$ for $\mathbf{r}'_{\parallel} \in \mathcal{A}_{\text{UC}}$. This choice has to be made, since, otherwise, artificial interactions between different layers in the out-of-plane direction would result. After Fourier expanding:

$$\begin{aligned} \varepsilon_{\text{mic}}^{-1}(\mathbf{r}_{\parallel}, \mathbf{r}'_{\parallel}, z, z') &= \frac{1}{\mathcal{A}} \sum_{\substack{\mathbf{q}_{\parallel}, \mathbf{G}_{\parallel}, \mathbf{G}'_{\parallel}, \\ G_z, G'_z}} e^{i(\mathbf{q}_{\parallel} + \mathbf{G}_{\parallel}) \cdot \mathbf{r}_{\parallel}} e^{iG_z z} \\ &\times (\varepsilon_{\text{mic}}^{-1})_{\mathbf{q}_{\parallel}, \mathbf{G}_{\parallel}, \mathbf{G}'_{\parallel}, G_z, G'_z} e^{-(\mathbf{q}_{\parallel} + \mathbf{G}'_{\parallel}) \cdot \mathbf{r}'_{\parallel}} e^{-iG'_z z'}, \end{aligned} \quad (63)$$

and rearranging Eq. (62), we obtain:

$$\begin{aligned} \frac{\phi_{\text{tot}, \mathbf{q}_{\parallel}}(0)}{\phi_{\text{ext}, \mathbf{q}_{\parallel}}} &= \sum_{G_z} \frac{1}{d} \int_{-\frac{d}{2}}^{\frac{d}{2}} dz e^{iG_z z} (\varepsilon_{\text{mic}}^{-1})_{\mathbf{q}_{\parallel}, \mathbf{0}, \mathbf{0}, G_z, 0} \\ &=: \frac{1}{\epsilon_{\mathbf{q}_{\parallel}}^{2D}} \quad (\text{two dimensions}), \end{aligned} \quad (64)$$

where the spatial integral can be explicitly evaluated as:

$$\frac{1}{d} \int_{-\frac{d}{2}}^{\frac{d}{2}} dz e^{iG_z z} = \begin{cases} \frac{\sin(G_z \frac{d}{2})}{G_z \frac{d}{2}}, & G_z \neq 0, \\ 1, & G_z = 0. \end{cases} \quad (65)$$

Note, that the summation over G_z in Eq. (64) is not a computational artifact. This way, a physically meaningful quantum-confined dielectric function for an isolated monolayer can be constructed from *ab initio* calculations, which use periodically arranged layers in the out-of-plane direction.

We note, that Eq. (64) can also be derived from Qiu's and Louie's approach [77, 79]. In contrast to Hüser, Lattini and Thygesen, Qiu and Louie work directly with the Green's functions giving rise to the total and external potentials induced by a test/active charge density. By rewriting Eq. (57), we obtain the following relation between the total screened Green's function G and the bare unscreened Green's function G_0 :

$$\begin{aligned} G(\mathbf{r}_{\parallel}, \mathbf{r}'_{\parallel}, z, z') &= \int d^2 r''_{\parallel} dz'' \varepsilon_{\text{mic}}^{-1}(\mathbf{r}_{\parallel}, \mathbf{r}''_{\parallel}, z, z'') G_0(\mathbf{r}''_{\parallel}, \mathbf{r}'_{\parallel}, z'', z'). \end{aligned} \quad (66)$$

We introduce a static, screened V (unscreened V_0) quantum-confined Coulomb potential, cf. Eq. (24):

$$V_{(0)}(\mathbf{r}_{\parallel}, \mathbf{r}'_{\parallel}) = \frac{e^2}{\mathcal{A}} \int dz dz' |\zeta(z)|^2 G_{(0)}(\mathbf{r}_{\parallel}, \mathbf{r}'_{\parallel}, z, z') |\zeta(z')|^2, \quad (67)$$

where $G_{(0)}(\mathbf{r}_{\parallel}, \mathbf{r}'_{\parallel}, z, z')$ is the screened (unscreened) Green's function solving Eq. (52) (Eq. (45)) and $|\zeta(z)|^2$ describes the charge distribution in the out-of-plane direction. Qiu and Louie now define a two-dimensional dielectric function ϵ_{2D}^{-1} via:

$$V(\mathbf{r}_{\parallel}, \mathbf{r}'_{\parallel}) = \int d^2r'' \epsilon_{2D}^{-1}(\mathbf{r}_{\parallel}, \mathbf{r}''_{\parallel}) V_0(\mathbf{r}''_{\parallel}, \mathbf{r}'_{\parallel}). \quad (68)$$

By Fourier expanding Eq. (68), we obtain the following relation in the in-plane macroscopic limit:

$$(\epsilon_{2D}^{-1})_{\mathbf{q}_{\parallel}, \mathbf{0}, \mathbf{0}} = \frac{V_{\mathbf{q}_{\parallel}, \mathbf{0}, \mathbf{0}}}{V_{0, \mathbf{q}_{\parallel}, \mathbf{0}, \mathbf{0}}}, \quad (69)$$

where:

$$V_{(0), \mathbf{q}_{\parallel}, \mathbf{0}, \mathbf{0}} = \frac{e^2}{A} \int dz dz' |\zeta(z)|^2 |\zeta(z')|^2 \times \sum_{G_z, G'_z} e^{iG_z z} G_{(0), \mathbf{q}_{\parallel}, \mathbf{0}, \mathbf{0}, G_z, G'_z} e^{-G'_z z'}. \quad (70)$$

If we now assume a step-function confinement around the material center z_0 : $|\zeta(z)|^2 = \frac{1}{d} \Theta(z - z_0 + \frac{d}{2}) \Theta(\frac{d}{2} + z_0 - z)$, Eq. (69) can be cast into Eq. (64) by using Eq. (66), so that $(\epsilon_{2D}^{-1})_{\mathbf{q}_{\parallel}, \mathbf{0}, \mathbf{0}} \equiv \frac{1}{\epsilon_{\mathbf{q}_{\parallel}}^{2D}}$. Hence, we observe, that the

definitions of the two-dimensional dielectric functions in Louie's and Thygesen's approaches are equal and the only difference stems from the exact choice of the out-of-plane confinement: A Dirac-delta confinement with $|\zeta(z)|^2 = \delta(z - z_0)$ in the former [77, 79] compared to a step-function confinement in the latter [82, 104].

A. Microscopic Screening

In this section, we derive an explicit expression of the microscopic dielectric function ϵ_{mic} . To keep the notation as simple as possible, we emphasize, that \mathbf{r} , \mathbf{q} and \mathbf{G} denote the three-dimensional position, momentum and reciprocal-lattice vector. We consider the total Coulomb Hamiltonian:

$$H_{\text{Coul,tot}} = \frac{1}{2} \int d^3r \rho_{\text{tot}}(\mathbf{r}, t) \phi_{\text{tot}}(\mathbf{r}, t). \quad (71)$$

Now, the idea is as follows: We split the total charge density in an active part and a background part: $\rho_{\text{tot}}(\mathbf{r}, t) = \rho_b(\mathbf{r}, t) + \rho_a(\mathbf{r}, t)$. The active part $\rho_a(\mathbf{r}, t)$ is, e.g., a reduced phase space of only one valence and one conduction band, whereas the background part $\rho_b(\mathbf{r})$ includes all other bands. Then, we calculate the response of the background due to the "perturbation" by the active part.

The total Hamiltonian in Fourier space reads:

$$\begin{aligned} \hat{H}_{\text{Coul,tot}} &= \frac{1}{2V} \sum_{\mathbf{q}, \mathbf{G}} \hat{\rho}_{\text{tot}, -\mathbf{q} - \mathbf{G}}(t) G_{0, \mathbf{q} + \mathbf{G}} \hat{\rho}_{\text{tot}, \mathbf{q} + \mathbf{G}}(t) \\ &= \hat{H}_{\text{Coul,bb}} + \hat{H}_{\text{Coul,ba}} + \hat{H}_{\text{Coul,aa}}. \end{aligned} \quad (72)$$

The background-background interaction $\hat{H}_{\text{Coul,bb}}$ reads:

$$\begin{aligned} \hat{H}_{\text{Coul,bb}} &= \frac{1}{2} \sum_{\lambda_1, \dots, \lambda_4, \mathbf{k}, \mathbf{k}', \mathbf{q}, \mathbf{G}, s, s'} V_{0, \mathbf{q} + \mathbf{G}} \bar{\Upsilon}_{\mathbf{k} + \mathbf{q} + \mathbf{G}, \mathbf{k}}^{\lambda_1, \lambda_4, s} \bar{\Upsilon}_{\mathbf{k}' - \mathbf{q} - \mathbf{G}, \mathbf{k}'}^{\lambda_2, \lambda_3, s'} \\ &\times \hat{a}_{\lambda_1, \mathbf{k} + \mathbf{q}}^{\dagger s}(t) \hat{a}_{\lambda_2, \mathbf{k}' - \mathbf{q}}^{\dagger s'}(t) \hat{a}_{\lambda_3, \mathbf{k}'}^s(t) \hat{a}_{\lambda_4, \mathbf{k}}^s(t), \end{aligned} \quad (73)$$

and the interaction between the background and active states $\hat{H}_{\text{Coul,ba}}$ reads:

$$\begin{aligned} \hat{H}_{\text{Coul,ba}} &= -e \sum_{\lambda_1, \lambda_2, \mathbf{k}, \mathbf{q}, \mathbf{G}, s} \tilde{\phi}_{\text{ext}, \mathbf{q} + \mathbf{G}}(t) \bar{\Upsilon}_{\mathbf{k} + \mathbf{q} + \mathbf{G}, \mathbf{k}}^{\lambda_1, \lambda_2, s} \\ &\times \hat{a}_{\lambda_1, \mathbf{k} + \mathbf{q}}^{\dagger s}(t) \hat{a}_{\lambda_2, \mathbf{k}}^s(t), \end{aligned} \quad (74)$$

where $\bar{\Upsilon}_{\mathbf{k}', \mathbf{k}}^{\lambda, \lambda', s}$ is the three-dimensional version of Eq. (30). In Eq. (74), the external potential $\tilde{\phi}_{\text{ext}, \mathbf{q} + \mathbf{G}}(t)$ induced by the active charges $\rho_{\mathbf{q} + \mathbf{G}}(t)$ reads:

$$\tilde{\phi}_{\text{ext}, \mathbf{q} + \mathbf{G}}(t) = \frac{1}{V} G_{0, \mathbf{q} + \mathbf{G}} \rho_{\mathbf{q} + \mathbf{G}}(t). \quad (75)$$

The active-active contribution $\hat{H}_{\text{Coul,aa}}$ is neglected, as it does not couple to the background. In the next step, we calculate the background charge density $\rho_b(\mathbf{q} + \mathbf{G})$:

$$\rho_b(\mathbf{q} + \mathbf{G})(t) = -e \sum_{\lambda, \lambda', \mathbf{k}, s} \bar{\Upsilon}_{\mathbf{k} - \mathbf{q} - \mathbf{G}, \mathbf{k}}^{\lambda, \lambda', s} \langle \hat{a}_{\lambda, \mathbf{k} - \mathbf{q}}^{\dagger s} \hat{a}_{\lambda', \mathbf{k}}^s \rangle(t), \quad (76)$$

where the coherences $\langle \hat{a}_{\lambda, \mathbf{k} - \mathbf{q}}^{\dagger s} \hat{a}_{\lambda', \mathbf{k}}^s \rangle(t)$ have to be evaluated via Heisenberg's equations of motion. In a Hartree-Fock- and a random-phase approximation, the equations of motion for $\langle \hat{a}_{\lambda, \mathbf{k} - \mathbf{q}}^{\dagger s} \hat{a}_{\lambda', \mathbf{k}}^s \rangle$ read:

$$\begin{aligned} &i\hbar \partial_t \langle \hat{a}_{\lambda, \mathbf{k} - \mathbf{q}}^{\dagger s} \hat{a}_{\lambda', \mathbf{k}}^s \rangle(t) \Big|_{0+ba+bb} \\ &= \left(\tilde{E}_{\lambda', \mathbf{k}}^s - \tilde{E}_{\lambda, \mathbf{k} - \mathbf{q}}^s - i\hbar\gamma \right) \langle \hat{a}_{\lambda, \mathbf{k} - \mathbf{q}}^{\dagger s} \hat{a}_{\lambda', \mathbf{k}}^s \rangle(t) \\ &- e \sum_{\mathbf{G}} \left(\tilde{\phi}_{\text{ext}, \mathbf{q} + \mathbf{G}}(t) + \tilde{\phi}_{b, \mathbf{q} + \mathbf{G}}(t) \right) \bar{\Upsilon}_{\mathbf{k} + \mathbf{G}, \mathbf{k} - \mathbf{q}}^{\lambda', \lambda, s} \\ &\times (f_{\lambda, \mathbf{k} - \mathbf{q}}^s - f_{\lambda', \mathbf{k}}^s), \end{aligned} \quad (77)$$

where $f_{\lambda, \mathbf{k}}^s$ are static Fermi distributions and γ is an additionally included dephasing due to higher-order correlation effects beyond a Hartree-Fock approximation. Note, that Eq. (77) does not describe excitonic effects as a consequence of the random-phase approximation. These excitonic effects are later calculated within a cluster-expansion approach by using Eq. (29) under the influence of the RPA-screening cloud from Eq. (77). $\tilde{E}_{\lambda, \mathbf{k}}^s$ are the energy dispersions renormalized by electron-electron interaction:

$$\tilde{E}_{\lambda, \mathbf{k}}^s = E_{\lambda, \mathbf{k}}^s - \sum_{\mathbf{q}', \mathbf{G}', \lambda'} V_{0, \mathbf{q}' + \mathbf{G}'} |\bar{\Upsilon}_{\mathbf{k}, \mathbf{k} + \mathbf{q}' + \mathbf{G}'}^{\lambda, \lambda'}|^2 f_{\lambda', \mathbf{k} + \mathbf{q}'}^s, \quad (78)$$

and $\tilde{\phi}_{b,\mathbf{q}+\mathbf{G}}$ is the background potential:

$$\tilde{\phi}_{b,\mathbf{q}+\mathbf{G}}(t) = \frac{1}{\mathcal{V}} G_{0,\mathbf{q}+\mathbf{G}} \rho_{b,\mathbf{q}+\mathbf{G}}(t). \quad (79)$$

Note, that the definitions for the external and background potentials ($\tilde{\phi}_{\text{ext},\mathbf{q}+\mathbf{G}}(t)$ and $\tilde{\phi}_{b,\mathbf{q}+\mathbf{G}}(t)$) used in Eq. (75) and Eq. (79) are *not* the bare Fourier transforms ($\phi_{\text{ext},\mathbf{q}+\mathbf{G}}(t)$ and $\phi_{b,\mathbf{q}+\mathbf{G}}(t)$), since we additionally included the semiconductor volume \mathcal{V} . This way, the (modified) Fourier transform $\tilde{\phi}_{\mathbf{q}+\mathbf{G}}(t)$ carries equal units compared to the corresponding real-space quantity $\phi(\mathbf{r})$. By identifying the total potential as $\tilde{\phi}_{\text{ext},\mathbf{q}+\mathbf{G}}(t) + \tilde{\phi}_{b,\mathbf{q}+\mathbf{G}}(t) = \tilde{\phi}_{\text{tot},\mathbf{q}+\mathbf{G}}(t)$, we find the following expression for the background charge density after solving Eq. (77) in frequency space:

$$\begin{aligned} \rho_{b,\mathbf{q}+\mathbf{G}}(\omega) &= e^2 \sum_{\lambda, \lambda', \mathbf{k}, \mathbf{G}'} \frac{\bar{\Upsilon}_{\mathbf{k}-\mathbf{q}-\mathbf{G}, \mathbf{k}}^{\lambda, \lambda', s} \bar{\Upsilon}_{\mathbf{k}, \mathbf{k}-\mathbf{q}-\mathbf{G}'}^{\lambda', \lambda, s} (f_{\lambda, \mathbf{k}-\mathbf{q}}^s - f_{\lambda', \mathbf{k}}^s)}{\tilde{E}_{\lambda, \mathbf{k}-\mathbf{q}}^s - \tilde{E}_{\lambda', \mathbf{k}}^s + \hbar\omega + i\hbar\gamma} \\ &\quad \times \tilde{\phi}_{\text{tot},\mathbf{q}+\mathbf{G}'}(\omega). \end{aligned} \quad (80)$$

Also, from Eq. (48), we obtain the following expression:

$$\begin{aligned} \rho_{b,\mathbf{q}+\mathbf{G}}(\omega) &= -\mathcal{V} \sum_{\mathbf{G}'} \frac{1}{2\pi} \int d\omega' (\mathbf{q} + \mathbf{G}) \cdot (\mathbf{q} + \mathbf{G}') \\ &\quad \times \epsilon_0 \chi_{\mathbf{q}, \mathbf{G}, \mathbf{G}'}(\omega, -\omega') \tilde{\phi}_{\text{tot},\mathbf{q}+\mathbf{G}'}(\omega'). \end{aligned} \quad (81)$$

By now comparing Eq. (80) with Eq. (81), we can find an explicit expression for the susceptibility $\chi_{\mathbf{q}, \mathbf{G}, \mathbf{G}'}(\omega, -\omega')$ determining the microscopic dielectric function:

$$\begin{aligned} \epsilon_{\text{mic}, \mathbf{q}, \mathbf{G}, \mathbf{G}'}(\omega, -\omega') &= 2\pi\delta(\omega - \omega')\delta_{\mathbf{G}, \mathbf{G}'} \\ &\quad + \frac{(\mathbf{q} + \mathbf{G}) \cdot (\mathbf{q} + \mathbf{G}')}{(\mathbf{q} + \mathbf{G}) \cdot (\mathbf{q} + \mathbf{G}')} \chi_{\mathbf{q}, \mathbf{G}, \mathbf{G}'}(\omega, -\omega'), \end{aligned} \quad (82)$$

and explicitly obtain:

$$\begin{aligned} \epsilon_{\text{mic}, \mathbf{q}, \mathbf{G}, \mathbf{G}'}(\omega, -\omega') &= 2\pi\delta(\omega - \omega')\delta_{\mathbf{G}, \mathbf{G}'} - 2\pi\delta(\omega - \omega')V_{0,\mathbf{q}+\mathbf{G}} \\ &\quad \times \sum_{\lambda, \lambda', \mathbf{k}} \frac{\bar{\Upsilon}_{\mathbf{k}-\mathbf{q}-\mathbf{G}, \mathbf{k}}^{\lambda, \lambda', s} \bar{\Upsilon}_{\mathbf{k}, \mathbf{k}-\mathbf{q}-\mathbf{G}'}^{\lambda', \lambda, s} (f_{\lambda, \mathbf{k}-\mathbf{q}}^s - f_{\lambda', \mathbf{k}}^s)}{\tilde{E}_{\lambda, \mathbf{k}-\mathbf{q}}^s - \tilde{E}_{\lambda', \mathbf{k}}^s + \hbar\omega + i\hbar\gamma}. \end{aligned} \quad (83)$$

Eq. (83) is the usual (renormalized) Lindhard formula from the literature [72, 73, 91, 105, 106], which describes interband ($\lambda \neq \lambda'$) screening, which dominates in charge-neutral semiconductors [107], and intraband ($\lambda = \lambda'$) screening of quasi-free carriers, which dominates in metals or doped semiconductors. By adding the corresponding Hamiltonians within our Heisenberg-equations-of-motion approach, cf. Eq. (77), the inclusion of other

screening mechanisms in Eq. (83) such as phonon screening [47, 108, 109] is straightforward.

We emphasize, that Eq. (82) and Eq. (83) describe the microscopic dielectric function ϵ as it appears in the relation between the total and bare potential or Green's function, Eq. (66) or Eq. (55), and *not* the dielectric function ϵ in the generalized Poisson equation in Eq. (50), which reads:

$$\begin{aligned} \epsilon_{\mathbf{q}, \mathbf{G}, \mathbf{G}'}(\omega, -\omega') &= 2\pi\delta(\omega - \omega')\delta_{\mathbf{G}, \mathbf{G}'} + \chi_{\mathbf{q}, \mathbf{G}, \mathbf{G}'}(\omega, -\omega'). \end{aligned} \quad (84)$$

Both expressions in Eq. (82) and Eq. (84) differ slightly, if all local-field effects with $\mathbf{G} \neq \mathbf{G}'$ are taken into account but coincide in the macroscopic limit with $\mathbf{G} = \mathbf{G}' = \mathbf{0}$.

We note, that the inverse of Eq. (83), $(\epsilon^{-1})_{\mathbf{q}, \mathbf{G}, \mathbf{G}'}$, is always well-defined, since, in practice, only a finite number of reciprocal lattice vectors is considered, as the matrix elements decay rapidly with increasing \mathbf{G} . To numerically calculate the dielectric matrix, a DFT approach with a many-body perturbation theory in GW approximation is usually employed [95, 110] via packages such as, e.g., QUANTUM ESPRESSO [111], YAMBO [112, 113], BERKELEYGW [91, 95], GPAW [114, 115] or VASP [116].

Usually, we make a static approximation with $\omega = 0$ in Eq. (83), i.e., we assume that the cloud of induced screening charges (virtual charges, i.e., polarizations if $\lambda \neq \lambda'$ or real charges if $\lambda = \lambda'$) follows the dynamics of a perturbing electron or hole *adiabatically*, which corresponds to a memory-free screening response of the singlet cloud and removes the time-integration in the many-body Coulomb Hamiltonian in Eq. (22). This is a reasonable approximation in the interband dielectric function, Eq. (83) with $\lambda \neq \lambda'$, as long as the exciton energy is much smaller than the resonance of the interband plasmon [74]. On the other hand, such an assumption fails, if we also take into account screening by a Fermi sea of dopants or an optically injected electron-hole/exciton gas, i.e., taking additional intraband contributions in the dielectric function, Eq. (83) with $\lambda = \lambda'$, into account [117]. In this regime, the screening cloud of induced charges cannot be assumed to follow the dynamics of the perturbing charges, e.g. optically induced electron-hole pairs, adiabatically, as the intraband plasmon frequency can be of similar magnitude compared to the coherence decay. Here, full quantum-kinetic calculations show, that the impact of time-dependent RPA screening is in the intermediate regime between an unscreened Coulomb potential and a statically screened Coulomb potential [118], at least within short timescales of coherence decay. This behavior might explain the observations, that simulations without a density-dependent dielectric function already yield good agreement with experiment in out-of-equilibrium ultrafast optics [15, 16, 21, 119–123], while the inclusion of a static density-dependent dielectric function is crucial in quasi-equilibrium conditions [124–130].

Now, we again distinguish between in-plane and out-

of-plane coordinates $\mathbf{r} \rightarrow (\mathbf{r}_\parallel \ z)^\top$, crystal momenta $\mathbf{q} \rightarrow (\mathbf{q}_\parallel \ q_z)^\top$ and reciprocal lattice vectors $\mathbf{G} \rightarrow (\mathbf{G}_\parallel \ G_z)^\top$. Having determined the dielectric function of the material, cf. Eq. (83), we now construct the quantum-confined Coulomb potential from Eq. (24) entering Eq. (29) by means of Eq. (66) with confinement wave functions $\zeta_n(z)$:

$$\begin{aligned} V_{\mathbf{q}_\parallel, \mathbf{G}_\parallel, \mathbf{G}'_\parallel}^{n_1, n_2, n_3, n_4}(\omega, \omega') &= \frac{e^2}{\mathcal{A}} \int dz dz' \zeta_{n_1}^*(z) \zeta_{n_4}(z) \\ &\times G_{\mathbf{q}_\parallel, \mathbf{G}_\parallel, \mathbf{G}'_\parallel}(z, z', \omega, \omega') \zeta_{n_2}^*(z') \zeta_{n_3}(z') \\ &= \frac{e^2}{\mathcal{A}} \int dz dz' \zeta_{n_1}^*(z) \zeta_{n_4}(z) \\ &\times \int dz'' (\varepsilon^{-1})_{\mathbf{q}_\parallel, \mathbf{G}_\parallel, \mathbf{G}'_\parallel}(z, z'', \omega, \omega') \\ &\times G_{0, \mathbf{q}_\parallel + \mathbf{G}'_\parallel}(z'' - z') \zeta_{n_2}^*(z') \zeta_{n_3}(z'). \quad (85) \end{aligned}$$

Fourier expanding the dielectric matrix in the out-of-plane direction and inserting a truncated bare Coulomb Green's function $G_{0, \mathbf{q}_\parallel}(z) \rightarrow G_{0, \mathbf{q}_\parallel}^{\text{trunc}}(z) = \frac{e^{-|\mathbf{q}_\parallel||z|}}{2\epsilon_0|\mathbf{q}_\parallel|} \Theta(z + \frac{L_{z, \text{SC}}}{2}) \Theta(\frac{L_{z, \text{SC}}}{2} - z)$, which eliminates electrostatic interactions between different supercells in the out-of-plane direction with supercell length $L_{z, \text{SC}}$ and total out-of-plane lattice length L_z , yields:

$$\begin{aligned} V_{\mathbf{q}_\parallel, \mathbf{G}_\parallel, \mathbf{G}'_\parallel}^{n_1, n_2, n_3, n_4}(\omega, \omega') &= \frac{e^2}{\mathcal{A}L_z} \int dz dz' \zeta_{n_1}^*(z) \zeta_{n_4}(z) \zeta_{n_2}^*(z') \zeta_{n_3}(z') \\ &\times \int_{z' - \frac{L_{z, \text{SC}}}{2}}^{z' + \frac{L_{z, \text{SC}}}{2}} dz'' \sum_{q_z, G_z, G'_z} e^{i(q_z + G_z)z} \\ &\times (\varepsilon^{-1})_{\mathbf{q}_\parallel, \mathbf{G}_\parallel, \mathbf{G}'_\parallel, q_z, G_z, G'_z}(\omega, \omega') e^{-i(q_z + G'_z)z''} \\ &\times \frac{e^{-|\mathbf{q}_\parallel + \mathbf{G}'_\parallel||z'' - z'|}}{2\epsilon_0|\mathbf{q}_\parallel + \mathbf{G}'_\parallel|}. \quad (86) \end{aligned}$$

Shifting $z'' \rightarrow z'' + z'$, defining confinement form factors:

$$F_{q_z + G_z}^{n, n'} = \int dz \zeta_n^*(z) \zeta_{n'}(z) e^{i(q_z + G_z)z}, \quad (87)$$

and evaluating the z'' -integral:

$$\begin{aligned} \int_{-\frac{L_{z, \text{SC}}}{2}}^{\frac{L_{z, \text{SC}}}{2}} dz'' e^{-i(q_z + G'_z)z''} e^{-|\mathbf{q}_\parallel + \mathbf{G}'_\parallel||z''|} \\ = \frac{2|\mathbf{q}_\parallel + \mathbf{G}'_\parallel|}{|\mathbf{q}_\parallel + \mathbf{G}'_\parallel|^2 + (q_z + G'_z)^2} \\ \times \left(1 - e^{-|\mathbf{q}_\parallel + \mathbf{G}'_\parallel| \frac{L_{z, \text{SC}}}{2}} \cos\left((q_z + G'_z) \frac{L_{z, \text{SC}}}{2}\right) \right), \quad (88) \end{aligned}$$

we obtain the following expression:

$$\begin{aligned} &V_{\mathbf{q}_\parallel, \mathbf{G}_\parallel, \mathbf{G}'_\parallel}^{n_1, n_2, n_3, n_4}(\omega, \omega') \\ &= \sum_{q_z, G_z, G'_z} (\varepsilon^{-1})_{\mathbf{q}_\parallel, \mathbf{G}_\parallel, \mathbf{G}'_\parallel, q_z, G_z, G'_z}(\omega, \omega') F_{q_z + G_z}^{n_1, n_4} F_{-q_z - G'_z}^{n_2, n_3} \\ &\times V_{0, \mathbf{q}_\parallel + \mathbf{G}'_\parallel, q_z + G'_z}^{\text{trunc}}, \quad (89) \end{aligned}$$

where $V_{0, \mathbf{q}_\parallel + \mathbf{G}'_\parallel, q_z + G_z}^{\text{trunc}}$ is the truncated bare Coulomb potential in reciprocal space [79, 102]:

$$\begin{aligned} &V_{0, \mathbf{q}_\parallel + \mathbf{G}_\parallel, q_z + G_z}^{\text{trunc}} \\ &= \frac{e^2}{\mathcal{A}L_z} \frac{1 - e^{-|\mathbf{q}_\parallel + \mathbf{G}_\parallel| \frac{L_{z, \text{SC}}}{2}} \cos\left((q_z + G_z) \frac{L_{z, \text{SC}}}{2}\right)}{\epsilon_0(|\mathbf{q}_\parallel + \mathbf{G}_\parallel|^2 + (q_z + G_z)^2)}. \quad (90) \end{aligned}$$

Note, that in practical calculations, the three-dimensional unscreened Coulomb potential $V_{0, \mathbf{q}_\parallel + \mathbf{G}_\parallel, q_z + G_z} = \frac{e^2}{\nu\epsilon_0(|\mathbf{q}_\parallel + \mathbf{G}_\parallel|^2 + (q_z + G_z)^2)}$ in Eq. (83) has also to be replaced by the truncated Coulomb $V_{0, \mathbf{q}_\parallel + \mathbf{G}_\parallel, q_z + G_z}^{\text{trunc}}$ potential from Eq. (90) to avoid electrostatic image interactions between layers in different supercells [79, 102]. Also note, that the dependence on q_z is usually dropped, since the allowed q_z -values are already small if the supercell length is chosen as correspondingly large, i.e., most of the spatial variation in the out-of-plane direction occurs *within* the supercell captured by G_z . Moreover, many DFT codes only provide the dominant $q_z = 0$ -components.

With Eq. (89), we have derived an explicit link between established *ab initio* methods of dielectric screening and our few-band Heisenberg-equations-of-motion approach to many-body exciton dynamics starting from the screened Coulomb Hamiltonian in Eq. (29).

B. Macroscopic Screening

In this section, we discuss material and environmental screening, which greatly influences the excitonic properties of layered semiconductor heterostructures, in a macroscopic continuum-electrostatics approach.

Since substrate screening mainly affects the screening at small momenta [82], where the macroscopic approach to the dielectric function – both the material dielectric function and the environmental screening – is valid [79, 82, 131], local-field contributions with $\mathbf{G}_\parallel \neq \mathbf{G}'_\parallel$ can be calculated reliably with an isolated layer in vacuum. Hence, in a first approximation, it is possible to circumvent microscopic approaches to the screening in layered dielectrics such as the performance-oriented Quantum Electrostatic Heterostructure (QEH) model [80, 132] or more rigorous but computationally more expensive ap-

proaches such as explicit multi-layer supercell calculations [49, 90].

We use the *ansatz* from Ref. [131], which incorporates material screening via a three-dimensional background dielectric function of the corresponding bulk material and solves the generalized Poisson equation in a layered dielectric environment, cf. Fig. 3, which is local in z -direction and time. While the inclusion of the dielec-

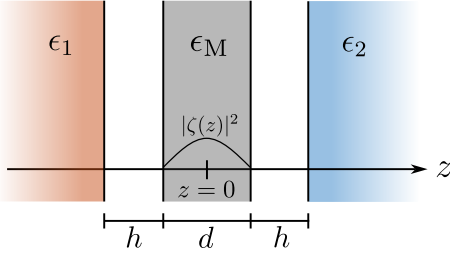


FIG. 3. Five dielectric volumes: The grey-colored volume represents the semiconductor monolayer ϵ_M with thickness d , red and blue denote superstrate ϵ_1 and substrate ϵ_2 , respectively, with a small vacuum gap h .

tric environment is crucial to obtain reasonable exciton binding energies [3, 82, 133], care should be taken not to overestimate its influence in a macroscopic approach. For that matter, we include a small vacuum gap h between the sample ϵ_M and the surrounding dielectric materials ϵ_1 and ϵ_2 , which is has to be adjusted to usual van der Waals distances [12, 110, 134]. Note, that the usually applied effective monolayer thickness d of 0.65 nm [135] actually already includes the van der Waals distance, since the real sample thickness, i.e., the chalcogen-chalcogen distance is on the order of 0.33 nm [136]. Hence, adding a small vacuum gap of h in the continuum-electrostatics approach results in slightly overestimated interlayer distances, but it is necessary in the macroscopic approach to obtain a reasonable exciton-trion splitting [134], i.e., a reasonable Coulomb interaction strength, which is not overscreened. Also note, that the dielectric constants used in our macroscopic model correspond to the *bulk* limit of the respective material. The confinement, i.e., reduction of dimensionality is then carried out via adjusting the layer thickness d .

The macroscopically screened quantum-confined Coulomb potential $V_{\mathbf{q}_{\parallel}}$ in the static limit ($\omega = \omega' = 0$) reads, cf. also Eq. (21) and Eq. (24):

$$V_{\mathbf{q}_{\parallel}, 0, 0}^{1, 1, 1, 1} \rightarrow V_{\mathbf{q}_{\parallel}} = \frac{e^2}{\mathcal{A}} \int dz dz' |\zeta(z)|^2 G_{\mathbf{q}_{\parallel}}^{\text{mac}}(z, z') |\zeta(z')|^2, \quad (91)$$

where $G_{\mathbf{q}_{\parallel}}^{\text{mac}}(z, z')$ solves the macroscopically screened Poisson equation in a layered dielectric environment with

dielectric constants ϵ_1/ϵ_2 of superstrate/substrate and material dielectric constant ϵ_M , cf. Fig. 3:

$$\epsilon_{\mathbf{q}_{\parallel}}(z) = \begin{cases} \epsilon_1, & z \leq -\frac{d}{2} - h \\ 1, & -\frac{d}{2} - h < z < -\frac{d}{2} \\ \epsilon_M, & -\frac{d}{2} < z \leq \frac{d}{2} \\ 1, & \frac{d}{2} < z \leq \frac{d}{2} + h, \\ \epsilon_2, & \frac{d}{2} + h < z, \end{cases} \quad (92)$$

which reads:

$$-|\mathbf{q}_{\parallel}|^2 \epsilon_{\mathbf{q}_{\parallel}}(z) G_{\mathbf{q}_{\parallel}}^{\text{mac}}(z, z') + \partial_z \left(\epsilon(z) \partial_z G_{\mathbf{q}_{\parallel}}^{\text{mac}}(z, z') \right) = -\delta(z - z'). \quad (93)$$

In Eq. (91), we already restricted the confinement wave functions $\zeta_n(z)$ to the respective ground state $n = 1$ and dropped the confinement quantum number index $\zeta_1(z) \equiv \zeta(z)$.

In the following, we solve the Poisson equation in a layered dielectric environment in Eq. (93) following a procedure similar to Refs. [137, 138].

1. Poisson's Equation in Layered Media

Since the permittivity $\epsilon(z)$ is defined as piecewise constant in each volume, i.e., $\epsilon(z) = \epsilon_i$, $z \in \mathcal{V}_i$, cf. Eq. (92), we can define the Poisson equation from Eq. (93) piecewise in each volume \mathcal{V}_i :

$$-|\mathbf{q}_{\parallel}|^2 G_{i, j, \mathbf{q}_{\parallel}}^{\text{mac}}(z, z') + \partial_z^2 G_{i, j, \mathbf{q}_{\parallel}}^{\text{mac}}(z, z') = -\frac{1}{\epsilon_{i, \mathbf{q}_{\parallel}}} \delta(z - z'), \quad (94)$$

where $z \in \mathcal{V}_i$ is the "point of observation" within the thin semiconductor, cf. Fig. 3, and $z' \in \mathcal{V}_j$ is the "source point".

The solution for the potential in the i -th volume induced by sources in the j -th volumes then reads:

$$\phi_{i, \mathbf{q}_{\parallel}}^{\text{mac}}(z) = \sum_{j=1}^n \int_{\mathcal{V}_j} dz' G_{i, j, \mathbf{q}_{\parallel}}^{\text{mac}}(z, z') \rho_{j, \mathbf{q}_{\parallel}}(z'). \quad (95)$$

The boundary conditions (which follow from $\mathbf{n} \times \mathbf{E}_i = \mathbf{n} \times \mathbf{E}_{i+1}$ and $\mathbf{n} \cdot \mathbf{D}_i = \mathbf{n} \cdot \mathbf{D}_{i+1}$ at the boundary between adjacent volumes \mathcal{V}_i and \mathcal{V}_{i+1} as well as from $\mathbf{E}(\pm\infty) = 0$ [139]) read:

$$\begin{aligned} G_{1, j, \mathbf{q}_{\parallel}}^{\text{mac}}(-\infty, z') &= G_{n, j, \mathbf{q}_{\parallel}}^{\text{mac}}(\infty, z') = 0, \\ G_{i, j, \mathbf{q}_{\parallel}}^{\text{mac}}(z_i, z') &= G_{i+1, j, \mathbf{q}_{\parallel}}^{\text{mac}}(z_i, z'), \\ \epsilon_i \partial_z G_{i, j, \mathbf{q}_{\parallel}}^{\text{mac}}(z, z') \Big|_{z=z_i} &= \epsilon_{i+1} \partial_z G_{i+1, j, \mathbf{q}_{\parallel}}^{\text{mac}}(z, z') \Big|_{z=z_i}. \end{aligned} \quad (96)$$

By solving the equations for the Green's function (Eq. (94)) we distinguish two cases. For $i = j$ (source

point and point of observation in the same volume) we have to solve the inhomogeneous equations:

$$-|\mathbf{q}_{\parallel}|^2 G_{i,i,\mathbf{q}_{\parallel}}^{\text{mac}}(z, z') + \partial_z^2 G_{i,i,\mathbf{q}_{\parallel}}^{\text{mac}}(z, z') = -\frac{1}{\epsilon_i} \delta(z - z'). \quad (97)$$

For $i \neq j$ (source point and point of observation in different volumes) we have to solve the homogeneous equations:

$$-|\mathbf{q}_{\parallel}|^2 G_{i,j,\mathbf{q}_{\parallel}}^{\text{mac}}(z, z') + \partial_z^2 G_{i,j,\mathbf{q}_{\parallel}}^{\text{mac}}(z, z') = 0, \quad i \neq j. \quad (98)$$

The particular solution of Eq. (97) obtained via complex integration reads:

$$G_{i,i,\mathbf{q}_{\parallel}}^{\text{mac,p}}(z, z') = \frac{1}{2\epsilon_i |\mathbf{q}_{\parallel}|} e^{-|\mathbf{q}_{\parallel}| |z - z'|}. \quad (99)$$

The homogeneous solution of Eq. (98) reads:

$$G_{i,j,\mathbf{q}_{\parallel}}^{\text{mac,h}}(z, z') = A_{i,j} e^{|\mathbf{q}_{\parallel}| z} + B_{i,j} e^{-|\mathbf{q}_{\parallel}| z}. \quad (100)$$

The complete solution reads:

$$G_{i,j,\mathbf{q}_{\parallel}}^{\text{mac}}(z, z') = \delta_{i,j} G_{i,i,\mathbf{q}_{\parallel}}^{\text{mac,p}}(z, z') + G_{i,j,\mathbf{q}_{\parallel}}^{\text{mac,h}}(z, z'). \quad (101)$$

Since we want to study electrons within the semiconductor monolayer, we have to calculate the Green's function whose source point and point of observation are both located within the volume of the monolayer semiconductor M, i.e., $i = j = M$ (cf. Fig. 3), which reads:

$$\begin{aligned} G_{M,M,\mathbf{q}_{\parallel}}^{\text{mac}}(z, z') &= \\ &= \frac{1}{2\epsilon_0 \epsilon_s |\mathbf{q}_{\parallel}|} e^{-|\mathbf{q}_{\parallel}| |z - z'|} + A_{M,M} e^{|\mathbf{q}_{\parallel}| z} + B_{M,M} e^{-|\mathbf{q}_{\parallel}| z}. \end{aligned} \quad (102)$$

The coefficients $A_{M,M}$ and $B_{M,M}$ are obtained by solving the linear system of equations provided by the boundary conditions in Eq. (96). We obtain for the Green's function in the semiconductor layer $G_{M,M,\mathbf{q}_{\parallel}}^{\text{mac}}(z, z') \equiv G_{\mathbf{q}_{\parallel}}^{\text{mac}}(z, z')$ [140]:

$$\begin{aligned} G_{\mathbf{q}_{\parallel}}^{\text{mac}}(z, z') &= \frac{1}{2\epsilon_0 \epsilon_M |\mathbf{q}_{\parallel}|} e^{-|\mathbf{q}_{\parallel}| |z - z'|} \\ &+ \frac{1}{2\epsilon_0 \epsilon_M |\mathbf{q}_{\parallel}| g_{\mathbf{q}_{\parallel}}} \left(\left(\epsilon_{M,-} \epsilon_{2,+} e^{h|\mathbf{q}_{\parallel}|} - \epsilon_{M,+} \epsilon_{2,-} e^{-h|\mathbf{q}_{\parallel}|} \right) \left(\epsilon_{1,+} \epsilon_{M,-} e^{h|\mathbf{q}_{\parallel}|} - \epsilon_{1,-} \epsilon_{M,+} e^{-h|\mathbf{q}_{\parallel}|} \right) e^{-d|\mathbf{q}_{\parallel}|} \left(e^{|\mathbf{q}_{\parallel}|(z-z')} + e^{-|\mathbf{q}_{\parallel}|(z-z')} \right) \right. \\ &\quad \left. + \left(\epsilon_{M,-} \epsilon_{2,+} e^{h|\mathbf{q}_{\parallel}|} - \epsilon_{M,+} \epsilon_{2,-} e^{-h|\mathbf{q}_{\parallel}|} \right) \left(\epsilon_{1,+} \epsilon_{M,+} e^{h|\mathbf{q}_{\parallel}|} - \epsilon_{1,-} \epsilon_{M,-} e^{-h|\mathbf{q}_{\parallel}|} \right) e^{|\mathbf{q}_{\parallel}|(z+z')} \right. \\ &\quad \left. + \left(\epsilon_{M,+} \epsilon_{2,+} e^{h|\mathbf{q}_{\parallel}|} - \epsilon_{M,-} \epsilon_{2,-} e^{-h|\mathbf{q}_{\parallel}|} \right) \left(\epsilon_{1,+} \epsilon_{M,-} e^{h|\mathbf{q}_{\parallel}|} - \epsilon_{1,-} \epsilon_{M,+} e^{-h|\mathbf{q}_{\parallel}|} \right) e^{-|\mathbf{q}_{\parallel}|(z+z')} \right), \end{aligned} \quad (103)$$

with the helper function $g_{\mathbf{q}_{\parallel}}$:

$$\begin{aligned} g_{\mathbf{q}_{\parallel}} &= \\ &- \epsilon_{M,-} \epsilon_{M,-} \left(\epsilon_{1,+} \epsilon_{2,+} e^{-d|\mathbf{q}_{\parallel}|} e^{2h|\mathbf{q}_{\parallel}|} - \epsilon_{1,-} \epsilon_{2,-} e^{d|\mathbf{q}_{\parallel}|} e^{-2h|\mathbf{q}_{\parallel}|} \right) \\ &- 2\epsilon_{M,+} \epsilon_{M,-} (\epsilon_1 \epsilon_2 - 1) \left(e^{d|\mathbf{q}_{\parallel}|} - e^{-d|\mathbf{q}_{\parallel}|} \right) \\ &+ \epsilon_{M,+} \epsilon_{M,+} \left(\epsilon_{1,+} \epsilon_{2,+} e^{d|\mathbf{q}_{\parallel}|} e^{2h|\mathbf{q}_{\parallel}|} - \epsilon_{1,-} \epsilon_{2,-} e^{-d|\mathbf{q}_{\parallel}|} e^{-2h|\mathbf{q}_{\parallel}|} \right), \end{aligned}$$

where we defined:

$$\epsilon_{i,\pm} = \epsilon_i \pm 1. \quad (105)$$

Note, that the limit of vanishing interlayer distance is discussed in Eq. (110). To calculate the quantum-confined Coulomb potential, Eq. (91), we make the following *ansatz* for the confinement wave function in z -direction:

$$\zeta(z) = \sqrt{\frac{2}{d}} \cos\left(\frac{\pi}{d} z\right), \quad (106)$$

which is the ground state of an infinitely deep potential well. Note, that, in principle, we cannot assume, that Eq. (106) for the ground state of an infinitely deep potential well $n = 1$ holds for the charge distributions in z -direction in every thin semiconductor: While Eq. (106) is a good approximation for conventional quantum wells [141, 142] and TMDCs [82] in the lowest conduction and highest valence bands, for h-BN, the first excited state (104) would be a better approximation to actual *ab initio* calculations of the charge distribution in z -direction [82].

The z -integrals occurring in Eq. (91) by employing

Eq. (103) and Eq. (106) then read:

$$\begin{aligned} \frac{4}{d^2} \int_{-\frac{d}{2}}^{\frac{d}{2}} dz dz' \cos^2\left(\frac{\pi}{d}z\right) e^{-|\mathbf{q}_\parallel||z-z'|} \cos^2\left(\frac{\pi}{d}z'\right) \\ = \frac{1}{|\mathbf{q}_\parallel|d(4\pi^2 + |\mathbf{q}_\parallel|^2 d^2)} \\ \times \left(8\pi^2 + 3|\mathbf{q}_\parallel|^2 d^2 - \frac{32\pi^4 (1 - e^{-|\mathbf{q}_\parallel|d})}{|\mathbf{q}_\parallel|d(4\pi^2 + |\mathbf{q}_\parallel|^2 d^2)} \right), \quad (107) \end{aligned}$$

and:

$$\begin{aligned} \frac{4}{d^2} \int_{-\frac{d}{2}}^{\frac{d}{2}} dz dz' \cos^2\left(\frac{\pi}{d}z\right) e^{\pm|\mathbf{q}_\parallel|(\pm z \pm z')} \cos^2\left(\frac{\pi}{d}z'\right) \\ = \left(\frac{8\pi^2 \sinh\left(\frac{|\mathbf{q}_\parallel|d}{2}\right)}{|\mathbf{q}_\parallel|d(4\pi^2 + |\mathbf{q}_\parallel|^2 d^2)} \right)^2. \quad (108) \end{aligned}$$

With these ingredients, an explicit expression for the macroscopically screened Coulomb potential from Eq. (91) can be derived:

$$\begin{aligned} V_{\mathbf{q}_\parallel} = \frac{e^2}{2\mathcal{A}\epsilon_0\epsilon_M|\mathbf{q}_\parallel|} \frac{1}{|\mathbf{q}_\parallel|d(4\pi^2 + |\mathbf{q}_\parallel|^2 d^2)} \left(8\pi^2 + 3|\mathbf{q}_\parallel|^2 d^2 - \frac{32\pi^4 (1 - e^{-|\mathbf{q}_\parallel|d})}{|\mathbf{q}_\parallel|d(4\pi^2 + |\mathbf{q}_\parallel|^2 d^2)} \right) \\ + \frac{e^2}{2\mathcal{A}\epsilon_0\epsilon_M|\mathbf{q}_\parallel|} \frac{1}{g_{\mathbf{q}_\parallel}} \left(\frac{8\pi^2 \sinh\left(\frac{|\mathbf{q}_\parallel|d}{2}\right)}{|\mathbf{q}_\parallel|d(4\pi^2 + |\mathbf{q}_\parallel|^2 d^2)} \right)^2 \left((\epsilon_{M,-} - \epsilon_{2,+} e^{h|\mathbf{q}_\parallel|} - \epsilon_{M,+} \epsilon_{2,-} e^{-h|\mathbf{q}_\parallel|}) (\epsilon_{1,+} \epsilon_{M,-} e^{h|\mathbf{q}_\parallel|} - \epsilon_{1,-} \epsilon_{M,+} e^{-h|\mathbf{q}_\parallel|}) 2e^{-d|\mathbf{q}_\parallel|} \right. \\ \left. + (\epsilon_{M,-} \epsilon_{2,+} e^{h|\mathbf{q}_\parallel|} - \epsilon_{M,+} \epsilon_{2,-} e^{-h|\mathbf{q}_\parallel|}) (\epsilon_{1,+} \epsilon_{M,+} e^{h|\mathbf{q}_\parallel|} - \epsilon_{1,-} \epsilon_{M,-} e^{-h|\mathbf{q}_\parallel|}) + (\epsilon_{M,+} \epsilon_{2,+} e^{h|\mathbf{q}_\parallel|} - \epsilon_{M,-} \epsilon_{2,-} e^{-h|\mathbf{q}_\parallel|}) \right. \\ \left. \times (\epsilon_{1,+} \epsilon_{M,-} e^{h|\mathbf{q}_\parallel|} - \epsilon_{1,-} \epsilon_{M,+} e^{-h|\mathbf{q}_\parallel|}) \right). \quad (109) \end{aligned}$$

For a vanishing vacuum gap ($h = 0$ nm), the macroscopic Green's function can also be expressed as:

$$\begin{aligned} G_{\mathbf{q}}^{\text{mac}}(z, z') = \frac{1}{2\epsilon_0\epsilon_M|\mathbf{q}_\parallel|} e^{-|\mathbf{q}_\parallel||z-z'|} \\ + \frac{1}{2\epsilon_0\epsilon_M|\mathbf{q}_\parallel|} \frac{1}{\delta_- e^{-|\mathbf{q}_\parallel|d} - \gamma_+ e^{|\mathbf{q}_\parallel|d}} \left(\gamma_- e^{|\mathbf{q}_\parallel|(z+z')} \right. \\ \left. + \delta_+ e^{-|\mathbf{q}_\parallel|(z+z')} - \delta_- e^{-|\mathbf{q}_\parallel|(z-z')} e^{-|\mathbf{q}_\parallel|d} \right. \\ \left. - \delta_- e^{|\mathbf{q}_\parallel|(z-z')} e^{-|\mathbf{q}_\parallel|d} \right), \quad (110) \end{aligned}$$

with:

$$\begin{aligned} \gamma_\pm &= (\epsilon_1 + \epsilon_M) (\epsilon_2 \pm \epsilon_M), \\ \delta_\pm &= (\epsilon_1 - \epsilon_M) (\epsilon_2 \pm \epsilon_M). \end{aligned} \quad (111)$$

The first term in Eq. (110) is the inhomogeneous contribution and the second term in Eq. (110) is the homoge-

neous contribution due to the dielectric environment, i.e., due to image charges. If we assume $\epsilon_1 = \epsilon_2 = \epsilon_M$, the second term in Eq. (110) vanishes and the Green's function is only given by the inhomogeneous contribution in the first term in Eq. (110). For the simplest case of a Dirac delta confinement of the charges, i.e., $|\zeta(z)|^2 = \delta(z)$, the quantum-confined macroscopic Coulomb potential $V_{\mathbf{q}_\parallel} = \frac{e^2}{\mathcal{A}} \int dz dz' |\zeta(z)|^2 G_{\mathbf{q}_\parallel}^{\text{mac}}(z, z') |\zeta(z')|^2$ reads:

$$V_{\mathbf{q}_\parallel} = \frac{e^2}{2\mathcal{A}\epsilon_0\epsilon_M|\mathbf{q}_\parallel|} \frac{\gamma_- + \delta_+ - \gamma_+ e^{|\mathbf{q}_\parallel|d} - \delta_- e^{-|\mathbf{q}_\parallel|d}}{\delta_- e^{-|\mathbf{q}_\parallel|d} - \gamma_+ e^{|\mathbf{q}_\parallel|d}}. \quad (112)$$

Comparing our results with the literature, we observe, that Eq. (110) is not equal to but similar to Rytova's formula derived in Refs. [143, 144]. Interestingly, the expression in Ref. [143] differs from the one in Ref. [144],

although both are derived with the same assumptions. If we assume $z \geq z'$, Eq. (110) corresponds exactly to Keldysh's formula in Ref. [145]. Regarding more recent calculations, our result matches exactly with Ref. [146] or, if $z = z' = 0$, with Ref. [147]. This validates our expression of the Green's function in Eq. (110) and it strongly indicates, that we have to slightly modify Rytova's expressions from Refs. [143, 144].

2. Analytical Model of Screening

Ab initio calculations suggest, that the constant approximation, i.e., $\mathbf{q} = \mathbf{0}$ -approximation, of the quasi-3D material dielectric function $\epsilon_{M,\mathbf{q}=\mathbf{0}}^{3D} = \epsilon_M$, cf. Fig. 3, significantly overestimates the screening at large momenta [77, 79, 82, 104]. While this is tolerable in the evaluation of interaction processes, which do not depend too strongly on the Coulomb-interaction strength such as exciton-phonon scattering, it underestimates biexciton and trion binding energies significantly and fails to describe the strength of the Coulomb interaction with large momentum transfers, e.g., Dexter coupling [41–43, 148], Auger coupling of momentum-dark excitons [149] or short-range exchange interaction [39, 78], correctly.

To capture this property in an analytical theory, we use the following analytic model of the 3D material dielectric function $\epsilon_{M,\mathbf{q}}^{3D}$ from Refs. [131, 150] in the static (or adiabatic) limit with $\omega = 0$:

$$\epsilon_{M,\mathbf{q}}^{3D} = 1 + \frac{1}{(\epsilon_M - 1)^{-1} + \alpha_{TF} \frac{|\mathbf{q}|^2}{q_{TF}^2} + \frac{\hbar^2 |\mathbf{q}|^4}{4m_0^2 \omega_{pl}^2}}. \quad (113)$$

Eq. (113) is designed to model the macroscopic three-dimensional interband dielectric function in RPA [107] from actual *ab initio* calculations at a temperature of $T = 0$ K, i.e., Eq. (83) for $\lambda \neq \lambda'$ in the macroscopic limit. We note, that there are other, more rigorous approaches [151, 152], which fulfill the Kramers-Kronig relations and can even be used to construct the full microscopic dielectric matrix with all local fields [152]. In Eq. (113), ϵ_M is the static bulk dielectric constant, cf. Fig. 3, the contribution “ $\alpha_{TF} \frac{|\mathbf{q}|^2}{q_{TF}^2}$ ” resembles the semiconductor Thomas-Fermi limit with fitting parameter α_{TF} and Thomas-Fermi wave vector $q_{TF}^3 = \sqrt{\frac{3\omega_{pl}^2 m_0^4}{\hbar^6 \pi^4 \epsilon_0^2}}$, and the contribution “ $\frac{\hbar^2 |\mathbf{q}|^4}{4m_0^2 \omega_{pl}^2}$ ” describes a single plasmon-pole contribution, where ω_{pl} is the bulk plasmon frequency. Note, that the Thomas-Fermi contribution in Eq. (113) should not be confused with the Thomas-Fermi limit of a quasi-free electron gas in metals or doped semiconductors derived from the *intraband* Lindhard function ($\lambda = \lambda'$ in Eq. (83)), as it describes the limit for small \mathbf{q} of the *interband* Lindhard function ($\lambda \neq \lambda'$ in Eq. (83)), i.e., the screening induced by an interband polarization cloud

and not by real carriers [153]. Consequently, ω_{pl} is related to the *interband* plasmon, which describes the collective mode of all possible transitions from fully occupied bands below the Fermi level including core bands to the empty conduction bands [154].

Eq. (113) serves as an analytical description of the macroscopic limit ($\mathbf{G} = \mathbf{G}' = \mathbf{0}$) of the *ab initio* theory of screening and replaces the constant approximation of the dielectric function of the material $\epsilon_M \rightarrow \epsilon_{M,\mathbf{q}}^{3D}$ in Eq. (109) and Eq. (112). Note, that substrate and superstrate material can be treated in an analog way.

To construct a two-dimensional material dielectric function $\epsilon_{M,\mathbf{q}_{||}}^{2D}$ from the three-dimensional dielectric function $\epsilon_{M,\mathbf{q}}^{3D}$ of the bulk material, which we include as the material "background" in our treatment of the layered dielectric structure, cf. Fig. 3, we employ Eq. (64) and Eq. (68) and write:

$$\left(\epsilon_{M,\mathbf{q}_{||}}^{2D} \right)^{-1} = \frac{V_{\mathbf{q}_{||}}}{V_{0,\mathbf{q}_{||}}} \quad (114)$$

where $V_{\mathbf{q}_{||}}$ is the macroscopically screened Coulomb potential from Eq. (91) and $V_{0,\mathbf{q}_{||}} = V_{\mathbf{q}_{||}}|_{\epsilon_{M,\mathbf{q}_{||}}^{3D}=1}$ is the unscreened Coulomb potential obtained from Eq. (91) by setting the background material dielectric function $\epsilon_{M,\mathbf{q}_{||}}^{3D}$, cf. Eq. (113), to unity. In Fig. 4(a), the effective two-dimensional dielectric function $\epsilon_{M,\mathbf{q}_{||}}^{2D}$ from Eq. (114) for a constant “ $\epsilon_{M,\mathbf{q}_{||}}^{2D}(\epsilon_{M,\mathbf{0}}^{3D})$ ” (blue solid line) and \mathbf{q} -dependent “ $\epsilon_{M,\mathbf{q}_{||}}^{2D}(\epsilon_{M,\mathbf{q}_{||}}^{3D})$ ” (red solid line) three-dimensional material dielectric background function from Eq. (113) is shown. Additionally, “ $\epsilon_{M,\mathbf{q}_{||}}^{R-K}$ ” (green solid line) depicts the Rytova-Keldysh thin-film limit in vacuum [145], which can be obtained in first order Taylor expansion in $|\mathbf{q}_{||}|d$:

$$\epsilon_{M,\mathbf{q}_{||}}^{R-K} = 1 + \frac{1}{2} \epsilon_{M,\mathbf{0}}^{3D} |\mathbf{q}_{||}|d, \quad (115)$$

and the black dots represent the dielectric function calculated by *ab initio* methods extracted from the Computational Materials Repository (CMR) [80]. Fig. 4(a) shows, that the constant approximation $\epsilon_{M,\mathbf{q}_{||}}^{2D}(\epsilon_{M,\mathbf{0}}^{3D})$ significantly overestimates the screening at large momenta and we are able to obtain a good agreement of the analytical model $\epsilon_{M,\mathbf{q}_{||}}^{2D}(\epsilon_{M,\mathbf{q}_{||}}^{3D})$ from Eq. (113) with *ab initio* calculations by adjusting the Thomas-Fermi parameter α_{TF} accordingly. The linear Rytova-Keldysh limit (green solid line) is only a good approximation at crystal momenta $|\mathbf{q}_{||}| \leq \frac{1}{d}$ and becomes even worse than the constant approximation at larger $\mathbf{q}_{||}$ (blue solid line). In Fig. 4(b), we depict the two-dimensional dielectric function from Eq. (114) for three different layer thicknesses d and the three-dimensional dielectric function from Eq. (113). We observe, that the two-dimensional dielectric function approaches the three-dimensional dielectric function, if d increases, which re-

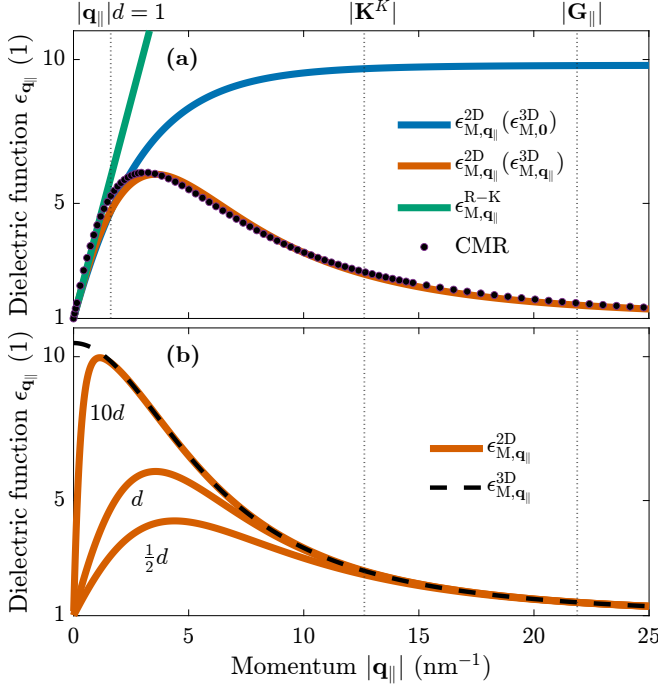


FIG. 4. (a) The two-dimensional dielectric function $\epsilon_{M,q||}^{2D}$ from Eq. (114) of an example MoS₂ monolayer ($\epsilon_{M,\parallel} = 15.5$, $\epsilon_{M,\perp} = 6.2$, $\epsilon_{M,\text{bulk}} = 10.5$ [155], $d = 0.618 \text{ nm}$ [135], $\hbar\omega_{\text{pl}} = 22.5 \text{ eV}$ [156]) suspended in vacuum ($\epsilon_1 = \epsilon_2 = 1$) is shown. $\epsilon_{M,q||}^{2D}(\epsilon_{M,0}^{3D})$ uses a constant approximation of the three-dimensional material background dielectric function $\epsilon_{M,0}^{3D}$ and $\epsilon_{M,q||}^{2D}(\epsilon_{M,q||}^{3D})$ uses the q_{\parallel} -dependent model from Eq. (113). $\epsilon_{M,q||}^{\text{R-K}}$ denotes the Rytova-Keldysh thin-film limit in vacuum from Eq. (115) and "CMR" denotes *ab initio* calculations extracted from the Computational Materials Repository (CMR) [80]. \mathbf{K}^K is a K valley momentum, cf. Sec. II B, and \mathbf{G}_{\parallel} is a reciprocal lattice vector. (b) The two-dimensional dielectric function $\epsilon_{M,q||}^{2D}$ from Eq. (114) for three different layer thicknesses and the three-dimensional dielectric function $\epsilon_{M,q||}^{3D}$ from Eq. (113) are shown.

sembles actual *ab initio* results [82, 104], validating our approach.

In general, the attenuation of the dielectric function at large momenta stems predominantly from the local-field effects, i.e., from the contributions with $\mathbf{G} \neq \mathbf{0}$ and $\mathbf{G}' \neq \mathbf{0}$. Since screening affects the Coulomb interaction via the inverse $(\epsilon^{-1})_{\mathbf{q},\mathbf{G},\mathbf{G}'}$ all local fields with \mathbf{G} and \mathbf{G}' affect the $\mathbf{G} = \mathbf{G}' = \mathbf{0}$ -component of the inverse dielectric matrix $(\epsilon^{-1})_{\mathbf{q},\mathbf{0},\mathbf{0},\mathbf{0}}$, which is not just the inverse of the $\mathbf{G} = \mathbf{G}' = \mathbf{0}$ -component of the dielectric matrix $(\epsilon_{\mathbf{q},\mathbf{0},\mathbf{0}})^{-1}$.

Hence, with a properly parametrized analytical model of the bulk material dielectric function $\epsilon_{M,\mathbf{q}}^{3D}$ from Eq. (113) combined with the analytical dielectric slab model, cf. Fig. 3, we obtain a good agreement with *ab initio* approaches including environmental screening and

the evaluation of the microscopic dielectric function from Eq. (83) via *ab initio* methods can be circumvented, as long as we do not explicitly need local-field effects with $\mathbf{G} \neq \mathbf{G}'$.

IV. EXCITONS AND OPTICAL SPECTRA

In this section, we discuss the occurrence of bound electron-hole pairs, the excitons. First, we derive the Bethe-Salpeter equation, which is used in full *ab initio* calculations, then we discuss a simplified version used in few-band excitonic approaches, the Wannier equation, and excitonic signatures in optical spectra.

From Eq. (29), we extract the following contributions, the hole-hole interaction:

$$\hat{H}_{\text{Coul-hh}} = \frac{1}{2} \sum_{\substack{\mathbf{k}, \mathbf{k}', \mathbf{q}, \mathbf{G}, \mathbf{G}', \\ v_1, v_2, v_3, v_4}} V_{\mathbf{q}, \mathbf{G}, \mathbf{G}'} \times \bar{\Upsilon}_{\mathbf{k}+\mathbf{q}+\mathbf{G}, \mathbf{k}}^{v_1, v_4} \bar{\Upsilon}_{\mathbf{k}'-\mathbf{q}-\mathbf{G}', \mathbf{k}'}^{v_2, v_3} \hat{v}_{1, \mathbf{k}+\mathbf{q}}^{\dagger} \hat{v}_{2, \mathbf{k}'-\mathbf{q}}^{\dagger} \hat{v}_{3, \mathbf{k}'} \hat{v}_{4, \mathbf{k}}, \quad (116)$$

the electron-electron interaction:

$$\hat{H}_{\text{Coul-ee}} = \frac{1}{2} \sum_{\substack{\mathbf{k}, \mathbf{k}', \mathbf{q}, \mathbf{G}, \mathbf{G}', \\ c_1, c_2, c_3, c_4}} V_{\mathbf{q}, \mathbf{G}, \mathbf{G}'} \times \bar{\Upsilon}_{\mathbf{k}+\mathbf{q}+\mathbf{G}, \mathbf{k}}^{c_1, c_4} \bar{\Upsilon}_{\mathbf{k}'-\mathbf{q}-\mathbf{G}', \mathbf{k}'}^{c_2, c_3} \hat{c}_{1, \mathbf{k}+\mathbf{q}}^{\dagger} \hat{c}_{2, \mathbf{k}'-\mathbf{q}}^{\dagger} \hat{c}_{3, \mathbf{k}'} \hat{c}_{4, \mathbf{k}}, \quad (117)$$

the direct electron-hole interaction:

$$\hat{H}_{\text{Coul-eh}}^{\text{dir}} = \sum_{\substack{\mathbf{k}, \mathbf{k}', \mathbf{q}, \mathbf{G}, \mathbf{G}', \\ v_1, v_2, c_1, c_2}} \frac{1}{2} (V_{\mathbf{q}, \mathbf{G}, \mathbf{G}'} + V_{-\mathbf{q}, -\mathbf{G}', -\mathbf{G}}) \times \bar{\Upsilon}_{\mathbf{k}+\mathbf{q}+\mathbf{G}, \mathbf{k}}^{c_1, c_2} \bar{\Upsilon}_{\mathbf{k}'-\mathbf{q}-\mathbf{G}', \mathbf{k}'}^{v_1, v_2} \hat{c}_{1, \mathbf{k}+\mathbf{q}}^{\dagger} \hat{v}_{1, \mathbf{k}'-\mathbf{q}}^{\dagger} \hat{v}_{2, \mathbf{k}'} \hat{c}_{2, \mathbf{k}}, \quad (118)$$

and the exchange electron-hole interaction:

$$\hat{H}_{\text{Coul-eh}}^{\text{exch}} = \sum_{\substack{\mathbf{k}, \mathbf{k}', \mathbf{q}, \mathbf{G}, \mathbf{G}', \\ v_1, v_2, c_1, c_2}} \frac{1}{2} (V_{\mathbf{q}, \mathbf{G}, \mathbf{G}'} + V_{-\mathbf{q}, -\mathbf{G}', -\mathbf{G}}) \times \bar{\Upsilon}_{\mathbf{k}+\mathbf{q}+\mathbf{G}, \mathbf{k}}^{c_1, c_2} \bar{\Upsilon}_{\mathbf{k}'-\mathbf{q}-\mathbf{G}', \mathbf{k}'}^{v_1, v_2} \hat{c}_{1, \mathbf{k}+\mathbf{q}}^{\dagger} \hat{v}_{1, \mathbf{k}'-\mathbf{q}}^{\dagger} \hat{c}_{2, \mathbf{k}'-\mathbf{q}} \hat{v}_{2, \mathbf{k}}. \quad (119)$$

Note, that we use a compound index for the bands and spins $\lambda \equiv \lambda, s$ here and restricted ourselves the the ground state in the out-of-plane direction: $V_{\mathbf{q}, \mathbf{G}, \mathbf{G}'} \equiv V_{\mathbf{q}, \mathbf{G}, \mathbf{G}'}^{1, 1, 1, 1}(\omega = 0)$ in the static limit, cf. Eq. (24). Moreover, we assume three-dimensional quasi-momenta for notational simplicity. Then, we calculate the Heisenberg equations of motion for the optically active interband transition $\langle \hat{v}_{\mathbf{q}}^{\dagger} \hat{c}_{\mathbf{q}} \rangle$ at zero center-of-mass momentum:

$$i\hbar \partial_t \langle \hat{v}_{\mathbf{q}}^{\dagger} \hat{c}_{\mathbf{q}} \rangle = \langle [\hat{v}_{\mathbf{q}}^{\dagger} \hat{c}_{\mathbf{q}}, \hat{H}_{\text{tot}}] \rangle, \quad (120)$$

with the total (full) solid-state Hamiltonian in Born-Oppenheimer approximation:

$$\begin{aligned} \hat{H}_{\text{tot}} &= \hat{H}_0 + \hat{H}_{\text{Coul-hh}} + \hat{H}_{\text{Coul-ee}} + \hat{H}_{\text{Coul-eh}}^{\text{dir}} + \hat{H}_{\text{Coul-eh}}^{\text{exch}}, \end{aligned} \quad (121)$$

where the single-particle Hamiltonian reads:

$$\hat{H}_0 = \sum_{\mathbf{k}, c} E_{c, \mathbf{k}} \hat{c}_{\mathbf{k}}^\dagger \hat{c}_{\mathbf{k}} + \sum_{\mathbf{k}, v} E_{v, \mathbf{k}} \hat{v}_{\mathbf{k}}^\dagger \hat{v}_{\mathbf{k}} \quad (122)$$

with Bloch-electron dispersion $E_{\lambda, \mathbf{k}}$ for valence-band states ($\lambda = v$) and conduction-band states ($\lambda = c$), and perform a Hartree-Fock approximation assuming completely filled valence bands and empty conduction bands, which corresponds to the limit of linear optics in a charge-neutral semiconductor. Note, that under these circumstances, the electron-electron interaction Hamiltonian $\hat{H}_{\text{Coul-ee}}$ does not contribute at all. At last, we expand the electron-hole transitions as follows:

$$\langle \hat{v}_{\mathbf{q}}^\dagger \hat{c}_{\mathbf{q}} \rangle = \sum_{\mu} \Phi_{\mu, v, c, \mathbf{q}} P_{\mu}, \quad (123)$$

For demonstration purposes, here, we assume only optically bright transitions with zero center-of-mass momentum. In Eq. (140), where we discuss the effective-mass approach, we depict the general expansion, which also considers excitonic transitions with nonzero center-of-mass momenta. The expansion coefficients $\Phi_{\mu, v, c, \mathbf{q}}$ in Eq. (123) satisfy the following eigenvalue equation:

$$\begin{aligned} & (E_{c, \mathbf{q}} - E_{v, \mathbf{q}} + \Sigma_{v, c, \mathbf{q}}^{\text{H}} + \Sigma_{v, c, \mathbf{q}}^{\text{COH}} + \Sigma_{v, c, \mathbf{q}}^{\text{SEX}}) \Phi_{\mu, v, c, \mathbf{q}} \\ & + \sum_{\mathbf{q}', v', c'} \left(K_{\text{eh}}^{\text{dir} v', c', \mathbf{q}'} + K_{\text{eh}}^{\text{exch} v', c', \mathbf{q}'} \right) \Phi_{\mu, v', c', \mathbf{q}'} \\ & = E_{\mu} \Phi_{\mu, v, c, \mathbf{q}}. \end{aligned} \quad (124)$$

Eq. (124) is the *Bethe-Salpeter equation* for optically active electron-hole pairs in COHSEX- and Tamm-Danoff approximation. The latter occurs naturally within our equations-of-motion approach, since we already neglected those exchange electron-hole Hamiltonians containing operator products such as $\hat{v}^\dagger \hat{v}^\dagger \hat{c} \hat{c}$ or $\hat{c}^\dagger \hat{c}^\dagger \hat{v} \hat{v}$, which are responsible for a coupling between $\langle \hat{v}_{\mathbf{q}}^\dagger \hat{c}_{\mathbf{q}} \rangle$ and $\langle \hat{c}_{\mathbf{q}}^\dagger \hat{v}_{\mathbf{q}} \rangle$, i.e., the anti-resonant contributions. Resonant-anti-resonant coupling due to direct electron-hole interaction does not occur in Hartree-Fock approximation.

In Eq. (124), $E_{c/v, \mathbf{q}}$ are the unrenormalized electron-/hole single-particle dispersions dependent on the quasi-momenta \mathbf{q} covering the entire Brillouin zone. They are renormalized via the Hartree self-energy $\Sigma_{v, c, \mathbf{q}}^{\text{H}}$:

$$\Sigma_{v, c, \mathbf{q}}^{\text{H}} = \sum_{\mathbf{q}', \mathbf{G}, \mathbf{G}', v'} \bar{V}_{\mathbf{0}, \mathbf{G}, \mathbf{G}'} \bar{\Upsilon}_{\mathbf{q}'+\mathbf{G}, \mathbf{q}'}^{v', v'} \left(\bar{\Upsilon}_{\mathbf{q}-\mathbf{G}', \mathbf{q}}^{c, c} - \bar{\Upsilon}_{\mathbf{q}-\mathbf{G}', \mathbf{q}}^{v, v} \right), \quad (125)$$

which vanishes for $\mathbf{G} = \mathbf{G}' = \mathbf{0}$, via the direct Coulomb-

hole self-energy $\Sigma_{v, \mathbf{q}}^{\text{COH}}$:

$$\Sigma_{v, \mathbf{q}}^{\text{COH}} = \sum_{\mathbf{q}', \mathbf{G}, \mathbf{G}', v'} \bar{V}_{\mathbf{q}', \mathbf{G}, \mathbf{G}'} \bar{\Upsilon}_{\mathbf{q}+\mathbf{q}'+\mathbf{G}, \mathbf{q}}^{v', v} \bar{\Upsilon}_{\mathbf{q}, \mathbf{q}+\mathbf{q}'+\mathbf{G}'}^{v', v}, \quad (126)$$

and the screened exchange self-energy $\Sigma_{c, \mathbf{q}}^{\text{SEX}}$:

$$\Sigma_{c, \mathbf{q}}^{\text{SEX}} = - \sum_{\mathbf{q}', \mathbf{G}, \mathbf{G}', v'} \bar{V}_{\mathbf{q}', \mathbf{G}, \mathbf{G}'} \bar{\Upsilon}_{\mathbf{q}, \mathbf{q}-\mathbf{q}'-\mathbf{G}}^{c, v'} \bar{\Upsilon}_{\mathbf{q}-\mathbf{q}'-\mathbf{G}', \mathbf{q}}^{v', c} \quad (127)$$

The electron-hole interaction is governed by the direct electron-hole interaction kernel $K_{\text{eh}}^{\text{dir} v', c', \mathbf{q}'}$:

$$K_{\text{eh}}^{\text{dir} v', c', \mathbf{q}'} = - \sum_{\mathbf{G}, \mathbf{G}'} \bar{V}_{\mathbf{q}-\mathbf{q}', \mathbf{G}, \mathbf{G}'} \bar{\Upsilon}_{\mathbf{q}, \mathbf{q}'-\mathbf{G}}^{c, c'} \bar{\Upsilon}_{\mathbf{q}'-\mathbf{G}', \mathbf{q}'}^{v', v}, \quad (128)$$

which acts attractive, and the exchange electron-hole interaction kernel $K_{\text{eh}}^{\text{exch} v', c', \mathbf{q}'}$:

$$K_{\text{eh}}^{\text{exch} v', c', \mathbf{q}'} = \sum_{\mathbf{G}, \mathbf{G}'} \bar{V}_{\mathbf{0}, \mathbf{G}, \mathbf{G}'} \bar{\Upsilon}_{\mathbf{q}, \mathbf{q}-\mathbf{G}}^{c, v} \bar{\Upsilon}_{\mathbf{q}'-\mathbf{G}', \mathbf{q}'}^{v', c'} \quad (129)$$

which usually acts repulsive. Here, we use the following abbreviation:

$$\bar{V}_{\mathbf{q}, \mathbf{G}, \mathbf{G}'} = \frac{1}{2} (V_{\mathbf{q}, \mathbf{G}, \mathbf{G}'} + V_{-\mathbf{q}, -\mathbf{G}', -\mathbf{G}}). \quad (130)$$

Note, that all interaction mechanisms, direct and exchange, are screened due to the background of inactive states, cf. Sec. III A, since we only include a few active states, which are optically addressed, explicitly in the Bethe-Salpeter equation in Eq. (124).

If we reduce Eq. (124) to a two-band model, expand around the extrema of the Brillouin zone, where an effective-mass approximation of the band structure is applicable, perform a low-wavenumber approximation in the Bloch form factors, which removes the coupling between different valence bands ($v \leftrightarrow v'$) and conduction bands ($c \leftrightarrow c'$), disregard scattering terms involving a large valley-momentum transfer (Dexter interaction) and exchange contributions coupling distinct excitonic configurations (Förster interaction), the Bethe-Salpeter equation can be reduced to a Schrödinger-like equation [157], the *Wannier equation* [158] for $\Phi_{\mu, v, c, \mathbf{q}} \rightarrow \varphi_{\mu, \mathbf{q}}^{\xi, \xi', s, s'}$:

$$\begin{aligned} & \left(\tilde{E}_{\text{gap}}^{\xi, \xi', s, s'} + \frac{\hbar^2 \mathbf{q}^2}{2m_{\text{r}, s, s'}^{\xi, \xi'}} \right) \varphi_{\mu, \mathbf{q}}^{\xi, \xi', s, s'} - \sum_{\mathbf{q}'} K_{\text{eh}}^{\text{dir} \xi, \xi', s, s'} \varphi_{\mu, \mathbf{q}-\mathbf{q}'}^{\xi, \xi', s, s'} \\ & = E_{\mu}^{\xi, \xi', s, s'} \varphi_{\mu, \mathbf{q}}^{\xi, \xi', s, s'}. \end{aligned} \quad (131)$$

Here, $\tilde{E}_{\text{gap}}^{\xi, \xi', s, s'}$ is the renormalized band gap:

$$\begin{aligned} \tilde{E}_{\text{gap}}^{\xi, \xi', s, s'} &= E_{c,0}^{\xi, s} - E_{v,0}^{\xi, s} + \Sigma_{v,c,0}^{\text{H}, \xi, \xi', s, s'} + \Sigma_{v,0}^{\text{COH}, \xi, s} + \Sigma_{c,0}^{\text{SEX}, \xi', s'}, \end{aligned} \quad (132)$$

where $E_{c/v,0}^{\xi, s}$ is the unrenormalized conduction/valence band edge with respect to valley ξ and spin s , $\Sigma_{v,c,0}^{\text{H}, \xi, \xi', s, s'}$ is the (reduced) Hartree self-energy:

$$\begin{aligned} \Sigma_{v,c,0}^{\text{H}, \xi, \xi', s, s'} &= \sum_{\substack{\mathbf{G}, \mathbf{G}' \\ \xi', s'}} \bar{V}_{\mathbf{0}, \mathbf{G}, \mathbf{G}'} \bar{\Upsilon}_{\mathbf{G}, \mathbf{0}}^{v, v, \xi'', \xi'', s''} \left(\bar{\Upsilon}_{\mathbf{0}, \mathbf{G}'}^{c, c, \xi', \xi', s'} - \bar{\Upsilon}_{\mathbf{0}, \mathbf{G}'}^{v, v, \xi, \xi, s} \right), \end{aligned} \quad (133)$$

and $\Sigma_{v,0}^{\text{COH}, \xi, s}$ is the (reduced) Coulomb-hole self-energy:

$$\begin{aligned} \Sigma_{v,0}^{\text{COH}, \xi, s} &= \sum_{\mathbf{q}, \mathbf{G}, \mathbf{G}', \xi''} \bar{V}_{\mathbf{q} + \mathbf{K}^{\xi''}, \mathbf{G}, \mathbf{G}'} \bar{\Upsilon}_{\mathbf{q} + \mathbf{G}, \mathbf{0}}^{v, v, \xi + \xi'', \xi, s} \bar{\Upsilon}_{\mathbf{0}, \mathbf{q} + \mathbf{G}'}^{v, v, \xi, \xi + \xi'', s}, \end{aligned} \quad (134)$$

and $\Sigma_{c,0}^{\text{SEX}, \xi', s'}$ is the (reduced) screened exchange self-energy:

$$\begin{aligned} \Sigma_{c,0}^{\text{SEX}, \xi', s'} &= - \sum_{\mathbf{q}, \mathbf{G}, \mathbf{G}', \xi''} \bar{V}_{\mathbf{q} + \mathbf{K}^{\xi''}, \mathbf{G}, \mathbf{G}'} \bar{\Upsilon}_{\mathbf{0}, -\mathbf{q} - \mathbf{G}}^{c, v, \xi', \xi' - \xi'', s'} \bar{\Upsilon}_{-\mathbf{q} - \mathbf{G}', \mathbf{0}}^{v, c, \xi' - \xi'', \xi', s'}. \end{aligned} \quad (135)$$

In Eq. (131), \mathbf{q}_{\parallel} is the relative momentum, $m_{r,s,s'}^{\xi, \xi'} = \left(\frac{1}{m_h^{\xi, s}} + \frac{1}{m_e^{\xi', s'}} \right)^{-1}$ is the reduced mass with effective masses of the hole/electron $m_{h/e}^{\xi, s}$ and $\varphi_{\mu, \mathbf{q}}^{\xi, \xi', s, s'}$ is the excitonic wave function with excitonic quantum number μ , where the first (second) valley and spin index always belongs to the hole (electron), and $E_{\mu}^{\xi, \xi', s, s'}$ is the corresponding excitonic energy. The excitonic wave functions are normalized according to:

$$\sum_{\mathbf{q}} \varphi_{\mu, \mathbf{q}}^{*, \xi, \xi', s, s'} \varphi_{\mu, \mathbf{q}}^{\xi, \xi', s, s'} = \delta_{\mu, \nu}, \quad (136)$$

and obey the completeness relation:

$$\sum_{\mu} \varphi_{\mu, \mathbf{q}}^{*, \xi, \xi', s, s'} \varphi_{\mu, \mathbf{q}'}^{\xi, \xi', s, s'} = \delta_{\mathbf{q}, \mathbf{q}'}. \quad (137)$$

In Eq. (131), the (reduced) direct electron-hole interaction kernel reads:

$$K_{\text{eh}}^{\text{dir} \xi, \xi', s, s'} = \sum_{\mathbf{G}, \mathbf{G}'} \bar{V}_{\mathbf{q}', \mathbf{G}, \mathbf{G}'} \bar{\Upsilon}_{\mathbf{0}, -\mathbf{q}' - \mathbf{G}}^{c, c, \xi', \xi', s'} \bar{\Upsilon}_{-\mathbf{q}' - \mathbf{G}', \mathbf{0}}^{v, v, \xi, \xi, s}. \quad (138)$$

By neglecting all local fields and applying a Taylor expansion in the form factors with respect to the momentum transfer \mathbf{q}' in zeroth order, cf. Eq. (40), the electron-hole kernel from Eq. (138) can be written as:

$$K_{\text{eh}}^{\text{dir} \xi, \xi', s, s'} \approx V_{\mathbf{q}'}, \quad (139)$$

where $V_{\mathbf{q}} \equiv \bar{V}_{\mathbf{q}, \mathbf{0}, \mathbf{0}}$, cf. Eq. (130).

Note that, while we provided the Bethe-Salpeter equation only for optically bright excitons in Eq. (124) – which can be straightforwardly extended to account for all optically dark excitons as well – the Wannier equation in Eq. (131) explicitly takes into account valley-momentum-bright intravalley excitons ($\xi = \xi'$) and valley-momentum-dark intervalley excitons ($\xi \neq \xi'$), as well as spin-bright ($s = s'$) and spin-dark ($s \neq s'$) excitons.

In the few-band effective-mass excitonic picture, electron-hole (interband) transitions are transformed into excitonic transitions as follows [2]:

$$\hat{P}_{\mu, \mathbf{Q}}^{\xi, \xi', s, s'} = \sum_{\mathbf{q}} \varphi_{\mu, \mathbf{q}}^{*, \xi, \xi', s, s'} \hat{v}_{\mathbf{q} + \beta_{\xi, \xi'}^s \mathbf{Q}}^{\dagger \xi, s} \hat{c}_{\mathbf{q} - \alpha_{\xi, \xi'}^s \mathbf{Q}}^{\xi', s'}, \quad (140)$$

where $\hat{P}_{\mu, \mathbf{Q}}^{\xi, \xi', s, s'} (\hat{P}_{\mu, \mathbf{Q}}^{\dagger \xi, \xi', s, s'})$ annihilates (creates) an exciton at excitonic state μ and center-of-mass momentum \mathbf{Q} with spin-valley configuration ξ, ξ', s, s' , cf. Fig. 5. The first (second) index belongs to the hole (electron). The effective-mass ratios read:

$$\alpha_{\xi, \xi'}^{s, s'} = \frac{m_e^{\xi, s'}}{m_h^{\xi, s} + m_e^{\xi', s'}}, \quad \beta_{\xi, \xi'}^{s, s'} = \frac{m_h^{\xi, s}}{m_h^{\xi, s} + m_e^{\xi', s'}}. \quad (141)$$

In Eq. (140), we explicitly take into account momentum-dark electron-hole pairs with $\mathbf{Q} \neq \mathbf{0}$.

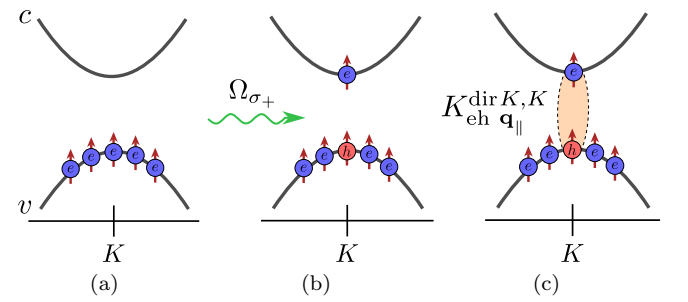


FIG. 5. Fully occupied valence band (a), optical excitation with Rabi frequency Ω_{σ_+} in σ_+ -polarization creates an electron-hole pair at the K valley (b) [159], which binds via electron-hole Coulomb attraction $K_{\text{eh}}^{\text{dir} K, K_{\parallel}}$, cf. Eq. (138), forming an exciton at zero center-of-mass momentum $\hat{P}_{\mu, 0}^{K, K_{\parallel}, K_{\parallel}}$ (c).

By coupling the excitons to a classical transverse Maxwell field [160–162] in a thin-film- and rotating-wave

approximation, we can derive an expression for the linear absorption $\alpha(\omega)$:

$$\alpha(\omega) = \frac{\omega}{c_0} \Im \left(\frac{\mathcal{A}}{\epsilon_0} \sum_{\mu} \frac{|\mathbf{d}_0^{c,v,K,K,\uparrow} \varphi_{\mu}^{*K,K,\uparrow,\uparrow}(\mathbf{r}_{\parallel} = \mathbf{0})|^2}{E_{\mu}^{K,K,\uparrow,\uparrow} - \hbar\omega - i\hbar\gamma_{\mu}^{K,K,\uparrow,\uparrow}} \right), \quad (142)$$

for σ_+ -polarized light without loss of generality, which corresponds to the Elliott formula [163]. In Eq. (142), the (half) homogeneous linewidth reads: $\hbar\gamma_{\mu}^{\xi,\xi',s,s'} = \hbar\gamma_{\text{rad},\mu}^{\xi,\xi',s,s'} + \hbar\gamma_{\text{nrad},\mu}^{\xi,\xi',s,s'}$, where $\hbar\gamma_{\text{rad},\mu}^{\xi,\xi',s,s'}$ is the radiative (half) linewidth:

$$\hbar\gamma_{\text{rad},\mu}^{\xi,\xi',s,s'} = \frac{E_{\mu}^{\xi,\xi,s,s} \mu_0 c_0 \mathcal{A}}{\hbar n_{\text{ref}}} |\mathbf{d}_0^{cv,\xi,\xi,s} \varphi_{\mu}^{*\xi,\xi,s,s}(\mathbf{r}_{\parallel} = \mathbf{0})|^2 \delta_{\xi,\xi'}, \quad (143)$$

where n_{ref} is the mean refractive index of the dielectric environment, and $\hbar\gamma_{\text{nrad},\mu}^{\xi,\xi',s,s'}$ is the nonradiative (half) linewidth due to, e.g., exciton-phonon interaction [164, 165] or uniformly distributed impurities [166, 167]. In principle, inhomogeneous contributions to the linewidth can also be included [168–170], but entail ensemble averages, which we do not consider here. The oscillator strength of $\alpha(\omega)$ is determined by the transition dipole moment $\mathbf{d}_0^{c,v,K,K,\uparrow}$ in low-wavenumber approximation and by the excitonic wave function $\varphi_{\mu}^{*K,K,\uparrow,\uparrow}(\mathbf{r}_{\parallel} = \mathbf{0})$ denoting the probability of finding an electron and a hole at the same position in real space. The transition dipole moment can be analytically calculated via the eigenfunctions of the few-band $k \cdot p$ -Hamiltonian from Ref. [84]:

$$\mathbf{d}_0^{cv,\xi,\xi,s} = (\delta_{\xi,K} - \delta_{\xi,K'}) \frac{i e \gamma_{k \cdot p} \sqrt{2}}{E_{c,0}^{\xi,s} - E_{v,0}^{\xi,s}} \mathbf{e}_{\delta_{\xi,K'} - \delta_{\xi,K}}, \quad (144)$$

with momentum matrix element $\gamma_{k \cdot p}$ and Jones vectors $\mathbf{e}_{\pm} = \frac{1}{\sqrt{2}} (1 \pm i)^{\top}$.

In Fig. 6, we depict the linear absorption spectrum $\alpha(\omega)$, cf. Eq. (142), of a h-BN-encapsulated MoSe₂ monolayer by taking the A- and B-series into account. The blue solid line in Fig. 6 depicts the full calculations using Eq. (131), the "excitonic" limit, and the red solid line depicts calculations without electron-hole Coulomb attraction, i.e., Eq. (131) with $K_{\text{eh}}^{\text{dir},\xi,\xi',s,s'} \approx V_{\mathbf{q}_{\parallel}} = 0$, the "free-particle" limit.

There are several features to discuss.

First, by comparing the free-particle limit to the excitonic case, additional resonances below the free-particle band gap E_{gap} appear, the *excitonic resonances*. They are labeled as $1s, 2s \dots$, in analogy to the hydrogen atom, since they denote bound eigenstates of the problem of

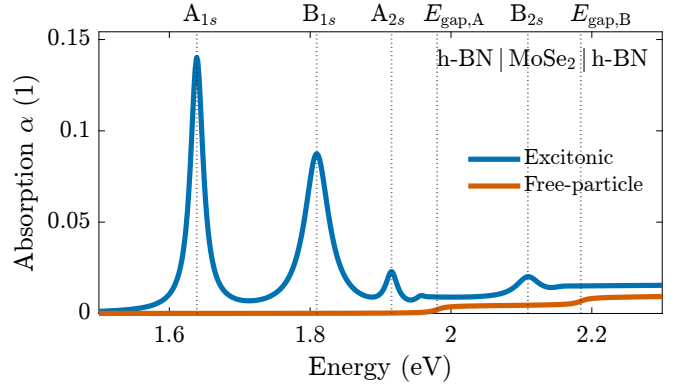


FIG. 6. Linear absorption $\alpha(\omega)$ from Eq. (142) of a h-BN-encapsulated monolayer MoSe₂ by taking the A- and B-series into account. Parameters are shown in Tab. A1.

electrons and holes interacting via an attractive Coulomb potential.

Second, at and above the free-particle band gap, the excitonic absorption is larger than the free-particle absorption. This is called *Sommerfeld enhancement* [171–173] and stems from the fact, that the unbound eigenstates of the interacting electron-hole problem above the band gap do not fully behave as free plane waves but are still perturbed by the Coulomb interaction and form so-called *Coulomb waves* [163, 174, 175]. It can be quantified as:

$$S(\omega) = \frac{\alpha_{\text{excitonic}}(\omega)}{\alpha_{\text{free-particle}}(\omega)}. \quad (145)$$

For the conditions in Fig. 6, we obtain a Sommerfeld enhancement factor of $S\left(\omega > \frac{E_{\text{gap},B}}{\hbar}\right) \approx 1.6$, similar to conventional quantum wells [173].

Third, the spectrum depicts two distinct excitonic series, the *A-series* and the *B-series*, which are energetically different. The A-series corresponds to electron-hole pairs at the K valley, where both electrons and holes are in the spin-up state, whereas the B-series corresponds to electron-hole pairs at the K valley with spin-down states. The energy difference between, e.g., the A_{1s} and the B_{1s} exciton is caused by the conduction and valence band splitting due to spin-orbit interaction via intrinsic in-plane electric fields [84, 159, 176–179] as well as differences in their respective binding energies due to different band curvatures, i.e., different effective masses. In case of σ_- -excitation, the spin- and valley labeling swaps.

Note, that we assume a slightly idealized spin structure with pure spin-up and spin-down states. *ab initio* calculations show [180, 181], that even directly at the band extrema, the spins are slightly mixed due to spin-orbit interaction via intrinsic out-of-plane electric fields. Both field components, in-plane (inducing spin splitting) and out-of-plane (inducing spin mixing), are induced by the ions and vary rapidly within the unit cell.

Also note, that our calculated spectrum in Fig. 6 does not include other excitonic contributions due to, e.g.,

higher-lying C-excitons, which are delocalized along the Γ - K direction in the Brillouin zone [79, 129] and significantly affect the absorption spectrum at higher energies. These cannot be properly described in an effective-mass approximation and have to be described via the full Bethe-Salpeter equation in Eq. (124).

V. COULOMB SCATTERING PROCESSES

Since the Wannier equation in Eq. (131) takes – next to the Coulomb-induced band gap renormalization – into account only one specific Coulomb interaction process, i.e., electron-hole Coulomb attraction involving momentum transfers in the vicinity of a band extrema (valley), which are small compared to the distance between different valleys, Eq. (131) lacks the description of other exciton scattering processes relevant in time-dependent optical experiments. Hence, its eigenstates rather provide a suitable basis in materials with strong Coulomb interaction as a starting point. In this section, we describe exciton-scattering processes at all center-of-mass momenta \mathbf{Q}_{\parallel} potentially reaching well outside the light cone formulated in a basis constructed from the eigenstates of the Wannier equation, cf. Eq. (131).

In the following, we disregard the subscript " \parallel " for notational simplicity. Even though we discuss two-dimensional materials, the concepts are equally valid in three dimensions.

Recall the many-body Coulomb Hamiltonian from Eq. (35) in a valley-expanded description:

$$\begin{aligned} \hat{H}_{\text{Coul}} &= \frac{1}{2} \sum_{\substack{\lambda_1, \dots, \lambda_4, \\ \mathbf{k}, \mathbf{k}', \mathbf{q}, \\ \mathbf{G}, \mathbf{G}' \\ \xi, \xi', \xi'', s, s'}} V_{\mathbf{q} + \mathbf{K}^{\xi''}, \mathbf{G}, \mathbf{G}'} \bar{T}_{\mathbf{k} + \mathbf{q}, \mathbf{k}, \mathbf{G}}^{\lambda_1, \lambda_4, \xi + \xi'', \xi, s} \bar{T}_{\mathbf{k}' - \mathbf{q}, \mathbf{k}', -\mathbf{G}'}^{\lambda_2, \lambda_3, \xi' - \xi'', \xi', s'} \\ &\quad \times \hat{a}_{\lambda_1, \mathbf{k} + \mathbf{q}}^{\dagger, \xi + \xi'', s} \hat{a}_{\lambda_2, \mathbf{k}' - \mathbf{q}}^{\dagger, \xi' - \xi'', s'} \hat{a}_{\lambda_3, \mathbf{k}'}^{\xi', s'} \hat{a}_{\lambda_4, \mathbf{k}}^{\xi, s}. \end{aligned} \quad (146)$$

Here, we already restricted the out-of-plane confinement to the respective ground state with $V_{\mathbf{q}, \mathbf{G}, \mathbf{G}'}^{1,1,1,1} \equiv V_{\mathbf{q}, \mathbf{G}, \mathbf{G}'}$ and assumed a statically screened Coulomb potential.

In the following, we illustrate only direct electron-hole and exchange electron-hole processes in the *density-independent* limit, i.e., we disregard all density-dependent processes such as nonlinear energy renormalizations, linewidth broadening or Auger scattering [15–17, 22, 124, 127, 149, 182, 183]. In this limit, electron-electron processes do not occur and hole-hole processes only renormalize the band gap via the Coulomb-hole self-energy in Eq. (134). Hence, the processes outlined in the following are only sufficient up to a strict $\chi^{(3)}$ -limit, e.g., weakly nonlinear pump-probe experiments with energy-averaged timetraces around well separated excitonic resonances, where all spectral signatures besides Pauli-blocking-induced bleaching have been averaged out.

A. Direct Electron-Hole Interaction

From Eq. (146), we consider electron-hole interaction processes, where the respective electrons and holes remain in their bands ($\lambda_1 = \lambda_4$ and $\lambda_2 = \lambda_3$). These processes are usually referred to as direct Coulomb interactions. In a two-band model, they are described by:

$$\begin{aligned} \hat{H}_{\text{Coul-eh}}^{\text{dir}} &= \sum_{\substack{\mathbf{k}, \mathbf{k}', \mathbf{q}, \mathbf{G}, \mathbf{G}' \\ \xi, \xi', \xi'', s, s'}} \bar{V}_{\mathbf{q} + \mathbf{K}^{\xi''}, \mathbf{G}, \mathbf{G}'} \bar{T}_{\mathbf{k} + \mathbf{q} + \mathbf{G}, \mathbf{k}}^{\xi, s} \bar{T}_{\mathbf{k}' - \mathbf{q} - \mathbf{G}', \mathbf{k}'}^{\xi' - \xi'', \xi', s'} \\ &\quad \times \hat{c}_{\mathbf{k} + \mathbf{q}}^{\dagger, \xi + \xi'', s} \hat{v}_{\mathbf{k}' - \mathbf{q}}^{\dagger, \xi' - \xi'', s'} \hat{v}_{\mathbf{k}'}^{\xi', s'} \hat{c}_{\mathbf{k}}^{\xi, s}. \end{aligned} \quad (147)$$

In Fig. 7, we display the direct electron-hole interaction in a two-band model for arbitrary momentum transfers \mathbf{q} .

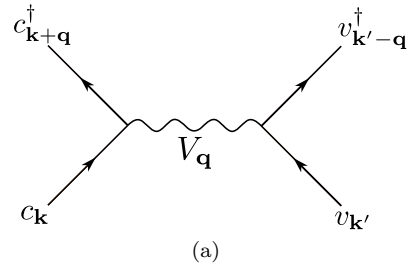


FIG. 7. Direct electron-hole Coulomb interaction.

Small Momentum Transfer

Direct electron-hole Coulomb interaction processes with small momentum transfer ($\mathbf{K}^{\xi''} = \mathbf{0}$) give rise to the binding of electron-hole pairs and are diagonalized together with the free-particle Hamiltonian within the transformation into the excitonic picture, cf. Eq. (140), by means of solving the Wannier equation in Eq. (131).

This procedure results in the free excitonic Hamiltonian:

$$\hat{H}_{\text{X-0}} = \sum_{\mu, \mathbf{Q}, \xi, \xi', s, s'} E_{\mu, \mathbf{Q}}^{\xi, \xi', s, s'} \hat{P}_{\mu, \mathbf{Q}}^{\dagger, \xi, \xi', s, s'} P_{\mu, \mathbf{Q}}^{\xi, \xi', s, s'}, \quad (148)$$

where:

$$E_{\mu, \mathbf{Q}}^{\xi, \xi', s, s'} = E_{\mu}^{\xi, \xi', s, s'} + \frac{\hbar^2 \mathbf{Q}^2}{2(m_h^{\xi, s} + m_e^{\xi', s'})}, \quad (149)$$

is the exciton dispersion with exciton energy $E_{\mu}^{\xi, \xi', s, s'}$ obtained by solving the Wannier equation in Eq. (131) and center-of-mass momentum \mathbf{Q} .

Large Momentum Transfer

The direct electron-hole interaction for large momentum transfer ($\mathbf{K}^{\xi''} \neq \mathbf{0}$) represents the valley analog in momentum space of Coulomb-induced charge transfer in real space, i.e., Dexter interaction [184]. It occurs between distinct valleys in the Brillouin zone and is always spin-conserving with regard to the individual electron and hole scattering. The corresponding Hamiltonian is given by Eq. (150) with the condition $\mathbf{K}^{\xi''} \neq \mathbf{0}$:

$$\begin{aligned} \hat{H}_{\text{Dex}}^{\text{dir}} &= \sum_{\substack{\mathbf{k}, \mathbf{k}', \mathbf{q}, \mathbf{G}, \mathbf{G}', \\ \xi, \xi', \xi'', \\ (\xi'' \neq 0), s, s'}} \bar{V}_{\mathbf{q} + \mathbf{K}^{\xi''}, \mathbf{G}, \mathbf{G}'} \bar{\Upsilon}_{\mathbf{k} + \mathbf{q} + \mathbf{G}, \mathbf{k}}^{c, c, \xi + \xi'', \xi, s} \bar{\Upsilon}_{\mathbf{k}' - \mathbf{q} - \mathbf{G}', \mathbf{k}'}^{v, v, \xi' - \xi'', \xi', s'} \\ &\quad \times \hat{c}_{\mathbf{k} + \mathbf{q}}^{\dagger} \xi + \xi'', s \hat{v}_{\mathbf{k}' - \mathbf{q}}^{\dagger} \xi' - \xi'', s' \hat{v}_{\mathbf{k}'}^{\xi', s'} \hat{c}_{\mathbf{k}}^{\xi, s}. \end{aligned} \quad (150)$$

In the excitonic picture with Eq. (140), the Dexter Hamiltonian reads:

$$\begin{aligned} \hat{H}_{\text{X-Dex}} &= \sum_{\substack{\mu, \nu, \mathbf{Q}, \\ \xi, \xi', \xi'', \\ (\xi'' \neq 0), s, s'}} D_{\mu, \nu, \mathbf{K}^{\xi''}}^{\xi, \xi', \xi'', s, s'} \hat{P}_{\mu, \mathbf{Q}}^{\dagger} \xi, \xi' + \xi'', s, s' \hat{P}_{\nu, \mathbf{Q}}^{\xi - \xi'', \xi', s, s'}, \end{aligned} \quad (151)$$

with matrix element:

$$\begin{aligned} D_{\mu, \nu, \mathbf{K}^{\xi''}}^{\xi, \xi', \xi'', s, s'} &= -C_{\text{Dex}}^{\text{dir}} V_{\mathbf{K}^{\xi''}} \sum_{\mathbf{q}} \varphi_{\mu, \mathbf{q}}^{*\xi, \xi' + \xi'', s, s'} \sum_{\mathbf{q}'} \varphi_{\nu, \mathbf{q}'}^{\xi - \xi'', \xi', s, s'}, \end{aligned} \quad (152)$$

where:

$$\begin{aligned} C_{\text{Dex}}^{\text{dir}} &= \left(V_{\mathbf{K}^{\xi''}} \sum_{\mathbf{q}} \varphi_{\mu, \mathbf{q}}^{*\xi, \xi' + \xi'', s, s'} \sum_{\mathbf{q}'} \varphi_{\nu, \mathbf{q}'}^{\xi - \xi'', \xi', s, s'} \right)^{-1} \\ &\times \sum_{\mathbf{q}, \mathbf{q}', \mathbf{G}, \mathbf{G}'} \bar{V}_{\mathbf{q} - \mathbf{q}' + \mathbf{K}^{\xi''}, \mathbf{G}, \mathbf{G}'} \bar{\Upsilon}_{\mathbf{q} - \mathbf{q}' + \mathbf{G}, \mathbf{0}}^{c, c, \xi' + \xi'', \xi', s'} \bar{\Upsilon}_{-\mathbf{q} + \mathbf{q}' - \mathbf{G}', \mathbf{0}}^{v, v, \xi - \xi'', \xi, s} \\ &\quad \times \varphi_{\mu, \mathbf{q}}^{*\xi, \xi' + \xi'', s, s'} \varphi_{\nu, \mathbf{q}'}^{\xi - \xi'', \xi', s, s'}, \end{aligned} \quad (153)$$

carries all corrections including possible local-field effects compared to the rough estimate $V_{\mathbf{K}^{\xi''}}$. We note that, as the Dexter matrix element does not vanish at zero center-of-mass momentum $\mathbf{Q} = \mathbf{0}$, Dexter interaction already affects linear spectra by introducing minor energy shifts and broadening due to intervalley A-B coupling [42].

First, we discuss intervalley scattering of *intravalley* excitons. If we restrict ourselves to the energetically lowest excitons, there exists one process:

$$K-K \leftrightarrow K'-K', \quad (154)$$

of which we depict the direction $K-K \rightarrow K'-K'$ in Fig. 8 for the spin-up-spin-up configuration. For the example Dexter process depicted in Fig. 8, the reduced form factor $\bar{\Upsilon}$, Eq. (30), has to be calculated between different valleys:

$$\bar{\Upsilon}_{\mathbf{k} + \mathbf{q}, \mathbf{G}, \mathbf{k}}^{c, c, K', K, s} \quad \text{and} \quad \bar{\Upsilon}_{\mathbf{k}' - \mathbf{q} - \mathbf{G}', \mathbf{k}'}^{v, v, K, K', s}. \quad (155)$$

For an exact evaluation of Eq. (153), first-principle methods are needed. However, in many cases, it is sufficient to disregard the local fields and approximate the form factors as follows: $\bar{\Upsilon}_{\mathbf{k} + \mathbf{q}, \mathbf{k}}^{c, c, K', K, s} = \bar{\Upsilon}_{\mathbf{k}' - \mathbf{q}, \mathbf{k}'}^{v, v, K, K', s} \approx 1$, which entails:

$$C_{\text{Dex}}^{\text{dir}} \approx 1, \quad (156)$$

serving as an upper estimate. In Fig. 8(a,b) we depict the scattering of the conduction-band electron (a) and the valence-band electron (b) of the corresponding Dexter process, where the grey-shaded areas denote the total set of possible momentum transfers $\mathbf{K}^{\xi''} + \mathbf{q}$. Here, even though there are three equivalent processes, the total scattering amplitude is not multiplied by three, since each K or K' valley as a final state is only covered by one third. Note, that we refrain from drawing specific reciprocal lattice vectors \mathbf{G}'' and \mathbf{G}''' denoting possible Umklapp processes *in the narrower sense* (not to be confused with the local-field contributions \mathbf{G} and \mathbf{G}'), as the form factors $\bar{\Upsilon}$ do not depend on \mathbf{G}'' and \mathbf{G}''' , cf. Sec. II A for a discussion. The combined process is depicted in Fig. 8(c) for electron-hole pairs in a reduced band structure. Note, that the hole in Fig. 8(c) scatters in the opposite direction compared to the valence-band electron in Fig. 8(b). The estimate in Eq. (156) already yields a reasonable Dexter interaction strength, which has back-up from measurements [41–43, 148]. One reason is, that the interaction strength of Dexter processes is mainly governed by a Coulomb potential carrying a large argument, i.e. $V_{\mathbf{q} + \mathbf{K}^{\xi''}} \approx V_{\mathbf{K}^{\xi''}}$, where $\mathbf{K}^{\xi''}$ is a valley momentum. The resulting interaction strength is of the order of tens of meV, which is one order of magnitude smaller than the excitonic binding energy governed by a Coulomb potential $V_{\mathbf{q}}$ carrying a small momentum argument $|\mathbf{q}| \ll |\mathbf{K}^{\xi''}|$.

Next to intervalley scattering of *intravalley* excitons as depicted in Fig. 8, Eq. (151) also encodes intervalley scattering of *intervalley* excitons. There are four possible processes for the energetically lowest electron-hole pairs involving holes at the K and Γ valleys and electrons at the K , K' , Λ and Λ' valleys:

$$\begin{aligned} K-K' &\leftrightarrow \Gamma-K \quad (K \text{ momentum transfer}), \\ K'-K &\leftrightarrow \Gamma-K' \quad (K \text{ momentum transfer}), \\ K-\Lambda &\leftrightarrow \Gamma-\Lambda' \quad (\Lambda \text{ momentum transfer}), \\ K'-\Lambda' &\leftrightarrow \Gamma-\Lambda \quad (\Lambda \text{ momentum transfer}). \end{aligned} \quad (157)$$

In Fig. 9, we depict the process $K-K' \rightarrow \Gamma-K$ for the spin-up-spin-up configuration exemplarily. As before, there

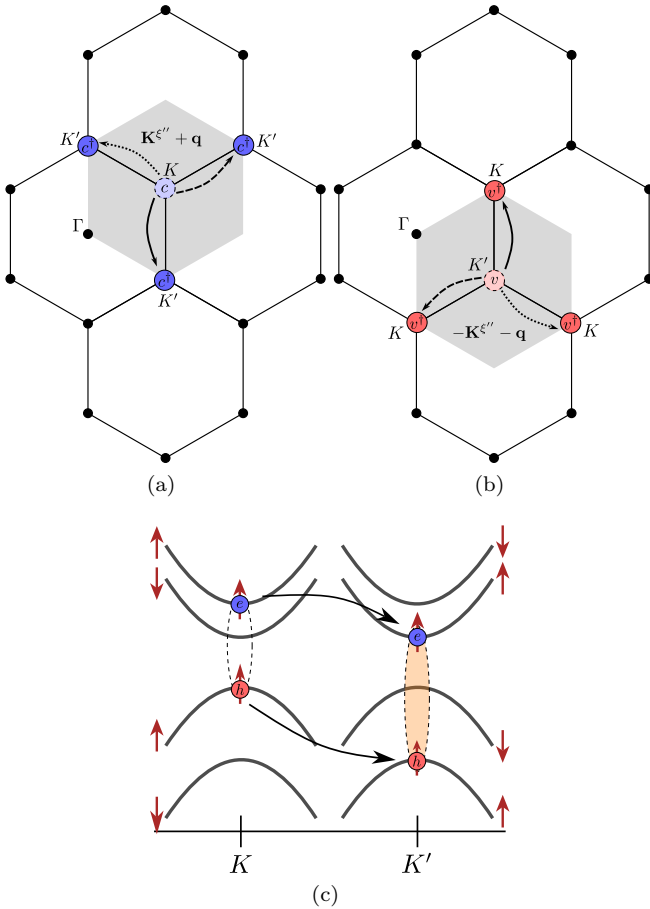


FIG. 8. Example process of intervalley interaction ($\xi'' \neq \Gamma$) of intravalley excitons ($\xi = \xi'$) involving simultaneous $K' \rightarrow K$ and $K \rightarrow K'$ intraband scattering (Dexter): Three equivalent processes denoted by solid, dashed and dotted arrows involving electron (a) and hole scattering (b). Grey-shaded areas denote the total set of possible momentum transfers $\mathbf{K}^{\xi''} + \mathbf{q}$ (conduction-band electron scattering) or $-\mathbf{K}^{\xi''} - \mathbf{q}$ (valence-band electron scattering). Combined process visualized in electron-hole pairs in a reduced band structure (c), cf. Eq. (151). Note, that the spin polarization is idealized, as spin-orbit interaction slightly mixes spins even directly at the band extrema [180, 181].

exist three equivalent processes, which are weighted each by one third. The reduced form factors for the process depicted in Fig. 9 read:

$$\bar{\Upsilon}_{\mathbf{k}+\mathbf{q}+\mathbf{G},\mathbf{k}}^{c,c,K,K',s} \quad \text{and} \quad \bar{\Upsilon}_{\mathbf{k}'-\mathbf{q}-\mathbf{G}',\mathbf{k}'}^{v,v,K,\Gamma,s}, \quad (158)$$

which have to be calculated via *ab initio* methods. It has been shown in Ref. [43], that the Dexter process involving intervalley excitons depicted in Fig. 9 plays a crucial role in the valley depolarization after ultrafast optical excitation of momentum-dark materials such as monolayer WSe₂ by breaking the quasi-stable K - K' configuration. Here, a good agreement with the experiment has already been obtained by neglecting all local fields and using a

rough approximation of $\bar{\Upsilon}_{\mathbf{k}+\mathbf{q}+\mathbf{G},\mathbf{k}}^{c,c,K,K',s} \approx \bar{\Upsilon}_{\mathbf{k}'-\mathbf{q}-\mathbf{G}',\mathbf{k}'}^{v,v,K,\Gamma,s} \approx 1$, which entails $C_{\text{Dex}}^{\text{dir}} \approx 1$ from Eq. (153) in Eq. (152).

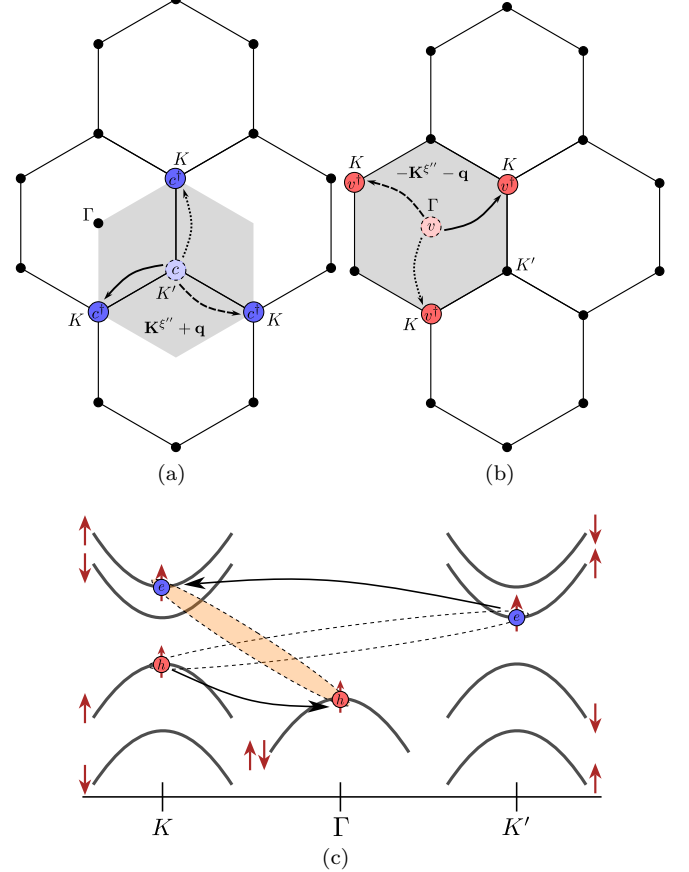


FIG. 9. Example process of intervalley interaction ($\xi'' \neq \Gamma$) of intervalley excitons ($\xi \neq \xi'$) involving simultaneous $\Gamma \rightarrow K$ and $K' \rightarrow K$ intraband scattering (Dexter): Three equivalent processes denoted by solid, dashed and dotted arrows involving electron (a) and hole scattering (b). Grey-shaded areas denote the total set of possible momentum transfers $\mathbf{K}^{\xi''} + \mathbf{q}$ (conduction-band electron scattering) or $-\mathbf{K}^{\xi''} - \mathbf{q}$ (valence-band electron scattering). Combined process visualized in electron-hole pairs in a reduced band structure (c), cf. Eq. (151).

B. Electron-Hole Exchange Interaction

From Eq. (146), we consider electron-hole interaction processes, where the respective electrons and holes flip their bands, cf. Fig. 10. These processes are usually re-

ferred to as Coulomb exchange interactions:

$$\begin{aligned} \hat{H}_{\text{Coul-eh}}^{\text{exch}} &= \sum_{\substack{\mathbf{k}, \mathbf{k}', \mathbf{q}, \mathbf{G}, \mathbf{G}', \\ \xi, \xi', \xi'', s, s'}} \bar{V}_{\mathbf{q} + \mathbf{K}^{\xi''}, \mathbf{G}, \mathbf{G}'} \bar{\Upsilon}_{\mathbf{k} + \mathbf{q} + \mathbf{G}, \mathbf{k}}^{c, v, \xi + \xi'', \xi, s} \bar{\Upsilon}_{\mathbf{k}' - \mathbf{q} - \mathbf{G}', \mathbf{k}'}^{v, c, \xi' - \xi'', \xi', s'} \\ &\quad \times \hat{c}_{\mathbf{k} + \mathbf{q}}^{\dagger} \xi + \xi'', s \hat{v}_{\mathbf{k}' - \mathbf{q}}^{\dagger} \xi' - \xi'', s' \hat{c}_{\mathbf{k}'}^{\xi', s'} \hat{v}_{\mathbf{k}}^{\xi, s}. \quad (159) \end{aligned}$$

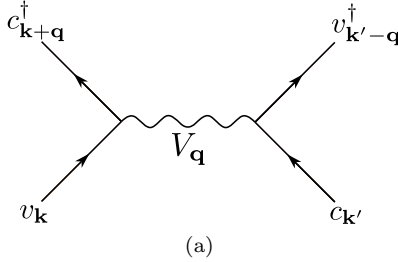


FIG. 10. Electron-hole Coulomb exchange interaction.

As before, we distinguish between processes involving small ($\mathbf{K}^{\xi''} = \mathbf{0}$) and large ($\mathbf{K}^{\xi''} \neq \mathbf{0}$) momentum transfers.

Small Momentum Transfer

The exchange Hamiltonian for small momentum transfer ($\mathbf{K}^{\xi''} = \mathbf{0}$) reads:

$$\begin{aligned} \hat{H}_{\text{Coul-eh}}^{\text{exch}} &= \sum_{\substack{\mathbf{k}, \mathbf{k}', \mathbf{q}, \mathbf{G}, \mathbf{G}', \\ \xi, \xi', s, s'}} \bar{V}_{\mathbf{q}, \mathbf{G}, \mathbf{G}'} \bar{\Upsilon}_{\mathbf{k} + \mathbf{q} + \mathbf{G}, \mathbf{k}}^{c, v, \xi, \xi, s} \bar{\Upsilon}_{\mathbf{k}' - \mathbf{q} - \mathbf{G}', \mathbf{k}'}^{v, c, \xi', \xi', s'} \\ &\quad \times \hat{c}_{\mathbf{k} + \mathbf{q}}^{\dagger} \xi, s \hat{v}_{\mathbf{k}' - \mathbf{q}}^{\dagger} \xi' \hat{c}_{\mathbf{k}'}^{\xi', s'} \hat{v}_{\mathbf{k}}^{\xi, s}. \quad (160) \end{aligned}$$

Due to the nature of the exchange interaction being an interband scattering process and the orthogonality of the Bloch factors at equal momenta, $\bar{\Upsilon}_{\mathbf{k}, \mathbf{k}}^{\lambda, \lambda', \xi, \xi, s} = \delta_{\lambda, \lambda'}$, it is beneficial to further distinguish between short-range ($\mathbf{G}, \mathbf{G}' \neq \mathbf{0}$) and long-range contributions ($\mathbf{G} = \mathbf{G}' = \mathbf{0}$). The former originates from spatially varying Coulomb fields on the scale of the unit cell, while the latter originates from spatially varying Coulomb fields on the scale of the total lattice.

Short-range interactions:

Contributions with $\mathbf{G}, \mathbf{G}' \neq \mathbf{0}$ in Eq. (160) are short-range interactions due to spatially varying local fields within a unit cell and they do not vanish at $\mathbf{q} = \mathbf{0}$, since $\bar{\Upsilon}_{\mathbf{k} + \mathbf{G}, \mathbf{k}}^{\lambda, \lambda', \xi, \xi, s} \neq 0$ for $\lambda \neq \lambda'$ due to the momentum mismatch with $\mathbf{G} \neq \mathbf{0}$. At $\mathbf{q} = \mathbf{0}$, these interactions involve reduced form factors as follows:

$$\bar{\Upsilon}_{\mathbf{k} + \mathbf{G}, \mathbf{k}}^{c, v, \xi, \xi, s}, \quad (161)$$

which have to be evaluated via first-principle methods, and a Coulomb potential with a large argument:

$V_{\mathbf{q}, \mathbf{G}, \mathbf{G}'} \approx V_{\mathbf{G}}$ if $\mathbf{G} = \mathbf{G}'$. With Eq. (140), the corresponding excitonic Hamiltonian reads:

$$\hat{H}_{\text{X-SR}}^{\text{exch}} = \sum_{\substack{\mu, \nu, \mathbf{Q}, \\ \xi, \xi', s, s'}} X_{\text{SR}, \mu, \nu, \mathbf{Q}}^{\xi, \xi', s, s'} \hat{P}_{\mu, \mathbf{Q}}^{\dagger} \xi, \xi, s \hat{P}_{\nu, \mathbf{Q}}^{\xi', \xi', s', s'}, \quad (162)$$

with matrix element:

$$X_{\text{SR}, \mu, \nu, \mathbf{Q}}^{\xi, \xi', s, s'} = \mathcal{C}_{\text{SR}}^{\text{exch}} V_{\mathbf{G}} \sum_{\mathbf{q}} \varphi_{\mu, \mathbf{q}}^{*, \xi, \xi, s, s} \sum_{\mathbf{q}'} \varphi_{\nu, \mathbf{q}'}^{\xi', \xi', s', s'}, \quad (163)$$

where:

$$\mathcal{C}_{\text{SR}}^{\text{exch}} = (V_{\mathbf{G}})^{-1} \sum_{\mathbf{G}, \mathbf{G}'} \bar{V}_{\mathbf{Q}, \mathbf{G}, \mathbf{G}'} \bar{\Upsilon}_{\mathbf{Q} + \mathbf{G}, \mathbf{0}}^{c, v, \xi, \xi, s} \bar{\Upsilon}_{-\mathbf{Q} - \mathbf{G}', \mathbf{0}}^{v, c, \xi', \xi', s'}, \quad (164)$$

carries all corrections evaluated by *ab initio* methods [78] compared to a simple estimate of $V_{\mathbf{G}}$. Short-range exchange interactions in Eq. (162) only affect spin-bright intravalley excitons causing singlet-triplet splitting [78, 185], cf. Fig. 11(b) – in a slightly idealized picture, as spin-orbit interaction weakly mixes spins even directly at the band extrema [180, 181] – or double-spin-flip processes within equal valleys, cf. Fig. 11(c). Hence, it is possible to obtain a rough estimate of $\mathcal{C}_{\text{SR}}^{\text{exch}}$ in a few-band effective-mass model without *ab initio* methods, if the energy splitting of the corresponding spin-bright and spin-dark excitons is known from experiments.

An intriguing empirical fact is the existence of an *intravalley* short-range contribution ($\xi = \xi'$ in Eq. (163)), but the vanishing of an *intervalley* short-range contribution ($\xi \neq \xi'$ in Eq. (163)), since, otherwise, a valley hybridization between the $P_{\mu, \mathbf{Q}}^{K, K, \uparrow, \uparrow}$ and $P_{\mu, \mathbf{Q}}^{K', K', \downarrow, \downarrow}$ excitons would occur already at zero center-of-mass momentum $\mathbf{Q} = \mathbf{0}$, which should produce observable features such as valley-split exciton lines in linear absorption measurements or near-instantaneous valley depolarization in non-linear pump-probe experiments. However, such features have not been observed experimentally, since valley-split exciton lines do not appear and valley depolarization usually takes some time (ps scale) [43, 186, 187]. Hence, the matrix element for intervalley short-range exchange interaction must vanish or, at least, very small compared to its intravalley counterpart, which we illustrate in the following. Since the matrix element in Eq. (163) contains a summation over all $\mathbf{G} \neq \mathbf{0}$, cf. Eq. (164), the total matrix element is built from a multitude of terms. Even if we restrict the summation to the most relevant first reciprocal lattice vectors and assume $\mathbf{G} = \mathbf{G}'$, this would entail in total six terms. The individual intravalley exchange equal-spin overlaps in low-wavenumber approximation and $|\mathbf{q}| \ll |\mathbf{G}|$ read:

$$\sum_{\mathbf{G} \neq \mathbf{0}} V_{\mathbf{G}} \bar{\Upsilon}_{\mathbf{G}, \mathbf{0}}^{c, v, \xi, \xi, s} \bar{\Upsilon}_{-\mathbf{G}, \mathbf{0}}^{v, c, \xi, \xi, s} \quad (\text{intravalley}), \quad (165)$$

while the intervalley exchange opposite-spin overlaps read:

$$\sum_{\mathbf{G} \neq \mathbf{0}} V_{\mathbf{G}} \bar{\Upsilon}_{\mathbf{G}, \mathbf{0}}^{c, v, \xi, \xi, s} \bar{\Upsilon}_{-\mathbf{G}, \mathbf{0}}^{v, c, \bar{\xi}, \bar{\xi}, \bar{s}} \quad (\text{intervalley}), \quad (166)$$

Since the Bloch factors are connected via a time-reversal transformation $\mathbf{k} \rightarrow -\mathbf{k}$, $\xi \rightarrow \bar{\xi}$ (for $\xi \in \{K, K'\}$), $s \rightarrow \bar{s}$, we can write:

$$\begin{aligned} \sum_{\mathbf{G} \neq \mathbf{0}} V_{\mathbf{G}} \bar{\Upsilon}_{\mathbf{G}, \mathbf{0}}^{c, v, \xi, \xi, s} \bar{\Upsilon}_{-\mathbf{G}, \mathbf{0}}^{v, c, \bar{\xi}, \bar{\xi}, \bar{s}} \\ = \sum_{\mathbf{G} \neq \mathbf{0}} V_{\mathbf{G}} \bar{\Upsilon}_{\mathbf{G}, \mathbf{0}}^{c, v, \xi, \xi, s} \bar{\Upsilon}_{\mathbf{G}, \mathbf{0}}^{v, c, \xi, \xi, s} \quad (\text{intervalley}). \end{aligned} \quad (167)$$

Hence, the only difference between the intravalley exchange element in Eq. (165) and the intervalley exchange element in Eq. (167) is the sign of the phase factor in the second reduced Bloch factor ($e^{i\mathbf{G} \cdot \mathbf{r}}$ vs. $e^{-i\mathbf{G} \cdot \mathbf{r}}$). Thus, by summing over all relevant $\mathbf{G} \neq \mathbf{0}$ -vectors, the intervalley contributions should cancel each other due to their phase mismatch, while the intravalley contributions do not. Here, explicit *ab initio* calculations can shed more light on this issue.

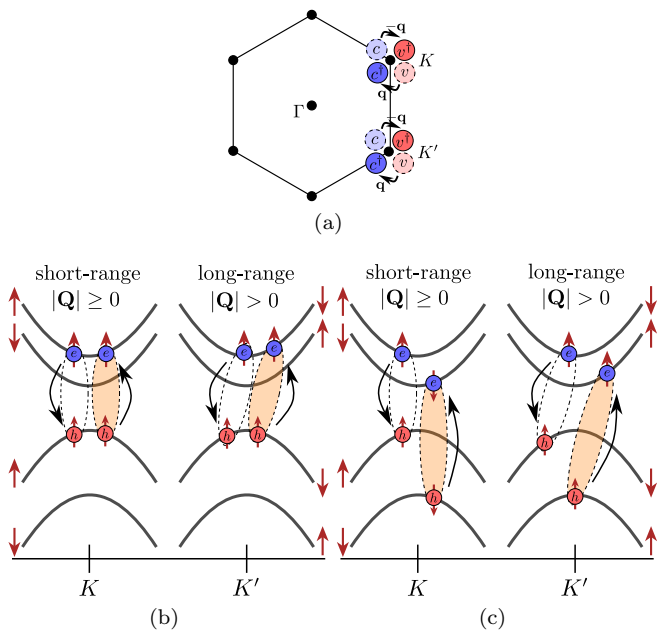


FIG. 11. Intravalley exchange interaction of intravalley excitons ($\xi = \xi'$) involving simultaneous $K \rightarrow K$ interband scattering (a): Spin-conserving ($s = s'$) (b) and spin-flip ($s \neq s'$) (c) coupling within the same valley ($\xi = \xi'$) due to short-range ($\mathbf{G} \neq \mathbf{0}$), cf. Eq. (162), and long-range ($\mathbf{G} = \mathbf{0}$), cf. Eq. (169), interactions.

Long-range interactions:

Contributions with $\mathbf{G} = \mathbf{G}' = \mathbf{0}$ in Eq. (160) are long-range interactions, as the interacting Coulombic fields can vary over multiple unit cells. These processes occur

within equal valleys ($\xi = \xi'$), cf. Fig. 11, and distinct valleys ($\xi \neq \xi'$), cf. Fig. 12. In contrast to the short-range contributions, they vanish at $\mathbf{q} = \mathbf{0}$. Hence, we can Taylor expand the form factors in $\mathbf{q} = \mathbf{0}$ up to the first non-vanishing order, cf. Eq. (41):

$$\bar{\Upsilon}_{\mathbf{k} + \mathbf{q}, \mathbf{k}}^{\lambda, \bar{\lambda}, \xi, \xi, s} \approx -\frac{i}{e} \mathbf{q} \cdot \mathbf{d}_{\mathbf{k}}^{\lambda, \bar{\lambda}, \xi, \xi, s} \approx -\frac{i}{e} \mathbf{q} \cdot \mathbf{d}_{\mathbf{0}}^{\lambda, \bar{\lambda}, \xi, \xi, s}, \quad (168)$$

where $\mathbf{d}_{\mathbf{0}}^{\lambda, \bar{\lambda}, \xi, \xi, s}$ is the dipole matrix element in low-wavenumber approximation, cf. Eq. (39). The corresponding excitonic Hamiltonian with Eq. (140) reads:

$$\hat{H}_{\text{X-LR}}^{\text{exch}} = \sum_{\mu, \nu, \mathbf{Q}, \xi, \xi', s, s'} X_{\text{LR}, \mu, \nu, \mathbf{Q}}^{\xi, \xi', s, s'} \hat{P}_{\mu, \mathbf{Q}}^{\dagger \xi, \xi, s, s} \hat{P}_{\nu, \mathbf{Q}}^{\xi', \xi', s', s'}, \quad (169)$$

with matrix element:

$$\begin{aligned} X_{\text{LR}, \mu, \nu, \mathbf{Q}}^{\xi, \xi', s, s'} \\ = V_{\mathbf{Q}} \left(\frac{1}{e^2} (\mathbf{Q} \cdot \mathbf{d}_{\mathbf{0}}^{cv, \xi, s}) (\mathbf{Q} \cdot \mathbf{d}_{\mathbf{0}}^{vc, \xi', s'}) + \mathcal{O}((\mathbf{Q} \cdot \mathbf{d})^3) \right) \\ \times \sum_{\mathbf{q}} \varphi_{\mu, \mathbf{q}}^{*\xi, \xi, s, s} \sum_{\mathbf{q}'} \varphi_{\nu, \mathbf{q}'}^{\xi, \xi, s', s'}. \end{aligned} \quad (170)$$

Long-range interactions between different excitonic configurations are the reciprocal-space analog to the Coulomb-induced energy transfer, i.e., Förster interaction [188], in real space: Nonresonant long-range interactions are responsible for the coupling of A and B excitons within equal valleys [189] (double spin flip scattering, $\xi = \xi'$, $s \neq s'$ in Eq. (169)), cf. Fig. 11(c), and for the coupling of A and B excitons between the K/K' valleys (spin-conserving scattering, $\xi \neq \xi'$, $s = s'$ in Eq. (169)), cf. Fig. 12(b). Moreover, resonant long-range exchange between the valleys gives rise to nonanalytic dispersions [78, 190] and double spin-flip scattering between K and K' valleys (Maialle-Silva-Sham- or Bir-Aronov-Pikus mechanism, $\xi \neq \xi'$, $s \neq s'$ in Eq. (169)) [37–39, 191–193], cf. Fig. 12(c). Additionally, within the same valley, long-range exchange further impacts the exciton dispersion at nonzero center-of-mass momenta \mathbf{Q} ($\xi = \xi'$, $s = s'$ in Eq. (169)), cf. Fig. 11(b). Hence, long-range exchange interaction causes a deviation from an otherwise purely quadratic effective-mass exciton dispersion possibly impairing biexciton binding [190].

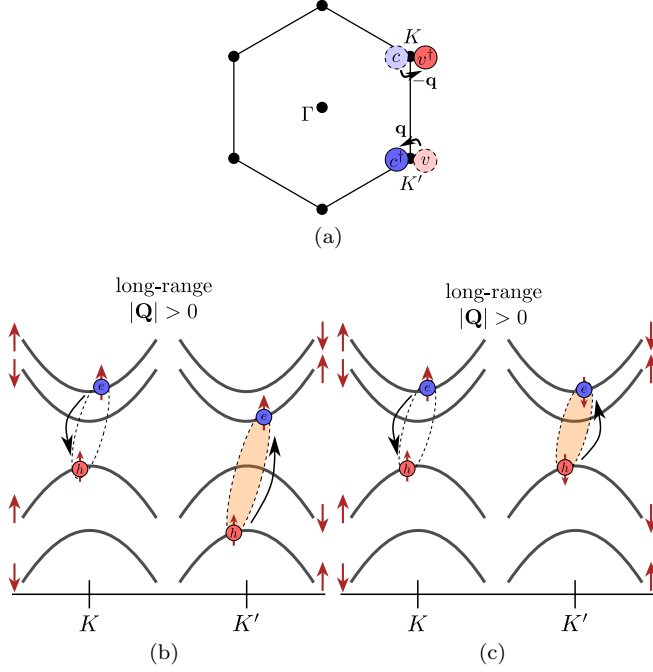


FIG. 12. Intervalley ($\xi \neq \xi'$) exchange interaction of intravalley excitons involving simultaneous $K' \rightarrow K'$ and $K \rightarrow K$ interband scattering (a): Spin-conserving ($s = s'$) valley transfer (b) and spin-flip ($s \neq s'$) valley transfer (c) via nonlocal fields ($\mathbf{G} = \mathbf{0}$) (Förster transfer), cf. Eq. (169).

Large Momentum Transfer

The exchange Hamiltonian for large momentum transfer ($\mathbf{K}^{\xi''} \neq \mathbf{0}$) is given by Eq. (159) with the condition $\xi'' \neq \Gamma$. Since the momentum transfer is already on the scale of a large valley momentum $\mathbf{K}^{\xi''}$, a distinction in short-range and long-range contributions is meaningless. Hence, we distinguish two cases as follows: Intravalley scattering between excitonic configurations in equal valleys with $\xi'' = \xi' - \xi \neq \Gamma$ and intervalley scattering with $\xi'' \neq \xi' - \xi$ and $\xi'' \neq \Gamma$ between excitonic configurations in unequal valleys.

Intravalley scattering with $\xi'' = \xi' - \xi \neq \Gamma$:

The corresponding excitonic Hamiltonian reads:

$$\hat{H}_{X-K,\text{intra}}^{\text{exch}} = \sum_{\mu,\nu,\mathbf{Q},\xi,\xi',s,s' \atop (\xi \neq \xi')} X_{K,\text{intra},\mathbf{Q},\mu,\nu}^{\xi,\xi',s,s'} \hat{P}_{\mu,\mathbf{Q}}^{\dagger\xi,\xi',s,s} \hat{P}_{\nu,\mathbf{Q}}^{\xi,\xi',s,s'}, \quad (171)$$

with matrix element:

$$X_{K,\text{intra},\mathbf{Q},\mu,\nu}^{\xi,\xi',s,s'} = \mathcal{C}_{K,\text{intra}}^{\text{exch}} V_{\mathbf{K}^{\xi'} - \mathbf{K}^{\xi}} \sum_{\mathbf{q}} \varphi_{\mu,\mathbf{q}}^{*\xi,\xi',s,s} \sum_{\mathbf{q}'} \varphi_{\nu,\mathbf{q}'}^{\xi,\xi',s,s'}. \quad (172)$$

where $\mathcal{C}_{K,\text{intra}}^{\text{exch}}$ is a correction to a simple estimate of $V_{\mathbf{K}^{\xi'} - \mathbf{K}^{\xi}}$ obtained from *ab initio* calculations:

$$\mathcal{C}_{K,\text{intra}}^{\text{exch}} = (V_{\mathbf{K}^{\xi'} - \mathbf{K}^{\xi}})^{-1} \times \sum_{\mathbf{G},\mathbf{G}'} \bar{V}_{\mathbf{Q} + \mathbf{K}^{\xi'} - \mathbf{K}^{\xi}, \mathbf{G}, \mathbf{G}'} \bar{\Upsilon}_{\mathbf{Q} + \mathbf{G}, \mathbf{0}}^{c,v,\xi,\xi',s,s'} \bar{\Upsilon}_{-\mathbf{Q} - \mathbf{G}', \mathbf{0}}^{v,c,\xi,\xi',s,s'}. \quad (173)$$

Large-momentum-transfer exchange interaction, where the corresponding electrons and holes do not change valleys ($\xi + \xi'' = \xi'$ and $\xi' - \xi'' = \xi$), occurs between all possible intervalley excitons with $\xi \neq \xi'$, cf. Eq. (171). Spin-conserving large-momentum-transfer exchange causes a blue shift of spin-bright intervalley excitons, cf. Fig. 13(c), and spin-flip large-momentum-transfer exchange couples intervalley A and B excitons, cf. Fig. 13(d), analog to the small-momentum-transfer counterpart acting on intravalley excitons, cf. Fig. 11. In particular, the spin-conserving large-momentum-transfer exchange interaction is responsible for the blue shift of the spin-bright intervalley $K, K' \uparrow, \uparrow$ exciton over the spin-dark intravalley $K, K \uparrow, \downarrow$ exciton [194–196], which would be otherwise energy-degenerate, since both conduction bands considered here, K', \uparrow and K, \downarrow have equal effective masses [84].

Intervalley scattering with $\xi'' \neq \xi' - \xi$ and $\xi'' \neq \Gamma$: The corresponding excitonic Hamiltonian reads:

$$\hat{H}_{X-K,\text{inter}}^{\text{exch}} = \sum_{\mu,\nu,\mathbf{Q},\xi,\xi',\xi'',s,s' \atop (\xi'' \neq \xi' - \xi, \xi'' \neq 0)} X_{K,\text{inter},\mathbf{Q},\mu,\nu}^{\xi,\xi',\xi'',s,s'} \hat{P}_{\mu,\mathbf{Q}}^{\dagger\xi,\xi+\xi'',s,s} \hat{P}_{\nu,\mathbf{Q}}^{\xi',\xi'',s,s'}, \quad (174)$$

with matrix element:

$$X_{K,\text{inter},\mathbf{Q},\mu,\nu}^{\xi,\xi',s,s'} = \mathcal{C}_{K,\text{inter}}^{\text{exch}} V_{\mathbf{K}^{\xi''}} \times \sum_{\mathbf{q}} \varphi_{\mu,\mathbf{q}}^{*\xi,\xi+\xi'',s,s} \sum_{\mathbf{q}'} \varphi_{\nu,\mathbf{q}'}^{\xi',\xi'',s,s'}, \quad (175)$$

where $\mathcal{C}_{K,\text{inter}}^{\text{exch}}$ is a correction to a simple estimate of $V_{\mathbf{K}^{\xi''}}$ obtained from *ab initio* calculations:

$$\mathcal{C}_{K,\text{inter}}^{\text{exch}} = (V_{\mathbf{K}^{\xi''}})^{-1} \times \sum_{\mathbf{G},\mathbf{G}'} \bar{V}_{\mathbf{Q} + \mathbf{K}^{\xi''}, \mathbf{G}, \mathbf{G}'} \bar{\Upsilon}_{\mathbf{Q} + \mathbf{G}, \mathbf{0}}^{c,v,\xi+\xi'',\xi,s,s'} \bar{\Upsilon}_{-\mathbf{Q} - \mathbf{G}', \mathbf{0}}^{v,c,\xi-\xi'',\xi,s,s'}. \quad (176)$$

On the other hand, large-momentum-transfer exchange interaction, where the corresponding electrons and holes change valleys ($\xi + \xi'' \neq \xi'$ and $\xi' - \xi'' \neq \xi$), occurs between the following spin-bright intervalley excitons, if we restrict ourselves to the energetically lowest holes at the

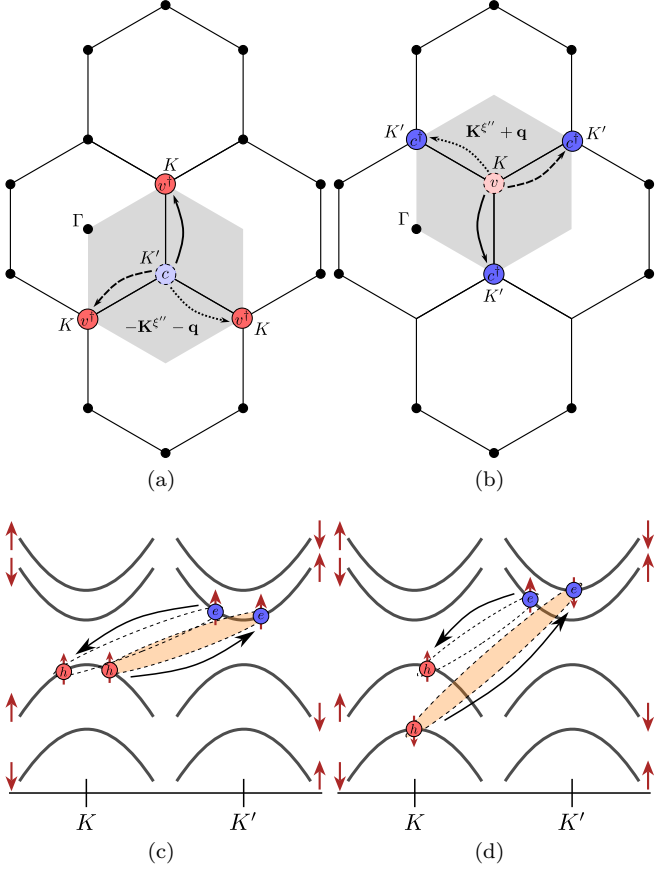


FIG. 13. Example scattering channel of intravalley exchange interaction $\xi'' = \xi' - \xi$ of intervalley excitons ($\xi \neq \xi'$) involving simultaneous $K \leftrightarrow K'$ interband scattering (a). (b): Three equivalent processes. Corresponding example spin-conserving ($s = s'$) (c) and spin-flip ($s \neq s'$) (d) process in the excitonic picture, cf. Eq. (171).

K , K' and Γ valleys and the electrons to the energetically lowest K , K' and Λ , Λ' valleys:

$$\begin{aligned} K-K' &\leftrightarrow \Gamma-K, \\ K'-K &\leftrightarrow \Gamma-K', \\ K-\Lambda &\leftrightarrow \Gamma-\Lambda', \\ K'-\Lambda' &\leftrightarrow \Gamma-\Lambda. \end{aligned} \quad (177)$$

These processes cause an energy transfer between distinct valleys, cf. Fig. 14, where we depict the spin-flip process $K-K' \rightarrow \Gamma-K$ exemplarily, which involves three equivalent processes analog to the charge-transfer process in Fig. 9. This process is expected to be of minor importance, since the large valley-momentum transfer and the exchange nature strongly suppress the magnitude of this process compared to other scattering processes. However, it can contribute to a slight acceleration of the valley depolarization process in dark materials such as monolayer WS₂ or WSe₂ [43], but no simulation has explicitly considered this process up to now.

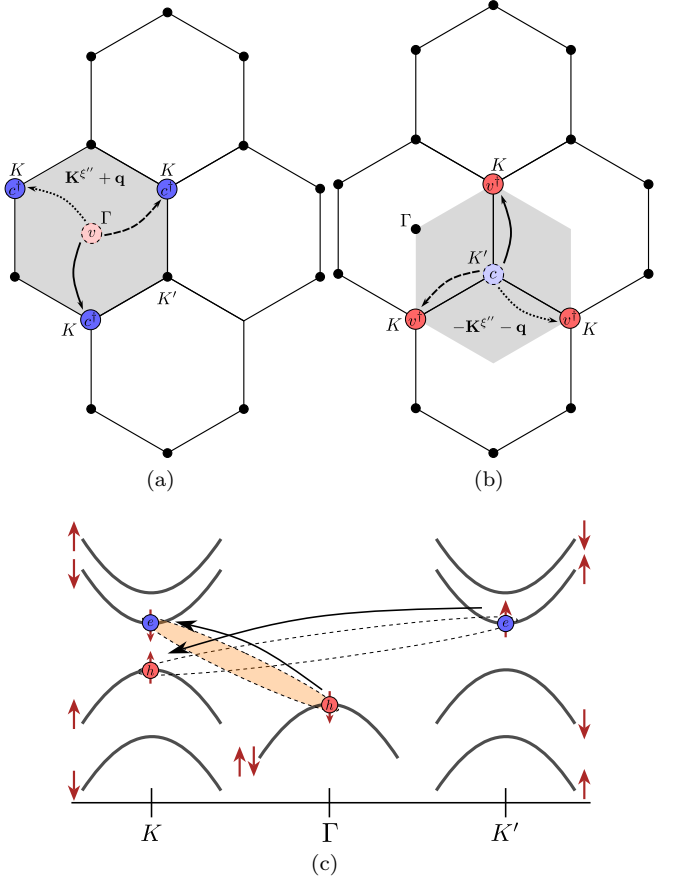


FIG. 14. Example scattering channel of intervalley exchange interaction ($\xi'' \neq \Gamma$) of intervalley excitons ($\xi'' \neq \xi' - \xi$) involving simultaneous $\Gamma \rightarrow K$ and $K' \rightarrow K$ and interband scattering (a) and (b): Three equivalent processes. Corresponding example spin-flip process ($s \neq s'$) in the excitonic picture, cf. Eq. (174).

VI. CONCLUSION

In this manuscript, we reviewed and discussed the second-quantized Coulomb interaction between Bloch electrons in 2D-confined semiconductors as a starting point for exciton quantum kinetics in a Heisenberg-equations-of-motion approach. We derived the many-body Coulomb interaction including all Umklapp processes, discussed the origin of microscopic screening and reviewed an effective macroscopic approach to screening including the dielectric environment for practical calculations. Further, we discussed the binding of electron-hole pairs, i.e., excitons, described by the Bethe-Salpeter equation and its few-band effective-mass manifestation, the Wannier equation in undoped semiconductors. At last, we provided a comprehensive discussion of all exciton-scattering processes relevant in the density-independent limit.

ACKNOWLEDGMENTS

Funded by the Deutsche Forschungsgemeinschaft (DFG, German Research Foundation) – Project No. 420760124 (H.M., A.K.); 556436549 (A.K.). H.M. acknowledges funding by project 21209528 (“proof of trust”). T.D. acknowledges financial support from the Deutsche Forschungsgemeinschaft (DFG, German Research Foundation) through Project No. 426726249 (DE 2749/2-1 and DE 2749/2-2).

H.M. thanks Alexander Steinhoff (Universität Oldenburg), Jonas Grumm (Technische Universität Berlin), Robert Lemke (Technische Universität Berlin) and Michiel Snoeken (Technische Universität Berlin) for fruitful discussions.

Appendix A: Supercell Hamiltonian

In this section, we derive the Coulomb Hamiltonian, which directly uses Bloch functions obtained from *ab initio* calculations using supercells. Since the Hamiltonian always describes the total system of interest in the first place, we need a description capturing the common *ab initio* supercell-setup with many layers, which is then reduced to a single-layer description as a starting point for practical quantum-kinetical calculations. For reasons of simplicity, we assume a static screening. Implementing a time-dependent dynamical screening as in Eq. (29) is straightforward.

The general Hamiltonian reads:

$$H_{\text{Coul}} = \frac{1}{2} \int d^2 r_{\parallel} dz d^2 r'_{\parallel} dz' \rho(\mathbf{r}_{\parallel}, z) G(\mathbf{r}_{\parallel}, \mathbf{r}'_{\parallel}, z, z') \rho(\mathbf{r}'_{\parallel}, z'). \quad (\text{A1})$$

The field operator reads:

$$\hat{\Psi}(\mathbf{r}_{\parallel}, z, t) = \sum_{\lambda, \mathbf{k}_{\parallel}, k_z, s} \psi_{\lambda, \mathbf{k}_{\parallel}, k_z}^s(\mathbf{r}_{\parallel}, z) \chi_s \hat{a}_{\lambda, \mathbf{k}_{\parallel}, k_z}^s(t), \quad (\text{A2})$$

where:

$$\psi_{\lambda, \mathbf{k}_{\parallel}, k_z}^s(\mathbf{r}_{\parallel}, z) = \frac{1}{\sqrt{\mathcal{A}L_z}} e^{i\mathbf{k}_{\parallel} \cdot \mathbf{r}_{\parallel}} e^{ik_z z} u_{\lambda, \mathbf{k}_{\parallel}, k_z}^s(\mathbf{r}_{\parallel}, z) \quad (\text{A3})$$

is the Bloch function of a three-dimensional lattice. To obtain a layer-resolved description, we Fourier expand the creation/annihilation operators as follows:

$$\hat{a}_{\lambda, \mathbf{k}_{\parallel}, k_z}^s = \frac{L_z}{N_z} \sum_{\ell} e^{-ik_z \ell} \hat{a}_{\lambda, \mathbf{k}_{\parallel}}^{\ell, s}, \quad (\text{A4})$$

where ℓ is a lattice vector in z -direction, L_z is the total lattice length in z -direction and N_z is the number of unit cells in z -direction. The field operator then becomes:

$$\hat{\Psi}(\mathbf{r}_{\parallel}, z, t) = \frac{\sqrt{L_z}}{\sqrt{\mathcal{A}N_z}} \sum_{\lambda, \mathbf{k}_{\parallel}, \ell, s} \chi_s e^{i\mathbf{k}_{\parallel} \cdot \mathbf{r}_{\parallel}} u_{\lambda, \mathbf{k}_{\parallel}}^{\ell, s}(\mathbf{r}_{\parallel}, z) \hat{a}_{\lambda, \mathbf{k}_{\parallel}}^{\ell, s}(t), \quad (\text{A5})$$

where:

$$u_{\lambda, \mathbf{k}_{\parallel}}^{\ell, s}(\mathbf{r}_{\parallel}, z) = \frac{1}{\sqrt{N_z}} \sum_{k_z} e^{ik_z(z-\ell)} u_{\lambda, \mathbf{k}_{\parallel}, k_z}^s(\mathbf{r}_{\parallel}, z), \quad (\text{A6})$$

with normalization condition:

$$\frac{1}{L_z} \int dz u_{\lambda, \mathbf{k}_{\parallel}}^{*\ell, s}(\mathbf{r}_{\parallel}, z) u_{\lambda, \mathbf{k}_{\parallel}}^{\ell', s}(\mathbf{r}_{\parallel}, z) = \delta_{\ell, \ell'}. \quad (\text{A7})$$

Hence, the expansion in Eq. (A5) constitutes a Bloch-state representation in the in-plane direction \mathbf{r}_{\parallel} and Wannier-state representation in the out-of-plane direction z . The Coulomb Hamiltonian becomes:

$$\begin{aligned} \hat{H}_{\text{Coul}} = & \frac{e^2 L_z^2}{2\mathcal{A}^2 N_z^2 \mathcal{A} L_z} \sum_{\substack{\lambda_1 \dots \lambda_4, \mathbf{k}_{\parallel 1} \dots \mathbf{k}_{\parallel 4}, \\ \ell_1 \dots \ell_4, \mathbf{q}_{\parallel}, \mathbf{G}_{\parallel}, \mathbf{G}'_{\parallel}, \\ q_z, G_z, G'_z, s, s'}} \\ & \times \int d^2 r_{\parallel} dz e^{i(\mathbf{k}_{\parallel 4} - \mathbf{k}_{\parallel 1} + \mathbf{q}_{\parallel} + \mathbf{G}_{\parallel}) \cdot \mathbf{r}_{\parallel}} \\ & \times u_{\lambda_1, \mathbf{k}_{\parallel 1}}^{*\ell_1, s}(\mathbf{r}_{\parallel}, z) u_{\lambda_4, \mathbf{k}_{\parallel 4}}^{\ell_4, s}(\mathbf{r}_{\parallel}, z) e^{i(q_z + G_z)z} \\ & \times \int d^2 r'_{\parallel} dz' e^{i(\mathbf{k}_{\parallel 3} - \mathbf{k}_{\parallel 2} - \mathbf{q}_{\parallel} - \mathbf{G}_{\parallel}) \cdot \mathbf{r}'_{\parallel}} u_{\lambda_2, \mathbf{k}_{\parallel 2}}^{*\ell_2, s'}(\mathbf{r}'_{\parallel}, z') \\ & \times u_{\lambda_3, \mathbf{k}_{\parallel 3}}^{\ell_3, s'}(\mathbf{r}'_{\parallel}, z') e^{-i(q_z + G'_z)z'} \\ & \times G_{\mathbf{q}_{\parallel}, \mathbf{G}_{\parallel}, \mathbf{G}'_{\parallel}, q_z, G_z, G'_z} \hat{a}_{\lambda_1, \mathbf{k}_{\parallel 1}}^{\dagger, \ell_1, s} \hat{a}_{\lambda_2, \mathbf{k}_{\parallel 2}}^{\dagger, \ell_2, s'} \hat{a}_{\lambda_3, \mathbf{k}_{\parallel 3}}^{\ell_3, s'} \hat{a}_{\lambda_4, \mathbf{k}_{\parallel 4}}^{\ell_4, s}. \end{aligned} \quad (\text{A8})$$

Evaluate the form factors:

$$\begin{aligned} & \frac{1}{\mathcal{A} L_z} \int d^2 r_{\parallel} dz e^{i(\mathbf{k}_{\parallel 4} - \mathbf{k}_{\parallel 1} + \mathbf{q}_{\parallel} + \mathbf{G}_{\parallel}) \cdot \mathbf{r}_{\parallel}} \\ & \times u_{\lambda_1, \mathbf{k}_{\parallel 1}}^{*\ell_1, s}(\mathbf{r}_{\parallel}, z) u_{\lambda_4, \mathbf{k}_{\parallel 4}}^{\ell_4, s}(\mathbf{r}_{\parallel}, z) e^{i(q_z + G_z)z} = \\ & \frac{1}{N_z} \sum_{\mathbf{G}_{\parallel}''} \delta_{\mathbf{G}_{\parallel}'' + \mathbf{k}_{\parallel 4} + \mathbf{q}_{\parallel} - \mathbf{k}_{\parallel 1}} e^{iq_z \ell_1} \sum_{q'_z, \mathbf{G}_{\parallel 1}, G_z, 1} e^{iq'_z(\ell_1 - \ell_4)} \\ & \times u_{\lambda_1, \mathbf{k}_{\parallel 4} + \mathbf{q}_{\parallel}, q'_z + q_z, \mathbf{G}_{\parallel 1}, \mathbf{G}_{\parallel 1} + G_z, G_{z, 1} + G_z}^s u_{\lambda_4, \mathbf{k}_{\parallel 4}, q'_z, \mathbf{G}_{\parallel 1}, G_{z, 1}}^s. \end{aligned} \quad (\text{A9})$$

Now, we assume, that the Bloch factors depend only weakly on q_z :

$$u_{\lambda, \mathbf{k}_{\parallel}, q_z, \mathbf{G}_{\parallel}, G_z}^s \approx u_{\lambda, \mathbf{k}_{\parallel}, 0, \mathbf{G}_{\parallel}, G_z}^s \equiv u_{\lambda, \mathbf{k}_{\parallel}, \mathbf{G}_{\parallel}, G_z}^s, \quad (\text{A10})$$

which is a good approximation, since the allowed q_z -values are already small if the supercell length $L_{z, \text{SC}}$ is chosen as correspondingly large, i.e., most of the spatial variation in the out-of-plane direction occurs *within* the supercell. In addition, many DFT codes provide the dominant $q_z = 0$ -components only. We then can perform

the q'_z -sum and obtain:

$$\begin{aligned} & \frac{1}{\mathcal{A}L_z} \int d^2r_{\parallel} dz e^{i(\mathbf{k}_{\parallel 4}-\mathbf{k}_{\parallel 1}+\mathbf{q}_{\parallel}+\mathbf{G}_{\parallel}) \cdot \mathbf{r}_{\parallel}} \\ & \times u_{\lambda_1, \mathbf{k}_{\parallel 1}}^{*, \ell_1, s}(\mathbf{r}_{\parallel}, z) u_{\lambda_4, \mathbf{k}_{\parallel 4}}^{\ell_4, s}(\mathbf{r}_{\parallel}, z) e^{i(q_z+G_z)z} = \\ & \sum_{\mathbf{G}_{\parallel}''} \delta_{\mathbf{G}_{\parallel}'' \cdot \mathbf{k}_{\parallel 4} + \mathbf{q}_{\parallel} - \mathbf{k}_{\parallel 1}} e^{iq_z \ell_1} \delta_{\ell_1, \ell_4} \\ & \times \sum_{\mathbf{G}_{\parallel 1}, G_{z,1}} u_{\lambda_1, \mathbf{k}_{\parallel 4} + \mathbf{q}_{\parallel}, \mathbf{G}_{\parallel 1} + \mathbf{G}_{\parallel}, G_{z,1} + G_z}^{*, s} u_{\lambda_4, \mathbf{k}_{\parallel 4}, \mathbf{G}_{\parallel 1}, G_{z,1}}^s, \end{aligned} \quad (\text{A11})$$

i.e., now only if $\ell_1 = \ell_4$ the form factor is nonzero. The multi-layer Coulomb Hamiltonian then becomes:

$$\begin{aligned} \hat{H}_{\text{Coul}} = & \frac{1}{2} \frac{L_z^4}{N_z^2} \sum_{\substack{\lambda, \lambda', \mathbf{k}_{\parallel}, \mathbf{k}'_{\parallel}, \\ \ell, \ell', \mathbf{q}_{\parallel}, \mathbf{G}_{\parallel}, \mathbf{G}'_{\parallel}, s, s'}} \\ & \times \sum_{G_z, G'_z} \bar{\Upsilon}_{\mathbf{k}_{\parallel} + \mathbf{q}_{\parallel} + \mathbf{G}_{\parallel}, \mathbf{k}_{\parallel}, G_z, 0}^{\text{sc} \lambda_1, \lambda_4, s} \bar{\Upsilon}_{\mathbf{k}'_{\parallel} - \mathbf{q}_{\parallel} - \mathbf{G}'_{\parallel}, \mathbf{k}'_{\parallel}, -G'_z, 0}^{\text{sc} \lambda_2, \lambda_3, s'} \\ & \times V_{\mathbf{q}_{\parallel}, \mathbf{G}_{\parallel}, \mathbf{G}'_{\parallel}, G_z, G'_z}^{\ell, \ell'} \hat{a}_{\lambda_1, \mathbf{k}_{\parallel} + \mathbf{q}_{\parallel}}^{\dagger, \ell, s} \hat{a}_{\lambda_2, \mathbf{k}'_{\parallel} - \mathbf{q}_{\parallel}}^{\dagger, \ell', s'} \hat{a}_{\lambda_3, \mathbf{k}_{\parallel}}^{\ell', s'} \hat{a}_{\lambda_4, \mathbf{k}_{\parallel}}^{\ell, s}, \end{aligned} \quad (\text{A12})$$

where $\bar{\Upsilon}_{\mathbf{k}_{\parallel}, \mathbf{k}'_{\parallel}, G_z, 0}^{\text{sc} \lambda, \lambda', s}$ is the (reduced) supercell form factor:

$$\begin{aligned} & \bar{\Upsilon}_{\mathbf{k}_{\parallel}, \mathbf{k}'_{\parallel}, G_z, G'_z}^{\text{sc} \lambda, \lambda', s} \\ = & \sum_{\mathbf{G}_{\parallel 1}, G_{z,1}} u_{\lambda, \mathbf{k}_{\parallel}, 0, \mathbf{G}_{\parallel 1}, G_{z,1} + G_z}^{*, s} u_{\lambda', \mathbf{k}'_{\parallel}, 0, \mathbf{G}_{\parallel 1}, G_{z,1} + G'_z}^s, \end{aligned} \quad (\text{A13})$$

and $V_{\mathbf{q}_{\parallel}, \mathbf{G}_{\parallel}, \mathbf{G}'_{\parallel}, G_z, G'_z}^{\ell, \ell'}$ is the layer-resolved Coulomb potential:

$$\begin{aligned} V_{\mathbf{q}_{\parallel}, \mathbf{G}_{\parallel}, \mathbf{G}'_{\parallel}, G_z, G'_z}^{\ell, \ell'} = & \sum_{q_z} e^{iq_z(\ell - \ell')} V_{\mathbf{q}_{\parallel}, \mathbf{G}_{\parallel}, \mathbf{G}'_{\parallel}, q_z, G_z, G'_z} \\ = & \sum_{q_z} e^{iq_z(\ell - \ell')} \frac{e^2}{\mathcal{A}L_z} G_{\mathbf{q}_{\parallel}, \mathbf{G}_{\parallel}, \mathbf{G}'_{\parallel}, q_z, G_z, G'_z}. \end{aligned} \quad (\text{A14})$$

Note, that the prefactor $\frac{L_z^4}{N_z^2}$ in Eq. (A12) arises due to the Fourier expansion in k_z , cf. Eq. (A4), which entails layer-resolved operators in units of one over length, i.e., $[\hat{a}^{(\dagger)}_{\lambda, \mathbf{k}_{\parallel}}]^{\ell, s} = \text{nm}^{-1}$. For the Green's function, it holds:

$$\begin{aligned} & G_{\mathbf{q}_{\parallel}, \mathbf{G}_{\parallel}, \mathbf{G}'_{\parallel}, q_z, G_z, G'_z} \\ = & (\varepsilon_{\text{mic}}^{-1})_{\mathbf{q}_{\parallel}, \mathbf{G}_{\parallel}, \mathbf{G}'_{\parallel}, q_z, G_z, G'_z} G_{0, \mathbf{q}_{\parallel} + \mathbf{G}'_{\parallel}, q_z + G'_z}. \end{aligned} \quad (\text{A15})$$

To obtain the monolayer limit without image charge interactions from the other layers, i.e., supercells, we apply a truncated Coulomb potential:

$$G_{0, \mathbf{q}_{\parallel}}(z) \rightarrow G_{0, \mathbf{q}_{\parallel}}^{\text{trunc}}(z) = \frac{e^{-|\mathbf{q}_{\parallel}| |z|}}{2\epsilon_0 |\mathbf{q}_{\parallel}|} \Theta\left(z + \frac{\Omega_z}{2}\right) \Theta\left(\frac{\Omega_z}{2} - z\right). \quad (\text{A16})$$

In reciprocal space, this transforms to:

$$G_{0, \mathbf{q}_{\parallel} + \mathbf{G}_{\parallel}, q_z + G_z}^{\text{trunc}} = \frac{1 - e^{-|\mathbf{q}_{\parallel} + \mathbf{G}_{\parallel}| \frac{\Omega_z}{2}} \cos((q_z + G_z) \frac{\Omega_z}{2})}{\epsilon_0 (|\mathbf{q}_{\parallel} + \mathbf{G}_{\parallel}|^2 + (q_z + G_z)^2)}. \quad (\text{A17})$$

Since q_z is small, we can safely assume, that the Green's function does not depend on it (similar argument as above):

$$\begin{aligned} G_{\mathbf{q}_{\parallel}, \mathbf{G}_{\parallel}, \mathbf{G}'_{\parallel}, q_z, G_z, G'_z}^{\text{trunc}} \approx & G_{\mathbf{q}_{\parallel}, \mathbf{G}_{\parallel}, \mathbf{G}'_{\parallel}, 0, G_z, G'_z}^{\text{trunc}} \\ \equiv & G_{\mathbf{q}_{\parallel}, \mathbf{G}_{\parallel}, \mathbf{G}'_{\parallel}, G_z, G'_z}^{\text{trunc}}. \end{aligned} \quad (\text{A18})$$

Hence, the layer-resolved Coulomb potential becomes:

$$\begin{aligned} V_{\mathbf{q}_{\parallel}, \mathbf{G}_{\parallel}, \mathbf{G}'_{\parallel}, G_z, G'_z}^{\ell, \ell'} \rightarrow & V_{\mathbf{q}_{\parallel}, \mathbf{G}_{\parallel}, \mathbf{G}'_{\parallel}, G_z, G'_z}^{\ell, \ell', \text{trunc}} \\ \approx & N_z \delta_{\ell, \ell'} V_{\mathbf{q}_{\parallel}, \mathbf{G}_{\parallel}, \mathbf{G}'_{\parallel}, G_z, G'_z}^{\text{trunc}}, \end{aligned} \quad (\text{A19})$$

where:

$$V_{\mathbf{q}_{\parallel}, \mathbf{G}_{\parallel}, \mathbf{G}'_{\parallel}, G_z, G'_z}^{\text{trunc}} = \frac{e^2}{\mathcal{A}L_z} G_{\mathbf{q}_{\parallel}, \mathbf{G}_{\parallel}, \mathbf{G}'_{\parallel}, G_z, G'_z}^{\text{trunc}}. \quad (\text{A20})$$

Now, interlayer, i.e., inter-supercell and, hence, unwanted, Coulomb interactions are removed. We obtain:

$$\begin{aligned} \hat{H}_{\text{Coul}} = & \frac{1}{2} \frac{L_z^4}{N_z} \sum_{\substack{\lambda, \lambda', \mathbf{k}_{\parallel}, \mathbf{k}'_{\parallel}, \\ \ell, \mathbf{q}_{\parallel}, \mathbf{G}_{\parallel}, \mathbf{G}'_{\parallel}, s, s'}} \sum_{G_z, G'_z} \bar{\Upsilon}_{\mathbf{k}_{\parallel} + \mathbf{q}_{\parallel} + \mathbf{G}_{\parallel}, \mathbf{k}_{\parallel}, G_z, 0}^{\text{sc} \lambda_1, \lambda_4, s} \\ & \times \bar{\Upsilon}_{\mathbf{k}'_{\parallel} - \mathbf{q}_{\parallel} - \mathbf{G}'_{\parallel}, \mathbf{k}'_{\parallel}, -G'_z, 0}^{\text{sc} \lambda_2, \lambda_3, s'} V_{\mathbf{q}_{\parallel}, \mathbf{G}_{\parallel}, \mathbf{G}'_{\parallel}, G_z, G'_z}^{\text{trunc}} \\ & \times \hat{a}_{\lambda_1, \mathbf{k}_{\parallel} + \mathbf{q}_{\parallel}}^{\dagger, \ell, s} \hat{a}_{\lambda_2, \mathbf{k}'_{\parallel} - \mathbf{q}_{\parallel}}^{\dagger, \ell', s'} \hat{a}_{\lambda_3, \mathbf{k}_{\parallel}}^{\ell', s'} \hat{a}_{\lambda_4, \mathbf{k}_{\parallel}}^{\ell, s}. \end{aligned} \quad (\text{A21})$$

By rescaling $L_z \hat{a}_{\lambda, \mathbf{k}_{\parallel}}^{(\dagger) \ell, s} \rightarrow \hat{a}_{\lambda, \mathbf{k}_{\parallel}}^{(\dagger) \ell, s}$, which retrieves unitless creation/annihilation operators, and dropping the layer index ℓ completely, as there are no interlayer interactions anymore, so that the layer-sum disappears: $\frac{1}{N_z} \sum_{\ell} = 1$, we obtain:

$$\begin{aligned} \hat{H}_{\text{Coul}} = & \frac{1}{2} \sum_{\lambda, \lambda', \mathbf{k}_{\parallel}, \mathbf{k}'_{\parallel}, \mathbf{q}_{\parallel}, \mathbf{G}_{\parallel}, \mathbf{G}'_{\parallel}, s, s'} \sum_{G_z, G'_z} V_{\mathbf{q}_{\parallel}, \mathbf{G}_{\parallel}, \mathbf{G}'_{\parallel}, G_z, G'_z}^{\text{trunc}} \\ & \times \bar{\Upsilon}_{\mathbf{k}_{\parallel} + \mathbf{q}_{\parallel} + \mathbf{G}_{\parallel}, \mathbf{k}_{\parallel}, G_z, 0}^{\text{sc} \lambda_1, \lambda_4, s} \bar{\Upsilon}_{\mathbf{k}'_{\parallel} - \mathbf{q}_{\parallel} - \mathbf{G}'_{\parallel}, \mathbf{k}'_{\parallel}, -G'_z, 0}^{\text{sc} \lambda_2, \lambda_3, s'} \\ & \times \hat{a}_{\lambda_1, \mathbf{k}_{\parallel} + \mathbf{q}_{\parallel}}^{\dagger, s} \hat{a}_{\lambda_2, \mathbf{k}'_{\parallel} - \mathbf{q}_{\parallel}}^{\dagger, s'} \hat{a}_{\lambda_3, \mathbf{k}_{\parallel}}^{\ell, s'} \hat{a}_{\lambda_4, \mathbf{k}_{\parallel}}^{\ell, s}. \end{aligned} \quad (\text{A22})$$

Eq. (A22) is the final second-quantized many-body Coulomb Hamiltonian, which directly uses Bloch factors and dielectric functions obtained from *ab initio* supercell calculations as input quantities.

Appendix B: Fourier Transformation in Periodic Lattices

In this section, we provide all relevant conventions and relations.

General Fourier transformation of an arbitrary function f with respect to time domain t and frequency domain ω :

$$f(t) = \frac{1}{2\pi} \int d\omega e^{-i\omega t} f(\omega), \quad f(\omega) = \int dt e^{i\omega t} f(t). \quad (\text{B1})$$

General Fourier transformation of an arbitrary function f with respect to real space \mathbf{r} and momentum space \mathbf{k} :

$$f(\mathbf{r}) = \frac{1}{(2\pi)^n} \int d^n k e^{i\mathbf{k}\cdot\mathbf{r}} f_{\mathbf{k}}, \quad f_{\mathbf{k}} = \int d^n r e^{-i\mathbf{k}\cdot\mathbf{r}} f(\mathbf{r}), \quad (\text{B2})$$

where n denotes the dimensionality.

Discrete Fourier series within Born-von Kármán boundary conditions [68]:

$$f(\mathbf{R}) = \frac{1}{\mathcal{V}_n} \sum_{\mathbf{q}} e^{i\mathbf{q}\cdot\mathbf{R}} f_{\mathbf{q}}, \quad f_{\mathbf{q}} = \frac{\mathcal{V}_n}{\mathcal{N}} \sum_{\mathbf{R}} e^{-i\mathbf{q}\cdot\mathbf{R}} f(\mathbf{R}), \quad (\text{B3})$$

where \mathbf{q} is a crystal momentum in the first Brillouin zone and \mathbf{R} is a lattice vector, \mathcal{N} is the total number of unit cells and \mathcal{V}_n is the n -dimensional volume of the total lattice. In the main text, we denote: $\mathcal{V}_{n=1} \equiv L$, $\mathcal{V}_{n=2} \equiv \mathcal{A}$ and $\mathcal{V}_{n=3} \equiv \mathcal{V}$. From Eq. (B3), it follows:

$$\begin{aligned} \frac{1}{\mathcal{N}} \sum_{\mathbf{R}} e^{i\mathbf{R}\cdot(\mathbf{q}-\mathbf{q}')} &= \delta_{\mathbf{q},\mathbf{q}'}, \\ \frac{1}{\mathcal{N}} \sum_{\mathbf{q}} e^{i\mathbf{q}\cdot(\mathbf{R}-\mathbf{R}')} &= \delta_{\mathbf{R},\mathbf{R}'}, \end{aligned} \quad (\text{B4})$$

and:

$$\begin{aligned} \frac{1}{\mathcal{V}_{n,UC}} \sum_{\mathbf{G}} e^{i\mathbf{G}\cdot\mathbf{r}} &= \sum_{\mathbf{R}} \delta(\mathbf{r}-\mathbf{R}), \\ \frac{1}{\mathcal{V}_{n,UC}} \int_{\mathcal{V}_{n,UC}} d^3 r e^{i(\mathbf{G}-\mathbf{G}')\cdot\mathbf{r}} &= \delta_{\mathbf{G},\mathbf{G}'}. \end{aligned} \quad (\text{B5})$$

Here, $\mathcal{V}_{n,UC}$ is the n -dimensional volume of the unit cell.

By expanding the arbitrary momentum \mathbf{k} in Eq. (B2) via $\mathbf{k} = \mathbf{q} + \mathbf{G}$, where \mathbf{q} is a momentum within the first Brillouin zone and \mathbf{G} is a reciprocal lattice vector, we can rewrite Eq. (B2):

$$f(\mathbf{r}) = \frac{1}{(2\pi)^n} \sum_{\mathbf{G}} \int_{\mathcal{V}_{n,BZ}} d^n q e^{i(\mathbf{q}+\mathbf{G})\cdot\mathbf{r}} f_{\mathbf{q}+\mathbf{G}}. \quad (\text{B6})$$

By using the conversion relation between discrete sums and integrals, which is valid as long as the crystal momenta \mathbf{q} lie sufficiently dense in the first Brillouin zone

[56]:

$$\sum_{\mathbf{q}} f_{\mathbf{q}} \leftrightarrow \frac{\mathcal{V}_n}{(2\pi)^n} \int_{\mathcal{V}_{n,BZ}} d^n q f_{\mathbf{q}}, \quad (\text{B7})$$

where $\mathcal{V}_{n,BZ}$ denotes the n -dimensional volume of the Brillouin zone (unit cell of the reciprocal lattice), we obtain:

$$f(\mathbf{r}) = \frac{1}{\mathcal{V}_n} \sum_{\mathbf{q},\mathbf{G}} e^{i(\mathbf{q}+\mathbf{G})\cdot\mathbf{r}} f_{\mathbf{q}+\mathbf{G}}. \quad (\text{B8})$$

The back transformation can be expressed as:

$$f_{\mathbf{q}+\mathbf{G}} = \sum_{\mathbf{R}} e^{-i(\mathbf{q}+\mathbf{G})\cdot\mathbf{R}} \int_{\mathcal{V}_{n,UC}} d^n r e^{-i(\mathbf{q}+\mathbf{G})\cdot\mathbf{r}} f(\mathbf{r}+\mathbf{R}). \quad (\text{B9})$$

If the function $f(\mathbf{r})$ is lattice periodic:

$$f(\mathbf{r}+\mathbf{R}) = f(\mathbf{r}), \quad (\text{B10})$$

the following relations hold:

$$f(\mathbf{r}) = \sum_{\mathbf{G}} e^{i\mathbf{G}\cdot\mathbf{r}} f_{\mathbf{G}}, \quad f_{\mathbf{G}} = \frac{1}{\mathcal{V}_{UC}} \int_{\mathcal{V}_{n,UC}} d^n r e^{-i\mathbf{G}\cdot\mathbf{r}} f(\mathbf{r}), \quad (\text{B11})$$

where we identified: $f_{\mathbf{q}+\mathbf{G}} \equiv f_{\mathbf{G}} \mathcal{V}_n \delta_{\mathbf{q},\mathbf{0}}$.

An arbitrary function with two arguments $f(\mathbf{r}, \mathbf{r}')$ can be Fourier expanded accordingly:

$$f(\mathbf{r}, \mathbf{r}') = \frac{1}{\mathcal{V}_n^2} \sum_{\mathbf{q}, \mathbf{G}, \mathbf{q}', \mathbf{G}'} e^{i(\mathbf{q}+\mathbf{G})\cdot\mathbf{r}} e^{i(\mathbf{q}'+\mathbf{G}')\cdot\mathbf{r}'} f_{\mathbf{q}, \mathbf{q}', \mathbf{G}, \mathbf{G}'}, \quad (\text{B12})$$

with back transformation:

$$\begin{aligned} f_{\mathbf{q}, \mathbf{q}', \mathbf{G}, \mathbf{G}'} &= \sum_{\mathbf{R}, \mathbf{R}'} e^{-i(\mathbf{q}+\mathbf{G})\cdot\mathbf{R}} e^{-i(\mathbf{q}'+\mathbf{G}')\cdot\mathbf{R}'} \\ &\times \int_{\mathcal{V}_{n,UC}} d^n r d^n r' e^{-i(\mathbf{q}+\mathbf{G})\cdot\mathbf{r}} e^{-i(\mathbf{q}'+\mathbf{G}')\cdot\mathbf{r}'} f(\mathbf{r}+\mathbf{R}, \mathbf{r}'+\mathbf{R}'). \end{aligned} \quad (\text{B13})$$

In case that the function $f(\mathbf{r}, \mathbf{r}')$ is lattice-periodic:

$$f(\mathbf{r}+\mathbf{R}, \mathbf{r}'+\mathbf{R}) = f(\mathbf{r}, \mathbf{r}'), \quad (\text{B14})$$

the Fourier expansion can be expressed as follows:

$$f(\mathbf{r}, \mathbf{r}') = \frac{1}{\mathcal{V}_n} \sum_{\mathbf{q}, \mathbf{G}, \mathbf{G}'} e^{i(\mathbf{q}+\mathbf{G})\cdot\mathbf{r}} e^{-i(\mathbf{q}+\mathbf{G}')\cdot\mathbf{r}'} f_{\mathbf{q}, \mathbf{G}, \mathbf{G}'}, \quad (\text{B15})$$

where we identified: $f_{\mathbf{q}, \mathbf{q}', \mathbf{G}, \mathbf{G}'} \equiv f_{\mathbf{q}, \mathbf{G}, -\mathbf{G}'} \mathcal{V}_n \delta_{\mathbf{q}, -\mathbf{q}'}$. Exploiting the lattice-periodicity of $f(\mathbf{r}, \mathbf{r}')$, the back transformation then reads:

$$\begin{aligned} f_{\mathbf{q}, \mathbf{G}, \mathbf{G}'} &= \frac{1}{\mathcal{V}_{n,UC}} \sum_{\mathbf{R}} e^{i\mathbf{q}\cdot\mathbf{R}} \\ &\times \int_{\mathcal{V}_{n,UC}} d^n r d^n r' e^{-i(\mathbf{q}+\mathbf{G})\cdot\mathbf{r}} e^{i(\mathbf{q}+\mathbf{G}')\cdot\mathbf{r}'} f(\mathbf{r}, \mathbf{r}'+\mathbf{R}). \end{aligned} \quad (\text{B16})$$

The Dirac delta distributions for arbitrary momenta \mathbf{k} and arbitrary spatial coordinates \mathbf{r} read:

$$\frac{1}{(2\pi)^n} \int d^n r e^{i\mathbf{k}\cdot\mathbf{r}} = \delta(\mathbf{k}), \quad \frac{1}{(2\pi)^n} \int d^n k e^{i\mathbf{k}\cdot\mathbf{r}} = \delta(\mathbf{r}). \quad (B17)$$

By expanding the spatial coordinates over the unit cells and the momenta over the Brillouin zones, we obtain:

$$\frac{1}{(2\pi)^n} \int d^n r e^{i(\mathbf{q}+\mathbf{G})\cdot\mathbf{r}} = \frac{\mathcal{V}_n}{(2\pi)^n} \delta_{\mathbf{q},\mathbf{0}} \delta_{\mathbf{G},\mathbf{0}} \quad (\mathbf{q} \in \mathcal{V}_{n,\text{BZ}}), \quad (B18)$$

$$\frac{1}{(2\pi)^n} \int d^n k e^{i\mathbf{k}\cdot(\mathbf{r}+\mathbf{R})} = \delta(\mathbf{r}) \delta_{\mathbf{R},\mathbf{0}} \quad (\mathbf{r} \in \mathcal{V}_{n,\text{UC}}). \quad (B19)$$

Hence, for a momentum \mathbf{q} within the first Brillouin zone, the following relation between the continuous Dirac delta function defined under integrals and the discrete Kronecker delta defined under sums can be obtained:

$$\delta(\mathbf{q}) \leftrightarrow \frac{\mathcal{V}_n}{(2\pi)^n} \delta_{\mathbf{q},\mathbf{0}} \quad (\mathbf{q} \in \mathcal{V}_{n,\text{BZ}}), \quad (B20)$$

cf. also Eq. (B7).

Appendix C: Parameters

1s excitonic energy $E_{A_{1s}}$	1.639 eV [197]
Nonradiative linewidth $\hbar\gamma_{\text{nrad},A_{1s}}$	10 meV
Nonradiative linewidth $\hbar\gamma_{\text{nrad},B_{1s}}$	$2\hbar\gamma_{\text{nrad},A_{1s}}$
Band structure parameters	
$k\cdot p$ -parameter $\gamma_{k\cdot p}$	$0.5(0.253 + 0.22)$ eV nm [84]
Effective electron mass $m_e^{K,\uparrow}/m_e^{K,\downarrow}$	$0.5m_0/0.58m_0$ [84]
Effective hole mass $m_h^{K,\uparrow}/m_h^{K,\downarrow}$	$0.6m_0/0.7m_0$ [84]
Conduction band splitting	20 meV [84]
Valence band splitting	184 meV [84]
Dielectric screening parameters	
Monolayer width d	0.6527 nm [135]
Static dielectric constant of bulk MoSe ₂ $\epsilon_{s,0} = \sqrt{\epsilon_{s,\parallel,0}\epsilon_{s,\perp,0}}$	12.0474 [155]
Interlayer gap h	0.3 nm [134]
Thomas-Fermi parameter α_{TF}	1.9 (fit to CMR [80])
Plasmon peak energy $\hbar\omega_{\text{pl}}$	22.0 eV [156]
Static dielectric constant of bulk h-BN $\epsilon_{\text{h-BN},0} = \sqrt{\epsilon_{\text{h-BN},0,\parallel}\epsilon_{\text{h-BN},0,\perp}}$	4.8 [82]
Optical in-plane dielectric constant of h-BN $\epsilon_{\parallel,\infty,\text{h-BN}}$	4.87 [198]
Selected calculated parameters	
A _{1s} binding energy	341.3 meV
B _{1s} binding energy	375.1 meV
A _{1s} Coulomb enhancement	0.916
$\sum_{\mathbf{q}} \varphi_{1s,\mathbf{q}}^{K,K,\uparrow,\uparrow}$	
B _{1s} Coulomb enhancement	1.038
$\sum_{\mathbf{q}} \varphi_{1s,\mathbf{q}}^{K,K,\downarrow,\downarrow}$	

TABLE AI. Parameters for the calculations of a h-BN-encapsulated MoSe₂ monolayer in Fig. 6.

[1] G. Wang, A. Chernikov, M. M. Glazov, T. F. Heinz, X. Marie, T. Amand, and B. Urbaszek, Colloquium: Excitons in atomically thin transition metal dichalcogenides, *Rev. Mod. Phys.* **90**, 021001 (2018).

[2] F. Katsch, M. Selig, A. Carmele, and A. Knorr, Theory of exciton-exciton interactions in monolayer transition metal dichalcogenides, *Phys. Status Solidi (B)* **255**, 1800185 (2018).

[3] A. Chernikov, T. C. Berkelbach, H. M. Hill, A. Rigosi, Y. Li, B. Aslan, D. R. Reichman, M. S. Hybertsen, and T. F. Heinz, Exciton binding energy and nonhydrogenic Rydberg series in monolayer WS₂, *Phys. Rev. Lett.* **113**, 076802 (2014).

[4] R. Perea-Causin, S. Brem, O. Schmidt, and E. Malic, Trion photoluminescence and trion stability in atomically thin semiconductors, *Phys. Rev. Lett.* **132**, 036903 (2024).

[5] D. Van Tuan and H. Dery, Excitons and trions in monolayer semiconductors with correlated electrons, *Phys. Rev. B* **108**, 085303 (2023).

[6] F. Katsch and A. Knorr, Excitonic theory of doping-dependent optical response in atomically thin semiconductors, *Phys. Rev. B* **105**, 045301 (2022).

[7] F. Katsch and A. Knorr, Doping-induced non-Markovian interference causes excitonic linewidth broadening in monolayer WSe₂, *Phys. Rev. B* **105**, L041401 (2022).

[8] D. K. Efimkin and A. H. MacDonald, Exciton-polarons in doped semiconductors in a strong magnetic field, *Phys. Rev. B* **97**, 235432 (2018).

[9] R. Combescot, Three-body Coulomb problem, *Phys. Rev. X* **7**, 041035 (2017).

[10] D. K. Efimkin and A. H. MacDonald, Many-body theory of trion absorption features in two-dimensional semiconductors, *Phys. Rev. B* **95**, 035417 (2017).

[11] A. Esser, R. Zimmermann, and E. Runge, Theory of trion spectra in semiconductor nanostructures, *Phys. Status Solidi (B)* **227**, 317 (2001).

[12] M. Drüppel, T. Deilmann, P. Krüger, and M. Rohlfing, Diversity of trion states and substrate effects in the optical properties of an MoS₂ monolayer, *Nat. Commun.* **8**, 2117 (2017).

[13] A. Arora, T. Deilmann, T. Reichenauer, J. Kern, S. Michaelis de Vasconcellos, M. Rohlfing, and R. Bratschitsch, Excited-state trions in monolayer WS₂, *Phys. Rev. Lett.* **123**, 167401 (2019).

[14] T. Deilmann and K. S. Thygesen, Interlayer trions in the MoS₂/WS₂ van der Waals heterostructure, *Nano Lett.* **18**, 1460 (2018).

[15] T. Deckert, H. Mittenzwey, O. Dogadov, M. Bertolotti,

G. Cerullo, D. Brida, A. Knorr, and S. Dal Conte, Coherent Coulomb intra- and intervalley many-body effects in single-layer transition metal dichalcogenides, *Phys. Rev. Lett.* **135**, 066902 (2025).

[16] F. Katsch, M. Selig, and A. Knorr, Exciton-scattering-induced dephasing in two-dimensional semiconductors, *Phys. Rev. Lett.* **124**, 257402 (2020).

[17] F. Katsch, M. Selig, and A. Knorr, Theory of coherent pump-probe spectroscopy in monolayer transition metal dichalcogenides, *2D Mater.* **7**, 015021 (2019).

[18] A. Steinhoff, M. Florian, A. Singh, K. Tran, M. Kolarczik, S. Helmrich, A. W. Achtstein, U. Woggon, N. Owschimikow, F. Jahnke, and X. Li, Biexciton fine structure in monolayer transition metal dichalcogenides, *Nat. Phys.* **14**, 1199 (2018).

[19] R. Takayama, N. H. Kwong, I. Rumyantsev, M. Kuwata-Gonokami, and R. Binder, T-matrix analysis of biexcitonic correlations in the nonlinear optical response of semiconductor quantum wells, *Eur. Phys. J. B* **25**, 445 (2002).

[20] J. Tang and C.-Z. Ning, Theoretical prediction of the quadruplon in a monolayer semiconductor, *Phys. Rev. B* **111**, L161409 (2025).

[21] F. Schäfer, H. Mittenzwey, M. Stein, O. Voigt, L. Greten, D. Anders, I. Müller, F. Dobener, M. Cuccu, C. Fuchs, K. Watanabe, T. Taniguchi, A. Chernikov, K. Volz, A. Knorr, and S. Chatterjee, Distinct Rabi splitting in confined systems of MoSe₂ monolayers and (Ga,In)As quantum wells, *Nat. Commun.* **16**, 8109 (2025).

[22] H. Mittenzwey, O. Voigt, and A. Knorr, Excitonic theory of the ultrafast optical response of 2D-quantum-confined semiconductors at elevated densities, arXiv preprint arXiv:2512.03198 [10.48550/arXiv.2512.03198](https://arxiv.org/abs/2512.03198) (2025).

[23] V. M. Axt, S. R. Bolton, U. Neukirch, L. J. Sham, and D. S. Chemla, Evidence of six-particle Coulomb correlations in six-wave-mixing signals from a semiconductor quantum well, *Phys. Rev. B* **63**, 115303 (2001).

[24] S. R. Bolton, U. Neukirch, L. J. Sham, D. S. Chemla, and V. M. Axt, Demonstration of sixth-order Coulomb correlations in a semiconductor single quantum well, *Phys. Rev. Lett.* **85**, 2002 (2000).

[25] T. Meier and S. W. Koch, Excitons versus unbound electron-hole pairs and their influence on exciton bleaching: A model study, *Phys. Rev. B* **59**, 13202 (1999).

[26] G. Bartels, G. C. Cho, T. Dekorsy, H. Kurz, A. Stahl, and K. Köhler, Coherent signature of differential transmission signals in semiconductors: Theory and experiment, *Phys. Rev. B* **55**, 16404 (1997).

[27] J. Choi, J. Li, D. Van Tuan, H. Dery, and S. A. Crooker, Emergence of composite many-body exciton states in WS₂ and MoSe₂ monolayers, *Phys. Rev. B* **109**, L041304 (2024).

[28] D. Van Tuan, S.-F. Shi, X. Xu, S. A. Crooker, and H. Dery, Six-body and eight-body exciton states in monolayer WSe₂, *Phys. Rev. Lett.* **129**, 076801 (2022).

[29] A. L. Ivanov and H. Haug, Self-consistent theory of the biexciton optical nonlinearity, *Phys. Rev. B* **48**, 1490 (1993).

[30] V. M. Axt and A. Stahl, A dynamics-controlled truncation scheme for the hierarchy of density matrices in semiconductor optics, *Z. Phys. B: Condens. Matter* **93**, 195 (1994).

[31] K. Victor, V. M. Axt, and A. Stahl, Hierarchy of density matrices in coherent semiconductor optics, *Phys. Rev. B* **51**, 14164 (1995).

[32] A. Thränhardt, S. Kuckenburg, A. Knorr, T. Meier, and S. W. Koch, Quantum theory of phonon-assisted exciton formation and luminescence in semiconductor quantum wells, *Phys. Rev. B* **62**, 2706 (2000).

[33] M. Herbst, V. M. Axt, and T. Kuhn, Temporally and spatially resolved electron-phonon quantum kinetics, *Phys. Status Solidi (B)* **221**, 419 (2000).

[34] V. M. Axt, K. Victor, and A. Stahl, Influence of a phonon bath on the hierarchy of electronic densities in an optically excited semiconductor, *Phys. Rev. B* **53**, 7244 (1996).

[35] M. Selig, G. Berghäuser, M. Richter, R. Bratschitsch, A. Knorr, and E. Malic, Dark and bright exciton formation, thermalization, and photoluminescence in monolayer transition metal dichalcogenides, *2D Mater.* **5**, 035017 (2018).

[36] S. Brem, A. Ekman, D. Christiansen, F. Katsch, M. Selig, C. Robert, X. Marie, B. Urbaszek, A. Knorr, and E. Malic, Phonon-assisted photoluminescence from indirect excitons in monolayers of transition-metal dichalcogenides, *Nano Lett.* **20**, 2849 (2020).

[37] M. Selig, F. Katsch, S. Brem, G. F. Mkrtchian, E. Malic, and A. Knorr, Suppression of intervalley exchange coupling in the presence of momentum-dark states in transition metal dichalcogenides, *Phys. Rev. Res.* **2**, 023322 (2020).

[38] M. Selig, F. Katsch, R. Schmidt, S. Michaelis de Vasconcellos, R. Bratschitsch, E. Malic, and A. Knorr, Ultrafast dynamics in monolayer transition metal dichalcogenides: Interplay of dark excitons, phonons, and intervalley exchange, *Phys. Rev. Res.* **1**, 022007 (2019).

[39] T. Yu and M. W. Wu, Valley depolarization due to intervalley and intravalley electron-hole exchange interactions in monolayer MoS₂, *Phys. Rev. B* **89**, 205303 (2014).

[40] M. Combescot, T. Amand, and S.-Y. Shiao, Ab initio quantum approach to electron-hole exchange for semiconductors hosting Wannier excitons, *Phys. Rev. B* **107**, 115206 (2023).

[41] G. Berghäuser, I. Bernal-Villamil, R. Schmidt, R. Schneider, I. Niehues, P. Erhart, S. Michaelis de Vasconcellos, R. Bratschitsch, A. Knorr, and E. Malic, Inverted valley polarization in optically excited transition metal dichalcogenides, *Nat. Commun.* **9**, 971 (2018).

[42] I. Bernal-Villamil, G. Berghäuser, M. Selig, I. Niehues, R. Schmidt, R. Schneider, P. Tonndorf, P. Erhart, S. M. de Vasconcellos, R. Bratschitsch, A. Knorr, and E. Malic, Exciton broadening and band renormalization due to Dexter-like intervalley coupling, *2D Mater.* **5**, 025011 (2018).

[43] O. Dogadov, H. Mittenzwey, M. Bertolotti, N. Olsen, T. Deckert, C. Trovatello, X. Zhu, D. Brida, G. Cerullo, A. Knorr, and S. Dal Conte, Dissecting intervalley coupling mechanisms in monolayer transition metal dichalcogenides, *npj 2D Mater. Appl.* **10**, 21 (2026).

[44] R. Schmidt, G. Berghäuser, R. Schneider, M. Selig, P. Tonndorf, E. Malic, A. Knorr, S. Michaelis de Vasconcellos, and R. Bratschitsch, Ultrafast Coulomb-induced intervalley coupling in atomically thin WS₂, *Nano Lett.* **16**, 2945 (2016).

[45] T. Amit, G. Vosco, M. Del Ben, and S. Refaelly-

Abramson, *Ab initio* density-matrix approach to exciton coherence: Phonon scattering, Coulomb interactions, and radiative recombination, *Phys. Rev. B* **112**, 115441 (2025).

[46] A. Steinhoff, F. Jahnke, and M. Florian, Wannier-function-based approach to coupled exciton-phonon-photon dynamics in two-dimensional semiconductors, *Phys. Rev. B* **112**, 115415 (2025).

[47] W. Lee, A. M. Alvertis, Z. Li, S. G. Louie, M. R. Filip, J. B. Neaton, and E. Kioupakis, Phonon screening of excitons in atomically thin semiconductors, *Phys. Rev. Lett.* **133**, 206901 (2024).

[48] Y.-h. Chan, J. B. Haber, M. H. Naik, S. G. Louie, J. B. Neaton, F. H. da Jornada, and D. Y. Qiu, Exciton thermalization dynamics in monolayer MoS₂: A first-principles Boltzmann equation study, *Phys. Rev. B* **111**, 184305 (2025).

[49] C. Hu, M. H. Naik, Y.-H. Chan, and S. G. Louie, Excitonic interactions and mechanism for ultrafast interlayer photoexcited response in van der Waals heterostructures, *Phys. Rev. Lett.* **131**, 236904 (2023).

[50] T. Amit and S. Refaely-Abramson, Ultrafast exciton decomposition in transition metal dichalcogenide heterostructures, *Phys. Rev. B* **108**, L220305 (2023).

[51] X.-W. Zhang and T. Cao, Ab initio calculations of spin-nonconserving exciton-phonon scattering in monolayer transition metal dichalcogenides, *J. Phys. Condens. Matter* **34**, 264002 (2022).

[52] E. Perfetto, Y. Pavlyukh, and G. Stefanucci, Real-time *GW*: Toward an ab initio description of the ultrafast carrier and exciton dynamics in two-dimensional materials, *Phys. Rev. Lett.* **128**, 016801 (2022).

[53] G. Stefanucci, R. van Leeuwen, and E. Perfetto, In and out-of-equilibrium ab initio theory of electrons and phonons, *Phys. Rev. X* **13**, 031026 (2023).

[54] A. Molina-Sánchez, D. Sangalli, L. Wirtz, and A. Marini, Ab initio calculations of ultrashort carrier dynamics in two-dimensional materials: Valley depolarization in single-layer WSe₂, *Nano Lett.* **17**, 4549 (2017).

[55] C. Attaccalite, M. Grüning, and A. Marini, Real-time approach to the optical properties of solids and nanostructures: Time-dependent Bethe-Salpeter equation, *Phys. Rev. B* **84**, 245110 (2011).

[56] G. Czycholl, *Theoretische Festkörperphysik: Von den klassischen Modellen zu modernen Forschungsthemen* (Springer, 2008).

[57] M. L. Cohen and S. G. Louie, *Fundamentals of Condensed Matter Physics* (Cambridge University Press, 2016).

[58] J. M. Ziman, *Electrons and Phonons: The Theory of Transport Phenomena in Solids* (Oxford University Press, 2001).

[59] G. D. Mahan, *Many-Particle Physics* (Springer New York, NY, 2000).

[60] H. Haug and S. W. Koch, *Quantum Theory of the Optical and Electronic Properties of Semiconductors*, 5th ed. (World Scientific, 2009).

[61] W. Schäfer and M. Wegener, *Semiconductor Optics and Transport Phenomena* (Springer-Verlag Berlin Heidelberg, 2002).

[62] C. Cohen-Tannoudji, J. Dupont-Roc, and G. Grynberg, *Photons and Atoms* (Wiley, New York, 1989).

[63] L. Hedin and S. Lundqvist, Effects of electron-electron and electron-phonon interactions on the one-electron states of solids, in *Solid state physics*, Vol. 23 (Elsevier, 1970) pp. 1–181.

[64] L. Á. Gergely, On Hamiltonian formulations of the Schrödinger system, *Ann. Phys. (NY)* **298**, 394 (2002).

[65] L. I. Schiff, *Quantum Mechanics*, 3rd ed. (McGraw-Hill, New York, 1968).

[66] D. Gitman and I. V. Tyutin, *Quantization of Fields with Constraints* (Springer Berlin, Heidelberg, 2012).

[67] K. Sundermeyer, *Constrained Dynamics*, 1st ed., Lecture Notes in Physics (Springer Berlin, Heidelberg, 1982).

[68] T. von Kármán and M. Born, Über Schwingungen in Raumgittern, *Phys. Z.* **13**, (1912).

[69] R. Resta, Manifestations of Berry's phase in molecules and condensed matter, *J. Phys. Condens. Matter* **12**, R107 (2000).

[70] R. M. Martin, *Electronic Structure: Basic Theory and Practical Methods* (Cambridge University Press, 2020).

[71] C. Kittel, *Quantum Theory of Solids* (Wiley, New York, 1963).

[72] N. Wiser, Dielectric constant with local field effects included, *Phys. Rev.* **129**, 62 (1963).

[73] S. L. Adler, Quantum theory of the dielectric constant in real solids, *Phys. Rev.* **126**, 413 (1962).

[74] M. Rohlfing and S. G. Louie, Electron-hole excitations and optical spectra from first principles, *Phys. Rev. B* **62**, 4927 (2000).

[75] M. S. Hybertsen and S. G. Louie, Ab initio static dielectric matrices from the density-functional approach. I. Formulation and application to semiconductors and insulators, *Phys. Rev. B* **35**, 5585 (1987).

[76] S. G. Louie, J. R. Chelikowsky, and M. L. Cohen, Local-field effects in the optical spectrum of silicon, *Phys. Rev. Lett.* **34**, 155 (1975).

[77] D. Y. Qiu, F. H. Da Jornada, and S. G. Louie, Optical spectrum of MoS₂: Many-body effects and diversity of exciton states, *Phys. Rev. Lett.* **111**, 216805 (2013).

[78] D. Y. Qiu, T. Cao, and S. G. Louie, Nonanalyticity, valley quantum phases, and lightlike exciton dispersion in monolayer transition metal dichalcogenides: Theory and first-principles calculations, *Phys. Rev. Lett.* **115**, 176801 (2015).

[79] D. Y. Qiu, F. H. Da Jornada, and S. G. Louie, Screening and many-body effects in two-dimensional crystals: Monolayer MoS₂, *Phys. Rev. B* **93**, 235435 (2016).

[80] K. Andersen, S. Latini, and K. S. Thygesen, Dielectric genome of van der Waals heterostructures, *Nano Lett.* **15**, 4616 (2015).

[81] A. H. Søndersted, M. Kuksma, J. K. Svaneborg, M. K. Svendsen, and K. S. Thygesen, Improved dielectric response of solids: Combining the Bethe-Salpeter equation with the random phase approximation, *Phys. Rev. Lett.* **133**, 026403 (2024).

[82] S. Latini, T. Olsen, and K. S. Thygesen, Excitons in van der Waals heterostructures: The important role of dielectric screening, *Phys. Rev. B* **92**, 245123 (2015).

[83] K. S. Thygesen, Calculating excitons, plasmons, and quasiparticles in 2D materials and van der Waals heterostructures, *2D Mater.* **4**, 022004 (2017).

[84] A. Kormányos, G. Burkard, M. Gmitra, J. Fabian, V. Zólyomi, N. D. Drummond, and V. Fal'ko, *k*·*p* theory for two-dimensional transition metal dichalcogenide semiconductors, *2D Mater.* **2**, 022001 (2015).

[85] S. Ismail-Beigi, E. K. Chang, and S. G. Louie, Coupling of nonlocal potentials to electromagnetic fields, *Phys. Rev. Lett.* **87**, 087402 (2001).

[86] M. Rösner, E. Şaşoğlu, C. Friedrich, S. Blügel, and T. O. Wehling, Wannier function approach to realistic Coulomb interactions in layered materials and heterostructures, *Phys. Rev. B* **92**, 085102 (2015).

[87] D. Erben, A. Steinhoff, C. Gies, G. Schönhoff, T. O. Wehling, and F. Jahnke, Excitation-induced transition to indirect band gaps in atomically thin transition-metal dichalcogenide semiconductors, *Phys. Rev. B* **98**, 035434 (2018).

[88] L. X. Benedict, Screening in the exchange term of the electron-hole interaction of the Bethe-Salpeter equation, *Phys. Rev. B* **66**, 193105 (2002).

[89] T. Deilmann and K. S. Thygesen, Important role of screening the electron-hole exchange interaction for the optical properties of molecules near metal surfaces, *Phys. Rev. B* **99**, 045133 (2019).

[90] D. Y. Qiu, F. H. da Jornada, and S. G. Louie, Environmental screening effects in 2D materials: Renormalization of the bandgap, electronic structure, and optical spectra of few-layer black phosphorus, *Nano Lett.* **17**, 4706 (2017).

[91] M. S. Hybertsen and S. G. Louie, Electron correlation in semiconductors and insulators: Band gaps and quasiparticle energies, *Phys. Rev. B* **34**, 5390 (1986).

[92] K. Kaasbjerg, K. S. Thygesen, and A.-P. Jauho, Acoustic phonon limited mobility in two-dimensional semiconductors: Deformation potential and piezoelectric scattering in monolayer MoS₂ from first principles, *Phys. Rev. B* **87**, 235312 (2013).

[93] P. Vogl, Microscopic theory of electron-phonon interaction in insulators or semiconductors, *Phys. Rev. B* **13**, 694 (1976).

[94] D. Pines, *Elementary Excitations in Solids* (CRC Press, 2018).

[95] J. Deslippe, G. Samsonidze, D. A. Strubbe, M. Jain, M. L. Cohen, and S. G. Louie, BerkeleyGW: A massively parallel computer package for the calculation of the quasiparticle and optical properties of materials and nanostructures, *Comput. Phys. Commun.* **183**, 1269 (2012).

[96] C. Aversa and J. E. Sipe, Nonlinear optical susceptibilities of semiconductors: Results with a length-gauge analysis, *Phys. Rev. B* **52**, 14636 (1995).

[97] D. Xiao, M.-C. Chang, and Q. Niu, Berry phase effects on electronic properties, *Rev. Mod. Phys.* **82**, 1959 (2010).

[98] G. F. Mkrtychian, A. Knorr, and M. Selig, Theory of second-order excitonic nonlinearities in transition metal dichalcogenides, *Phys. Rev. B* **100**, 125401 (2019).

[99] B. Pasenow, M. Reichelt, T. Stroucken, T. Meier, and S. W. Koch, Excitonic wave packet dynamics in semiconductor photonic-crystal structures, *Phys. Rev. B* **71**, 195321 (2005).

[100] A. Zimmermann, S. Kuhn, and M. Richter, Poisson Green's function method for increased computational efficiency in numerical calculations of Coulomb coupling elements, *Phys. Rev. B* **93**, 035308 (2016).

[101] C. A. Rozzi, D. Varsano, A. Marini, E. K. U. Gross, and A. Rubio, Exact Coulomb cutoff technique for supercell calculations, *Phys. Rev. B* **73**, 205119 (2006).

[102] S. Ismail-Beigi, Truncation of periodic image interactions for confined systems, *Phys. Rev. B* **73**, 233103 (2006).

[103] T. Tian, D. Scullion, D. Hughes, L. H. Li, C.-J. Shih, J. Coleman, M. Chhowalla, and E. J. G. Santos, Electronic polarizability as the fundamental variable in the dielectric properties of two-dimensional materials, *Nano Lett.* **20**, 841 (2019).

[104] F. Hüser, T. Olsen, and K. S. Thygesen, How dielectric screening in two-dimensional crystals affects the convergence of excited-state calculations: Monolayer MoS₂, *Phys. Rev. B* **88**, 245309 (2013).

[105] H. Ehrenreich and M. H. Cohen, Self-consistent field approach to the many-electron problem, *Phys. Rev.* **115**, 786 (1959).

[106] J. Lindhard, On the properties of a gas of charged particles, *Kgl. Danske Videnskab. Selskab Mat.-Fys. Medd.* **28**, (1954).

[107] J. P. Walter and M. L. Cohen, Wave-vector-dependent dielectric function for Si, Ge, GaAs, and ZnSe, *Phys. Rev. B* **2**, 1821 (1970).

[108] A. Steinhoff, M. Florian, and F. Jahnke, Dynamical screening effects of substrate phonons on two-dimensional excitons, *Phys. Rev. B* **101**, 045411 (2020).

[109] A. M. Alvertis, J. B. Haber, Z. Li, C. J. N. Coveney, S. G. Louie, M. R. Filip, and J. B. Neaton, Phonon screening and dissociation of excitons at finite temperatures from first principles, *Proc. Natl. Acad. Sci. U.S.A.* **121**, e2403434121 (2024).

[110] T. Deilmann, M. Rohlffing, and K. S. Thygesen, Optical excitations in 2D semiconductors, *Electron. Struct.* **5**, 033002 (2023).

[111] P. Giannozzi, S. Baroni, N. Bonini, M. Calandra, R. Car, C. Cavazzoni, D. Ceresoli, G. L. Chiarotti, M. Cococcioni, I. Dabo, A. Dal Corso, S. de Gironcoli, S. Fabris, G. Fratesi, R. Gebauer, U. Gerstmann, C. Gougoussis, A. Kokalj, M. Lazzeri, L. Martin-Samos, N. Marzari, F. Mauri, R. Mazzarello, S. Paolini, A. Pasquarello, L. Paulatto, C. Sbraccia, S. Scandolo, G. Sclauzero, A. P. Seitsonen, A. Smogunov, P. Umari, and R. M. Wentzcovitch, QUANTUM ESPRESSO: a modular and open-source software project for quantum simulations of materials, *J. Phys. Condens. Matter* **21**, 395502 (2009).

[112] A. Marini, C. Hogan, M. Grüning, and D. Varsano, yambo: An ab initio tool for excited state calculations, *Computer Physics Communications* **180**, 1392 (2009).

[113] D. Sangalli, A. Ferretti, H. Miranda, C. Attaccalite, I. Marri, E. Cannuccia, P. Melo, M. Marsili, F. Paleari, A. Marrazzo, G. Prandini, P. Bonfà, M. O. Atambo, F. Affinito, M. Palummo, A. Molina-Sánchez, C. Hogan, M. Grüning, D. Varsano, and A. Marini, Many-body perturbation theory calculations using the yambo code, *Journal of Physics: Condensed Matter* **31**, 325902 (2019).

[114] J. J. Mortensen, A. H. Larsen, M. Kuusma, A. V. Ivanov, A. Taghizadeh, A. Peterson, A. Haldar, A. O. Dohn, C. Schäfer, E. Ö. Jónsson, E. D. Hermes, F. A. Nilsson, G. Kastlunger, G. Levi, H. Jónsson, H. Häkkinen, J. Fojt, J. Kangsabanik, J. Södequist, J. Lehtomäki, J. Heske, J. Enkovaara, K. T. Winther, M. Dulak, M. M. Melander, M. Ovesen, M. Louhivuori, M. Walter, M. Gjerding, O. Lopez-Acevedo, P. Erhart, R. Warmbier, R. Würdemann, S. Kaappa, S. Latini, T. M. Boland, T. Bligaard, T. Skovhus, T. Susi, T. Maxson,

T. Rossi, X. Chen, Y. L. A. Schmerwitz, J. Schiøtz, T. Olsen, K. W. Jacobsen, and K. S. Thygesen, GPAW: An open Python package for electronic structure calculations, *J. Chem. Phys.* **160**, 092503 (2024).

[115] A. Hjorth Larsen, J. Jørgen Mortensen, J. Blomqvist, I. E. Castelli, R. Christensen, M. Dulak, J. Friis, M. N. Groves, B. Hammer, C. Hargus, E. D. Hermes, P. C. Jennings, P. Bjerre Jensen, J. Kermode, J. R. Kitchin, E. Leonhard Kolsbørg, J. Kubal, K. Kaasbørg, S. Lysgaard, J. Bergmann Maronsson, T. Maxson, T. Olsen, L. Pastewka, A. Peterson, C. Rostgaard, J. Schiøtz, O. Schütt, M. Strange, K. S. Thygesen, T. Vegge, L. Vilhelmsen, M. Walter, Z. Zeng, and K. W. Jacobsen, The atomic simulation environment—a Python library for working with atoms, *J. Phys. Condens. Matter* **29**, 273002 (2017).

[116] J. Hafner, Ab-initio simulations of materials using VASP: Density-functional theory and beyond, *J. Comput. Chem.* **29**, 2044 (2008).

[117] H. Haug and A.-P. Jauho, *Quantum Kinetics in Transport and Optics of Semiconductors*, Vol. 2 (Springer, 2008).

[118] L. Bányai, Q. T. Vu, B. Mieck, and H. Haug, Ultrafast quantum kinetics of time-dependent RPA-screened Coulomb scattering, *Phys. Rev. Lett.* **81**, 882 (1998).

[119] F. Schäfer, A. Trautmann, C. Ngo, J. T. Steiner, C. Fuchs, K. Volz, F. Dobener, M. Stein, T. Meier, and S. Chatterjee, Optical Stark effect in type-II semiconductor heterostructures, *Phys. Rev. B* **109**, 075301 (2024).

[120] C. Trovatello, F. Katsch, Q. Li, X. Zhu, A. Knorr, G. Cerullo, and S. Dal Conte, Disentangling many-body effects in the coherent optical response of 2D semiconductors, *Nano Lett.* **22**, 5322 (2022).

[121] C. Ciuti, C. Piermarocchi, V. Savona, P. E. Selbmann, P. Schwendimann, and A. Quattropani, Strongly driven exciton resonances in quantum wells: Light-induced dressing versus Coulomb scattering, *Phys. Rev. Lett.* **84**, 1752 (2000).

[122] A. Schülzgen, R. Binder, M. E. Donovan, M. Lindberg, K. Wundke, H. M. Gibbs, G. Khitrova, and N. Peyghambarian, Direct observation of excitonic Rabi oscillations in semiconductors, *Phys. Rev. Lett.* **82**, 2346 (1999).

[123] S. T. Cundiff, A. Knorr, J. Feldmann, S. W. Koch, E. O. Göbel, and H. Nickel, Rabi flopping in semiconductors, *Phys. Rev. Lett.* **73**, 1178 (1994).

[124] A. Steinhoff, E. Wietek, M. Florian, T. Schulz, T. Taniguchi, K. Watanabe, S. Zhao, A. Högele, F. Jahnke, and A. Chernikov, Exciton-exciton interactions in van der Waals heterobilayers, *Phys. Rev. X* **14**, 031025 (2024).

[125] A. Steinhoff, M. Rosner, F. Jahnke, T. O. Wehling, and C. Gies, Influence of excited carriers on the optical and electronic properties of MoS₂, *Nano Lett.* **14**, 3743 (2014).

[126] A. Steinhoff, M. Florian, M. Rösner, G. Schönhoff, T. O. Wehling, and F. Jahnke, Exciton fission in monolayer transition metal dichalcogenide semiconductors, *Nat. Commun.* **8**, 1166 (2017).

[127] D. Erkensten, S. Brem, R. Perea-Causín, and E. Malic, Microscopic origin of anomalous interlayer exciton transport in van der Waals heterostructures, *Phys. Rev. Mater.* **6**, 094006 (2022).

[128] A. Steinhoff, J.-H. Kim, F. Jahnke, M. Rösner, D.-S. Kim, C. Lee, G. H. Han, M. S. Jeong, T. O. Wehling, and C. Gies, Efficient excitonic photoluminescence in direct and indirect band gap monolayer MoS₂, *Nano Lett.* **15**, 6841 (2015).

[129] D. Erben, A. Steinhoff, M. Lorke, and F. Jahnke, Optical nonlinearities in the excited carrier density of atomically thin transition metal dichalcogenides, *Phys. Rev. B* **106**, 045409 (2022).

[130] F. Lohof, A. Steinhoff, M. Florian, M. Lorke, D. Erben, F. Jahnke, and C. Gies, Prospects and limitations of transition metal dichalcogenide laser gain materials, *Nano Lett.* **19**, 210 (2019).

[131] M. L. Trolle, T. G. Pedersen, and V. Véniard, Model dielectric function for 2D semiconductors including substrate screening, *Sci. Rep.* **7**, 39844 (2017).

[132] M. N. Gjerding, L. S. R. Cavalcante, A. Chaves, and K. S. Thygesen, Efficient ab initio modeling of dielectric screening in 2D van der Waals materials: Including phonons, substrates, and doping, *J. Phys. Chem. C* **124**, 11609 (2020).

[133] N. Peimyoo, H.-Y. Wu, J. Escolar, A. De Sanctis, G. Prando, F. Vollmer, F. Withers, A. C. Riis-Jensen, M. F. Craciun, K. S. Thygesen, and S. Russo, Engineering dielectric screening for potential-well arrays of excitons in 2D materials, *ACS Appl. Mater. Interfaces* **12**, 55134 (2020).

[134] M. Florian, M. Hartmann, A. Steinhoff, J. Klein, A. W. Holleitner, J. J. Finley, T. O. Wehling, M. Kaniber, and C. Gies, The dielectric impact of layer distances on exciton and trion binding energies in van der Waals heterostructures, *Nano Lett.* **18**, 2725 (2018).

[135] I. Kylänpää and H.-P. Komsa, Binding energies of exciton complexes in transition metal dichalcogenide monolayers and effect of dielectric environment, *Phys. Rev. B* **92**, 205418 (2015).

[136] R. Narciso Pedrosa, C. E. P. Villegas, A. Reily Rocha, R. G. Amorim, and W. Scopel, Interlayer excitons and radiative lifetimes in MoSe₂/SeWS bilayers: Implications for light-emitting diodes, *ACS Appl. Nano Mater.* **8**, 5051 (2025).

[137] N. Kang, *Green's Function for Poisson Equation in Layered Nano-Structures Including Graphene*, Master's thesis, University of Waterloo (2015).

[138] L. Meckbach, T. Stroucken, and S. W. Koch, Influence of the effective layer thickness on the ground-state and excitonic properties of transition-metal dichalcogenide systems, *Phys. Rev. B* **97**, 035425 (2018).

[139] J. D. Jackson, *Classical Electrodynamics* (Wiley, New York, 1999).

[140] W. R. Inc., *Mathematica, Version 14.2*, champaign, IL, 2024.

[141] E. Malic, M. J. P. Bormann, P. Hovel, M. Kuntz, D. Bimberg, A. Knorr, and E. Scholl, Coulomb damped relaxation oscillations in semiconductor quantum dot lasers, *IEEE J. Sel. Top. Quantum Electron.* **13**, 1242 (2007).

[142] A. Liu, Local-field effect on the linear optical intersubband absorption in multiple quantum wells, *Phys. Rev. B* **50**, 8569 (1994).

[143] N. S. Rytova, Coulomb interaction of electrons in a thin film, in *Dokl. Akad. Nauk SSSR*, Vol. 163 (Russian Academy of Sciences, 1965) pp. 1118–1120.

[144] N. S. Rytova, Screened potential of a point charge in a

thin film, *Mosc. Univ. Phys. Bull.* **3**, (1967).

[145] L. V. Keldysh, Coulomb interaction in thin semiconductor and semimetal films, *J. Exp. Theor. Phys.* **29**, 658 (1979).

[146] J. Neuhaus, S. C. Liebscher, L. Meckbach, T. Stroucken, and S. W. Koch, Microscopic Coulomb interaction in transition-metal dichalcogenides, *J. Phys. Condens. Matter* **33**, 035301 (2020).

[147] B. Scharf, D. Van Tuan, I. Žutić, and H. Dery, Dynamical screening in monolayer transition-metal dichalcogenides and its manifestations in the exciton spectrum, *J. Phys. Condens. Matter* **31**, 203001 (2019).

[148] D. Timmer, M. Gittinger, T. Quenzel, A. R. Cadore, B. L. T. Rosa, W. Li, G. Soavi, D. C. Lünemann, S. Stephan, M. Silies, T. Schulz, A. Steinhoff, F. Jahnke, G. Cerullo, A. C. Ferrari, A. De Sio, and C. Lienau, Ultrafast coherent exciton couplings and many-body interactions in monolayer WS₂, *Nano Lett.* **24**, 8117 (2024).

[149] D. Erkensten, S. Brem, K. Wagner, R. Gillen, R. Pereira-Causín, J. D. Ziegler, T. Taniguchi, K. Watanabe, J. Maultzsch, A. Chernikov, and E. Malic, Dark exciton-exciton annihilation in monolayer WSe₂, *Phys. Rev. B* **104**, L241406 (2021).

[150] G. Cappellini, R. Del Sole, L. Reining, and F. Bechstedt, Model dielectric function for semiconductors, *Phys. Rev. B* **47**, 9892 (1993).

[151] Z. H. Levine and S. G. Louie, New model dielectric function and exchange-correlation potential for semiconductors and insulators, *Phys. Rev. B* **25**, 6310 (1982).

[152] M. S. Hybertsen and S. G. Louie, Model dielectric matrices for quasiparticle self-energy calculations, *Phys. Rev. B* **37**, 2733 (1988).

[153] D. R. Penn, Wave-number-dependent dielectric function of semiconductors, *Phys. Rev.* **128**, 2093 (1962).

[154] F. Bechstedt and R. Enderlein, Electronic polarization (relaxation) effects in the core level spectra of semiconductors. I. General theory of electronic polarization (relaxation) in semiconductors, *Phys. Status Solidi (B)* **94**, 239 (1979).

[155] A. Laturia, M. L. Van de Put, and W. G. Vandenberghe, Dielectric properties of hexagonal boron nitride and transition metal dichalcogenides: from monolayer to bulk, *npj 2D Mater. Appl.* **2**, 6 (2018).

[156] A. Kumar and P. K. Ahluwalia, Tunable dielectric response of transition metals dichalcogenides MX₂ (M=Mo, W; X=S, Se, Te): Effect of quantum confinement, *Phys. B: Condens. Matter* **407**, 4627 (2012).

[157] L. J. Sham and T. M. Rice, Many-particle derivation of the effective-mass equation for the Wannier exciton, *Phys. Rev.* **144**, 708 (1966).

[158] G. H. Wannier, The structure of electronic excitation levels in insulating crystals, *Phys. Rev.* **52**, 191 (1937).

[159] D. Xiao, G.-B. Liu, W. Feng, X. Xu, and W. Yao, Coupled spin and valley physics in monolayers of MoS₂ and other group-VI dichalcogenides, *Phys. Rev. Lett.* **108**, 196802 (2012).

[160] A. Knorr, S. Hughes, T. Stroucken, and S. W. Koch, Theory of ultrafast spatio-temporal dynamics in semiconductor heterostructures, *Chem. Phys.* **210**, 27 (1996).

[161] E. Malic and A. Knorr, *Graphene and Carbon Nanotubes: Ultrafast Relaxation Dynamics and Optics* (John Wiley & Sons, Ltd, 2013).

[162] F. Jahnke, M. Kira, and S. W. Koch, Linear and non-linear optical properties of excitons in semiconductor quantum wells and microcavities, *Z. Phys. B: Condens. Matter* **104**, 559 (1997).

[163] R. J. Elliott, Intensity of optical absorption by excitons, *Phys. Rev.* **108**, 1384 (1957).

[164] M. Selig, G. Berghäuser, A. Raja, P. Nagler, C. Schüller, T. F. Heinz, T. Korn, A. Chernikov, E. Malic, and A. Knorr, Excitonic linewidth and coherence lifetime in monolayer transition metal dichalcogenides, *Nat. Commun.* **7**, 13279 (2016).

[165] F. Lengers, T. Kuhn, and D. E. Reiter, Theory of the absorption line shape in monolayers of transition metal dichalcogenides, *Phys. Rev. B* **101**, 155304 (2020).

[166] N. Ma and D. Jena, Charge scattering and mobility in atomically thin semiconductors, *Phys. Rev. X* **4**, 011043 (2014).

[167] D. Jena and A. Konar, Enhancement of carrier mobility in semiconductor nanostructures by dielectric engineering, *Phys. Rev. Lett.* **98**, 136805 (2007).

[168] S. Glutsch and F. Bechstedt, Theory of asymmetric broadening and shift of excitons in quantum structures with rough interfaces, *Phys. Rev. B* **50**, 7733 (1994).

[169] A. Thränhardt, C. Ell, S. Mosor, G. Rupper, G. Khitrova, H. M. Gibbs, and S. W. Koch, Interplay of phonon and disorder scattering in semiconductor quantum wells, *Phys. Rev. B* **68**, 035316 (2003).

[170] A. Raja, L. Waldecker, J. Zipfel, Y. Cho, S. Brem, J. D. Ziegler, M. Kulig, T. Taniguchi, K. Watanabe, E. Malic, T. F. Heinz, T. C. Berkelbach, and A. Chernikov, Dielectric disorder in two-dimensional materials, *Nat. Nanotechnol.* **14**, 832 (2019).

[171] A. Sommerfeld, Über die Beugung und Bremsung der Elektronen, *Ann. Phys.* **403**, 257 (1931).

[172] R. Zimmermann, Excitonic spectra in semiconductor nanostructures, *Jpn. J. Appl. Phys.* **34**, 228 (1995).

[173] R. Winkler, Excitons and fundamental absorption in quantum wells, *Phys. Rev. B* **51**, 14395 (1995).

[174] M. Shinada and S. Sugano, Interband optical transitions in extremely anisotropic semiconductors. I. Bound and unbound exciton absorption, *J. Phys. Soc. Jpn.* **21**, 1936 (1966).

[175] S. Gozem, A. O. Gumina, T. Ichino, D. L. Osborn, J. F. Stanton, and A. I. Krylov, Photoelectron wave function in photoionization: Plane wave or Coulomb wave?, *J. Phys. Chem. Lett.* **6**, 4532 (2015).

[176] R. Winkler, *Spin-Orbit Coupling Effects in Two-Dimensional Electron and Hole Systems*, Vol. 191 (Springer Berlin, Heidelberg, 2003).

[177] A. Kormányos, V. Zólyomi, N. D. Drummond, and G. Burkard, Spin-orbit coupling, quantum dots, and qubits in monolayer transition metal dichalcogenides, *Phys. Rev. X* **4**, 011034 (2014).

[178] K. Kośmider, J. W. González, and J. Fernández-Rossier, Large spin splitting in the conduction band of transition metal dichalcogenide monolayers, *Phys. Rev. B* **88**, 245436 (2013).

[179] M. Marsili, A. Molina-Sánchez, M. Palummo, D. Sangalli, and A. Marini, Spinorial formulation of the GW-BSE equations and spin properties of excitons in two-dimensional transition metal dichalcogenides, *Phys. Rev. B* **103**, 155152 (2021).

[180] T. Deilmann, P. Krüger, and M. Rohlfing, Ab initio studies of exciton g factors: Monolayer transition metal

dichalcogenides in magnetic fields, *Phys. Rev. Lett.* **124**, 226402 (2020).

[181] P. E. Faria Junior, K. Zollner, T. Woźniak, M. Kurpas, M. Gmitra, and J. Fabian, First-principles insights into the spin-valley physics of strained transition metal dichalcogenides monolayers, *New J. Phys.* **24**, 083004 (2022).

[182] G. Vosco and S. Refael-Y Abramson, Exciton-exciton annihilation mediated by many-body Coulomb and phonon interactions: An ab initio study, *Phys. Rev. Lett.* **135**, 206901 (2025).

[183] A. Steinhoff, F. Jahnke, and M. Florian, Microscopic theory of exciton-exciton annihilation in two-dimensional semiconductors, *Phys. Rev. B* **104**, 155416 (2021).

[184] D. L. Dexter, A theory of sensitized luminescence in solids, *J. Chem. Phys.* **21**, 836 (1953).

[185] D. Y. Qiu, F. H. da Jornada, and S. G. Louie, Solving the Bethe-Salpeter equation on a subspace: Approximations and consequences for low-dimensional materials, *Phys. Rev. B* **103**, 045117 (2021).

[186] S. Raiber, P. E. Faria Junior, D. Falter, S. Feldl, P. Marzena, K. Watanabe, T. Taniguchi, J. Fabian, and C. Schüller, Ultrafast pseudospin quantum beats in multilayer WSe₂ and MoSe₂, *Nat. Commun.* **13**, 4997 (2022).

[187] S. Dal Conte, F. Bottegoni, E. A. A. Pogna, D. De Fazio, S. Ambrogio, I. Bargigia, C. D'Andrea, A. Lombardo, M. Bruna, F. Ciccacci, A. C. Ferrari, G. Cerullo, and M. Finazzi, Ultrafast valley relaxation dynamics in monolayer MoS₂ probed by nonequilibrium optical techniques, *Phys. Rev. B* **92**, 235425 (2015).

[188] T. Förster, Zwischenmolekulare Energiewanderung und Fluoreszenz, *Ann. Phys.* **437**, 55 (1948).

[189] L. Guo, M. Wu, T. Cao, D. M. Monahan, Y.-H. Lee, S. G. Louie, and G. R. Fleming, Exchange-driven intravalley mixing of excitons in monolayer transition metal dichalcogenides, *Nat. Phys.* **15**, 228 (2019).

[190] N.-H. Kwong, J. R. Schaibley, and R. Binder, Effect of intravalley and intervalley electron-hole exchange on the nonlinear optical response of monolayer MoSe₂, *Phys. Rev. B* **104**, 245434 (2021).

[191] G. Bir, A. Aronov, and G. Pikus, Spin relaxation of electrons due to scattering by holes, *Zh. Eksp. Teor. Fiz.* **69**, 1382–1397 (1975).

[192] M. Z. Maialle, E. A. de Andrade e Silva, and L. J. Sham, Exciton spin dynamics in quantum wells, *Phys. Rev. B* **47**, 15776 (1993).

[193] C. Lechner and U. Rössler, Spin-dependent semiconductor Bloch equations: Microscopic theory of Bir-Aronov-Pikus spin relaxation, *Phys. Rev. B* **72**, 153317 (2005).

[194] P. Li, C. Robert, D. Van Tuan, L. Ren, M. Yang, X. Marie, and H. Dery, Intervalley electron-hole exchange interaction and impurity-assisted recombination of indirect excitons in WS₂ and WSe₂ monolayers, *Phys. Rev. B* **106**, 085414 (2022).

[195] M. Yang, L. Ren, C. Robert, D. Van Tuan, L. Lombez, B. Urbaszek, X. Marie, and H. Dery, Relaxation and darkening of excitonic complexes in electrostatically doped monolayer WSe₂: Roles of exciton-electron and trion-electron interactions, *Phys. Rev. B* **105**, 085302 (2022).

[196] M. He, P. Rivera, D. Van Tuan, N. P. Wilson, M. Yang, T. Taniguchi, K. Watanabe, J. Yan, D. G. Mandrus, H. Yu, H. Dery, W. Yao, and X. Xu, Valley phonons and exciton complexes in a monolayer semiconductor, *Nat. Commun.* **11**, 618 (2020).

[197] C. Robert, B. Han, P. Kapuscinski, A. Delhomme, C. Faugeras, T. Amand, M. R. Molas, M. Bartos, K. Watanabe, T. Taniguchi, B. Urbaszek, M. Potemski, and X. Marie, Measurement of the spin-forbidden dark excitons in MoS₂ and MoSe₂ monolayers, *Nat. Commun.* **11**, 4037 (2020).

[198] Y. Cai, L. Zhang, Q. Zeng, L. Cheng, and Y. Xu, Infrared reflectance spectrum of BN calculated from first principles, *Solid State Commun.* **141**, 262 (2007).